DOT/FAA/AR-98/28

Office of Aviation Research
Washington, D.C. 20591

Statistical Loads Data for Boeing 737-400 Aircraft in Commercial Operations

August 1998

Final Report

U.S. Department of Transportation
Federal Aviation Administration

NOTICE

Technical Report Documentation Page

1. Report No.	2. Government Accession No.	3. Recipient's Catalog No.
DOT/FAA/AR-98/28		

4. Title and Subtitle	5. Report Date
STATISTICAL LOADS DATA FOR BOEING 737-400 AIRCRAFT IN COMMERCIAL OPERATIONS	August 1998
	6. Performing Organization Code

7. Author(s)	8. Performing Organization Report No.
John Rustenburg, Donal Skinn, Daniel O. Tipps	URD-TR-98-00032

9. Performing Organization Name and Address	10. Work Unit No. (TRAIS)
University of Dayton Research Institute Structural Integrity Division 300 College Park Dayton, OH 45469-0120	RPD-510-1998-00032
	11. Contract or Grant No. FAA Grant No. 96-G-020

12. Sponsoring Agency Name and Address	13. Type of Report and Period Covered
U.S. Department of Transportation Federal Aviation Administration Office of Aviation Research Washington, DC 20591	Final Report
	14. Sponsoring Agency Code AAR-431

15. Supplementary Notes

The Federal Aviation Administration William J. Hughes Technical Center COTR is Thomas DeFiore

16. Abstract

The University of Dayton is supporting Federal Aviation Administration (FAA) research on the structural integrity requirements for the US commercial transport airplane fleet. The primary objective of this research is to support the FAA Airborne Data Monitoring Systems Research Program by developing new and improved methods and criteria for processing and presenting large commercial transport airplane flight and ground loads usage data. The scope of activities performed involved (1) defining the service related factors which affect the operational life of commercial aircraft; (2) designing an efficient software system to reduce, store, and process large quantities of optical quick access recorder data; and (3) providing processed data in formats that will enable the FAA to reassess existing certification criteria. Equally important, these new data will also enable the FAA, the aircraft manufacturers, and the airlines to better understand and control those factors which influence the structural integrity of commercial transport aircraft. Presented herein are analyses and statistical summaries of data collected from 11,721 flights representing 19,105 flight hours of 17 typical B-737-400 aircraft during operational usage recorded by a single airline. The statistical data presented include the initial recorded data previously reported in FAA report DOT/FAA/AR-95/21. The data include statistical information on accelerations, speeds, altitudes, flight duration and distance, gross weights, speed brake/spoiler cycles, thrust reverser usage, and gust velocities encountered.

17. Key Words	18. Distribution Statement
Optical quick access recorder, Flight profiles, Gust loads, Accelerations, Statistical summaries	This document is available to the public through the National Technical Information Service (NTIS), Springfield, Virginia 22161.

19. Security Classif. (of this report)	20. Security Classif. (of this page)	21. No. of Pages	22. Price
Unclassified	Unclassified	86	N/A

PREFACE

The Flight Systems Integrity Group of the Structural Integrity Division of the University of Dayton Research Institute (URDI) performed this work under Federal Aviation Administration (FAA) Grant No. 96-G-020 entitled "Aircraft Operational Usage for Service Life Management and Design Criteria Development." The Program Manager for the FAA was Mr. Thomas DeFiore of the FAA William J. Hughes Technical Center at Atlantic City International Airport, New Jersey, and the Program Technical Advisor was Mr. Terence Barnes of the FAA Aircraft Certification Office. Mr. Daniel Tipps was the Principal Investigator for the University of Dayton and provided oversight direction for this effort. Mr. Donald Skinn developed the data reduction algorithms, established data reduction criteria, and performed the data reduction. Mr. John Rustenburg performed the data analysis, created the graphical presentations, and prepared the report. Ms. Andrea Snell compiled and formatted the report for publication.

TABLE OF CONTENTS

LIST OF FIGURES

LIST OF TABLES

LIST OF SYMBOLS AND ABBREVIATIONS

$\overline{A}$	aircraft PSD gust response factor
a	speed of sound (ft/sec)
$\overline{c}$	wing mean geometric chord (ft)
$\overline{C}$	aircraft discrete gust response factor
C_{L_α}	aircraft lift curve slope per radian
$C_{L_{max}}$	maximum lift coefficient
CAS	calibrated air speed
c.g.	center of gravity
EAS	equivalent airspeed
F(PSD)	continuous gust alleviation factor
g	gravity constant, 32.17 ft/sec^2
H_p	pressure altitude, (ft)
K_g	discrete gust alleviation factor, $0.88\,\mu/(5.3 + \mu)$
KCAS	knots calibrated air speed
KEAS	knots equivalent air speed
KIAS	knots indicated air speed
kts	knots
L	turbulence scale length (ft)
n	load factor (g)
N	number of occurrences for U_σ (PSD gust procedure)
nm	nautical mile
n_x	longitudinal load factor (g)
n_y	lateral load factor (g)
n_z	normal load factor (g)
N_0	number of zero crossings per nautical mile (PSD gust procedure)
q	dynamic pressure (lbs/ft^2)
S	wing area (ft^2)
TAS	true airspeed
U_{de}	derived gust velocity (ft/sec)
U_σ	continuous turbulence gust intensity (ft/sec)

V_B	design speed for maximum gust
V_C	design cruise speed
V_D	design dive speed
V_e	equivalent airspeed
V_T	true airspeed
W	gross weight (lbs)
Δm	incremental acceleration due to a turning maneuver
Δn_z	incremental normal load factor, n_z - 1
$\Delta n_{z_{man}}$	incremental maneuver load factor
$\Delta n_{z_{gust}}$	incremental gust load factor
μ	airplane mass ratio, $\frac{2(W/S)}{\rho g \bar{c} C_{L_\alpha}}$
μ_p	statistical mean of p (parameter on plots)
ρ	air density, slugs/ft^3 (at altitude)
ρ_0	standard sea level air density, 0.0023769 slugs/ft^3
σ_p	standard deviation of p (parameter on plots)
φ	bank angle (degrees)

EXECUTIVE SUMMARY

The University of Dayton is supporting Federal Aviation Administration (FAA) research on the structural integrity requirements for the US commercial transport airplane fleet. The primary objective of this research is to support the FAA Airborne Data Monitoring Systems Research Program by developing new and improved methods and criteria for processing and presenting large commercial transport airplane flight and ground loads usage data. The scope of activities performed involved (1) defining the service related factors which affect the operational life of commercial aircraft; (2) designing an efficient software system to reduce, store, and process large quantities of optical quick access recorder data; and (3) providing processed data in formats that will enable the FAA to reassess existing certification criteria. Equally important, these new data will also enable the FAA, the aircraft manufacturers, and the airlines to better understand and control those factors which influence the structural integrity of commercial transport aircraft. Presented herein are analyses and statistical summaries of data collected from 11,721 flights representing 19,105 flight hours of 17 typical B-737-400 aircraft during operational usage recorded by a single airline. The statistical data presented includes the initial recorded data previously reported in FAA report DOT/FAA/AR-95/21. The data include statistical information on accelerations, speeds, altitudes, flight duration and distance, gross weights, speed brake/spoiler cycles, thrust reverser usage, and gust velocities encountered.

1. INTRODUCTION.

The Federal Aviation Administration (FAA) has an ongoing Airborne Data Monitoring Systems Research Program to collect, process, and evaluate statistical flight loads data from transport aircraft used in normal commercial airline operations. The objectives of this program are (a) to acquire, evaluate, and utilize typical operational in-service data for comparison with the prior data used in the design and qualification testing of civil transport aircraft and (b) to provide a basis to improve the structural criteria and methods of design, evaluation, and substantiation of future airplanes. Since the inception of the FAA's Airborne Data Monitoring Systems Research Program, the scope of the program has steadily increased to include data collection on additional aircraft, different aircraft models, and additional operators. The University of Dayton has supported the FAA's efforts and has responsibility for the data analysis and processing tasks and report preparation. In consultation with airplane manufacturers and operators, the University has enhanced and improved the data processing capabilities to allow reducing, analyzing, and reporting additional aircraft usage and statistical loads data from the digital flight loads recorders into a form that will fulfill the requests of the aircraft manufacturers, the airlines, and the FAA. The report presents data obtained from 17 airplanes over 11,721 flights and 19,105 hours of airline operations for the B-737-400 aircraft of a single operator.

2. AIRCRAFT DESCRIPTION.

Table 1 presents certain operational characteristics of the 17 Boeing 737-400 aircraft which were equipped with optical quick access recorders. Figure 1 shows front, top, and side views of the aircraft and identifies its major physical dimensions.

TABLE 1. BOEING 737-400 AIRCRAFT CHARACTERISTICS

Maximum Taxi Weight	143,000 lb
Maximum Takeoff Weight	142,500 lb
Maximum Landing Weight	121,000 lb
Zero-Fuel Weight	113,000 lb
Fuel Capacity	5311 U.S. gallons
2 CFM56-3 Engines	@ 22,000 lbs static thrust each
Wing Span	94 ft 9 in
Wing Reference Area	980 ft^2
Wing MAC	11 ft 2.46 in
Wing Sweep	25 degrees
Length	119 ft 7 in
Height	36 ft 6 in
Tread	17 ft 2 in
Wheel Base	46 ft 10 in

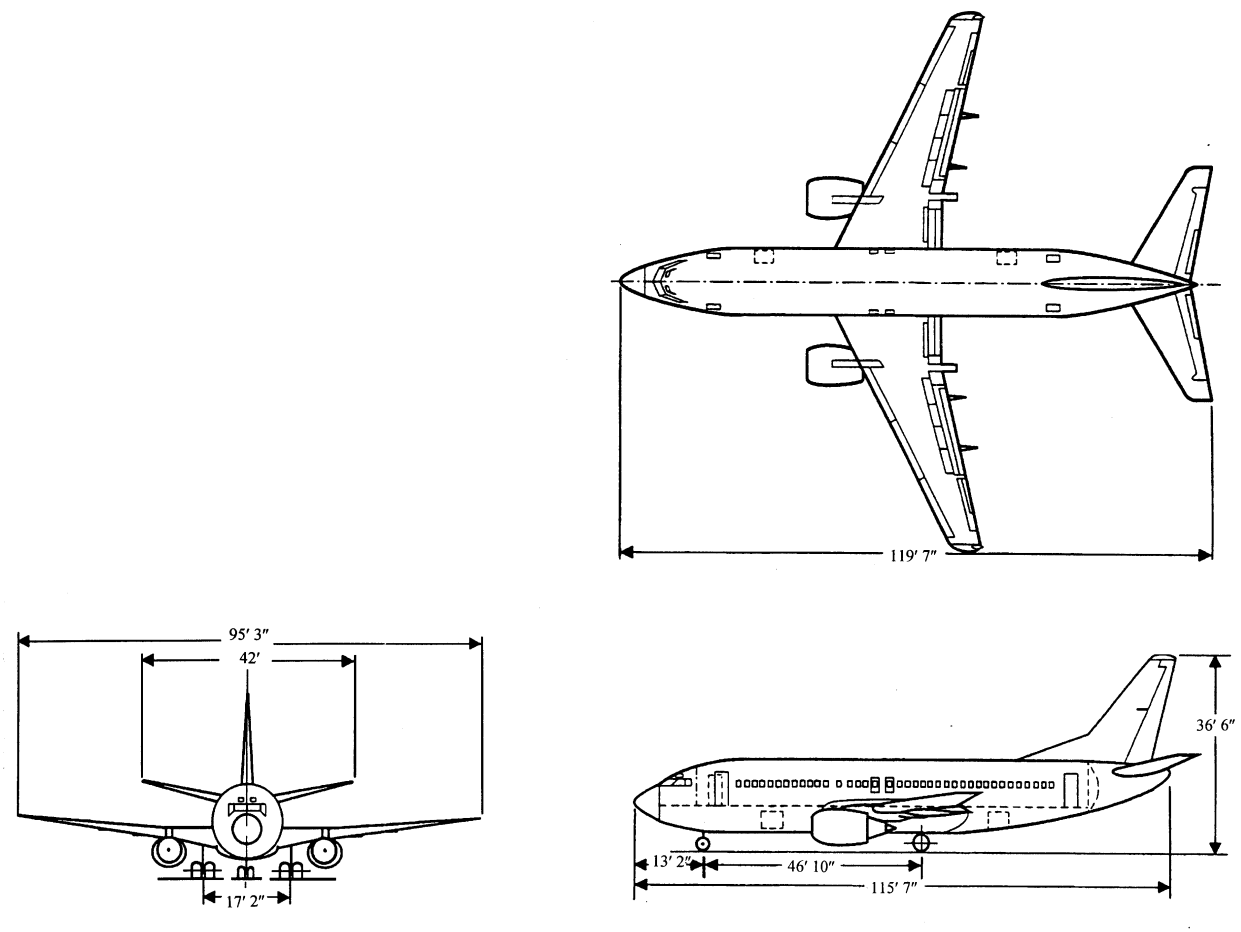

FIGURE 1. BOEING 737-400 THREE-VIEW DRAWING

3. AIRLINE DATA COLLECTION AND EDITING SYSTEMS.

The airline data collection and editing system consists of two major components: (1) the data collection system installed on board the aircraft and (2) the ground data editing station. A schematic overview of the system is given in figure 2. The requirements for the data acquisition and processing are defined in reference 1. The collection and editing systems are discussed below.

3.1 DATA COLLECTION SYSTEM.

The on-board data collection system consists of a Digital Flight Data Acquisition Unit (DFDAU), a Digital Flight Data Recorder (DFDR), and an Optical Quick Access Recorder (OQAR). The DFDAU collects sensor signals and sends parallel data signals to both the DFDR and the OQAR. The OQAR is programmed to start recording once certain data signals are detected. The OQAR is equipped with an optical disk which can store up to 200 hours of flight data, whereas the DFDR uses a 25-hour looptape. The optical disk is periodically removed from the OQAR and forwarded to the ground processing station.

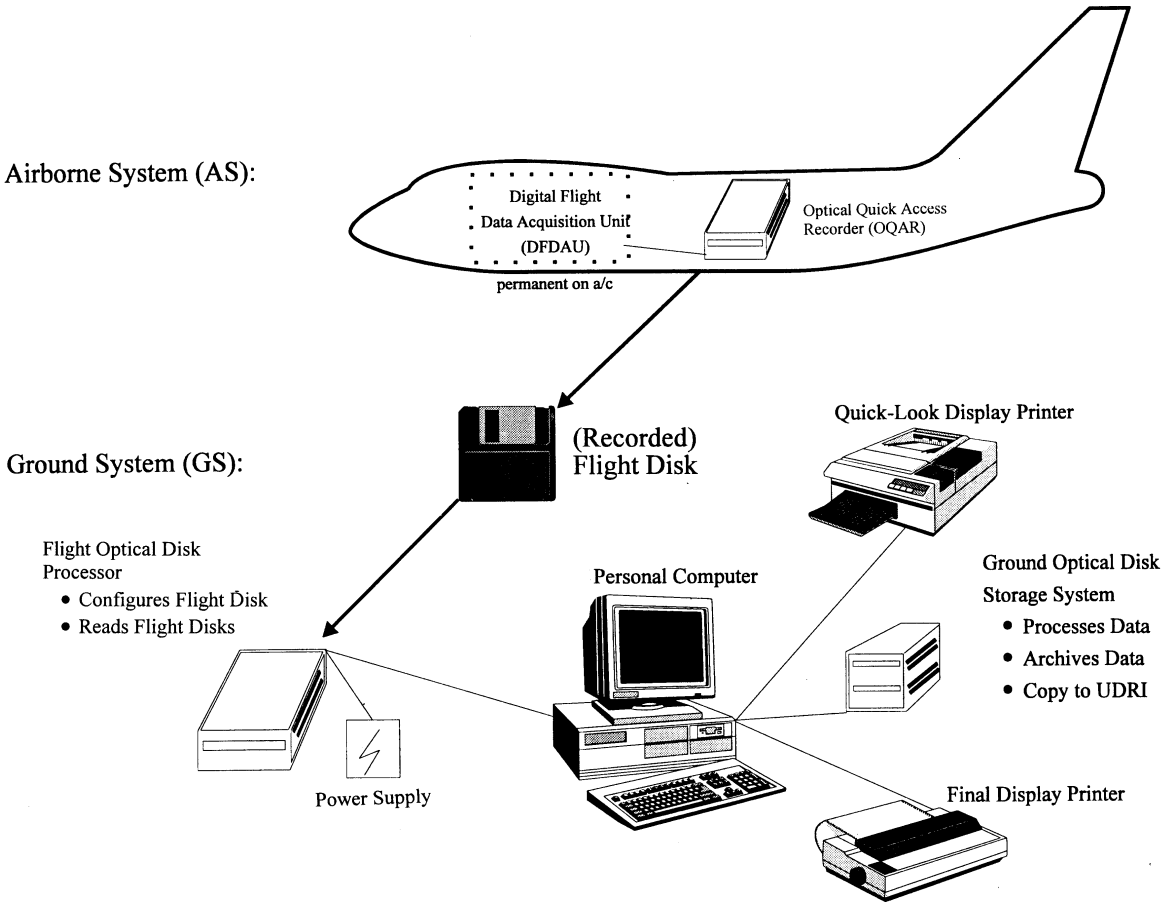

FIGURE 2. AIRLINE RECORDING AND EDITING SYSTEM

3.2 DATA EDITING SYSTEM.

The airline ground data editing station consists of a Pentium computer, a magneto-optical (MO) disk drive, and flight data editing software. The software performs a number of functions during the process of transferring the raw flight data into DOS file format onto the hard disk. The most important of these functions include a data integrity check and removal of flight sensitive information. Data considered sensitive are those which can be used to readily identify a specific flight. The desensitized data are forwarded to the University of Dayton Research Institute (UDRI) for flight loads processing and analysis. Table 2 presents the recorded data parameters provided by the airline to UDRI.

4. UNIVERSITY OF DAYTON RESEARCH INSTITUTE DATA PROCESSING.

The data parameters of table 2 are provided by the airline to UDRI for each recorded flight. The data are provided on magneto-optical disks containing binary files for multiple flights for different airplanes. These data are processed by UDRI to extract the parameters required for statistical flight loads presentation. This section describes the reduction of the data and the derivation of required parameters.

TABLE 2. RECORDED PARAMETERS PROVIDED TO UDRI

Parameter	Sample Rate
Normal Acceleration	8 per second
Lateral Acceleration	4 per second
Longitudinal Acceleration	4 per second
Aileron Position	1 per second
Elevator Position	1 per second
Rudder Position	2 per second
Pilot Trim Position	1 per second
Flap Handle Position	1 per second
Speed Brake Position	1 per second
N_1 Engine - Left	1 per second
N_1 Engine - Right	1 per second
Throttle #1 Position	1 per second
Throttle #2 Position	1 per second
Thrust Reverser Position	Discrete
Autopilot Status (on or off)	Discrete
Squat Switch (main gear)	Discrete
Gear Position	Discrete
Calibrated Airspeed	1 per second
Ground Speed	1 per second
Mach Number	1 per 4 seconds
Pressure Altitude	1 per second
Gross Weight	1 per 64 seconds
Bank Angle	2 per second
Pitch Angle	4 per second
Magnetic Heading	1 per second
Total Air Temperature	1 per second
Radio Altitude	1 per second

4.1 DATA REDUCTION.

Each file provided by the airline contains multiple flights for each airplane. These files are first separated into individual flight files and subsequently into individual time history files for each flight. The time history files are compressed and stored on the same 230 MB magneto-optical disks for later recall by the flight loads processing software.

Data editing and verification are performed on the data as the time histories are being prepared. Messages alert the user that obviously erroneous data have been removed and that questionable data have been retained but need to be manually reviewed prior to their acceptance. Table 3 lists the limits against which the data are compared.

TABLE 3. PARAMETER EDITING VALUES

Item		Condition	Min	Max
1.	Gross Weight	at start up	75,000 lbs	150,500 lbs
2.	Pressure Altitude (Hp)	at all times	-2,000 ft	45,000 ft
3.	Calibrated Airspeed	at all times during flight operations	45 kts	420 kts
4.	Normal Acceleration	at start up and shut down in flight	0 g	+4 g
5.	Lateral Acceleration	at all times	±0.5 g	±0.5 g
6.	Longitudinal Acceleration	at all times	±1.0 g	±1.0 g
7.	Flap Handle Position	at all times	0°	45°
8.	Elevator Position	at all times	±25°	±25°
9.	Aileron Position	at all times	±25°	±25°
10.	Rudder Position	at all times	±50°	±50°
11.	Trim Position	at all times	0°	20°
12.	Speed Brake Handle Position	at all times	0°	60°
13.	Throttles 1 and 2	at all times	-5°	75°
14.	Thrust Reverser Position	stowed at start up and shutdown	0	1
15.	Autopilot Status	off or on	0	1
16.	Squat Switch (main gear)	closed at start up and shutdown	0	1
17.	Landing Gear Position	down at start up and shutdown up within 10 seconds after takeoff down within 10 minutes before landing	0	1
18.	Pitch Attitude	at all times	-20°	+30°
19.	Bank Attitude	at all times	±60°	±60°
20.	Mach Number	at all times	0	1
21.	Ground Speed	at all times	0 kts	800 kts

Important characteristics about each set of flights received from the airline are recorded in a relational database. Airline identifier, aircraft tail number, and disk identifier of the disk received from the airline are in the data. Each flight is assigned a unique flight sequence number. The flight sequence number assigned to the first flight of the set and the number of flights in the set are also entered. Also recorded is the disk identifier of the MO disk, which contains the compressed time history files of all flights in the set.

4.2 RECORDED PARAMETERS.

Not all parameters listed in table 2 are used for statistical analysis and data presentation. Table 4 lists the parameters used in the data reduction and for which time history files are created and compressed on the magneto-optical disk. These parameters are used by the summarization software for statistical analysis and data presentation.

TABLE 4. RECORDED PARAMETERS USED IN DATA REDUCTION

Flight Parameter	Sample Rate
Gross Weight	1 per 64 seconds
Pressure Altitude	1 per second
Calibrated Airspeed	1 per second
Normal Acceleration (n_z)	8 per second
Lateral Acceleration (n_y)	4 per second
Longitudinal Acceleration (n_x)	4 per second
Flap Handle Position	1 per second
Speed Brake Handle Position	1 per second
Thrust Reverser Position	Discrete
Autopilot Status (on or off)	Discrete
Squat Switch (main gear)	Discrete
Landing Gear Position	Discrete
Pitch Angle	4 per second
Bank Angle	2 per second
Mach Number	1 per 4 seconds
Ground Speed	1 per second
Magnetic Heading	1 per second
N_1 Engine - Left	1 per second

4.3 COMPUTED PARAMETERS.

Derived gust velocity U_{de} and continuous gust intensity U_σ are important statistical load parameters which are derived from measured normal accelerations. This derivation of gust velocity U_{de} and continuous gust intensity U_σ from measured normal accelerations requires knowledge of atmospheric density, equivalent airspeed, and dynamic pressure. These values are calculated using equations that express the rate of change of density as a function of altitude based on the International Standard Atmosphere.

4.3.1 Atmospheric Density.

For altitudes below 36,089 feet, the density ρ is expressed as a function of altitude by

$$\rho = \rho_o (1 - 6.876 \times 10^{-6} \times H_p)^{4.256} \quad (1)$$

where ρ_0 is air density at sea level (0.0023769 slugs/ft^3) and H_p is pressure altitude (ft). Pressure altitude is a recorded parameter.

4.3.2 Equivalent Airspeed.

Equivalent air speed (V_e) is a function of true air speed (V_T) and the square root of the ratio of air density at altitude (ρ) to air density at sea level (ρ_0)

$$V_e = V_T \sqrt{\frac{\rho}{\rho_0}} \tag{2}$$

True airspeed is derived from Mach number (M) and speed of sound (a):

$$V_T = Ma\,. \tag{3}$$

Mach number is a dimensionless, recorded parameter. The speed of sound (a) is a function of pressure altitude (H_p) and the speed of sound at sea level and is

$$a = a_0 \sqrt{(1 - 6.876 \times 10^{-6} \times H_p)} \tag{4}$$

Substituting equations 1 and 4 into equation 2 gives

$$V_e = M \times a_0 \times (1 - 6.876 \times 10^{-6} \times H_p)^{0.5} \times (1 - 6.876 \times 10^{-6} \times H_p)^{2.128} \tag{5}$$

and

$$V_e = M \times a_0 \times (1 - 6.876 \times 10^{-6} \times H_p)^{2.626} \tag{6}$$

where the speed of sound at sea level a_0 is 1116.4 fps or 661.5 knots.

4.3.3 Dynamic Pressure (q).

The dynamic pressure (q) is calculated from the air density and velocity

$$q = \frac{1}{2} \rho V^2 \tag{7}$$

where

ρ = air density at altitude (slugs/ft^3)
V = true air speed (ft/sec)

4.3.4 Derived Gust Velocity (U_{de}).

The derived gust velocity, U_{de}, is computed from the peak values of gust incremental normal acceleration as

$$U_{de} = \frac{\Delta n_z}{\overline{C}} \tag{8}$$

where Δn_z is gust peak incremental normal acceleration and $\overline{C}$ is the aircraft response factor considering the plunge-only degree of freedom and is calculated from

$$\overline{C} = \frac{\rho_0 V_e C_{L_\alpha} S}{2W} K_g \tag{9}$$

where

ρ_0 = 0.002377 slugs/ft^3, standard sea level air density
V_e = equivalent airspeed (ft/sec)
C_{L_α} = aircraft lift-curve slope per radian
S = wing reference area (ft^2)
W = gross weight (lbs)
K_g = $\frac{0.88\mu}{5.3+\mu}$ = gust alleviation factor

μ = $\frac{2W}{\rho g \bar{c} C_{L_\alpha} S}$

ρ = air density, slug/ft^3, at pressure altitude (*Hp*), from equation 1

g = 32.17 ft/sec^2
$\bar{c}$ = wing mean geometric chord (ft)

In this program, the lift-curve slope, C_{L_α}, is the untrimmed flexible lift-curve slope for the entire airplane. For the flaps retracted conditions, the lift-curve slope is given as a function of Mach number and altitude; for flaps extended, the lift-curve slope is a function of flap deflection and calibrated airspeed (CAS).

4.3.5 Continuous Gust Intensity (U_σ).

Power Spectral Density (PSD) functions provide a turbulence description in terms of the probability distribution of the root-mean-square (rms) gust velocities. The root-mean-square gust velocities, U_σ, are computed from the peak gust value of normal acceleration using the power spectral density technique as described in reference 2. The procedure is

$$U_\sigma = \frac{\Delta n_z}{\overline{A}} \tag{10}$$

where Δn_z = gust peak incremental normal acceleration

$$\overline{A} = \text{aircraft PSD gust response factor} = \frac{\rho_0 V_e C_{L\alpha} S}{2W} \text{F(PSD) in } \frac{1}{ft/sec} \tag{11}$$

ρ_0 = 0.002377 slugs/ft^3, standard sea level air density
V_e = equivalent airspeed (ft/sec)
C_{L_α} = aircraft lift-curve slope per radian
S = wing reference area (ft^2)
W = gross weight (lbs)

$$F(PSD) = \frac{11.8}{\sqrt{\pi}}\left[\frac{\bar{c}}{2L}\right]^{\frac{1}{3}}\sqrt{\frac{\mu}{110+\mu}},\ \textit{dimensionless} \tag{12}$$

$\bar{c}$ = wing mean geometric chord (ft)
L = turbulence scale length, 2500 ft

$$\mu = \frac{2W}{\rho g \bar{c} C_{L_\alpha} S},\ \text{dimensionless} \tag{13}$$

ρ = air density (slugs/ft^3)
g = 32.17 ft/sec^2

To determine the number of occurrences (N) for U_σ, calculate

$$N = \frac{N_0(o)_{ref}}{N_0(o)} = \frac{\pi \bar{c}}{203}\left[\frac{\rho}{\rho_0}\mu\right]^{0.46},\ \text{dimensionless} \tag{14}$$

where $\bar{c}$, ρ, ρ_0, and μ are defined above. Then each U_σ peak is counted as N counts at that U_σ value. This number of counts is used to determine the number of counts per nautical mile (*nm*)

or
$$\frac{\text{counts}}{nm} = \left(\frac{N}{\text{distance flown in counting interval}}\right) \tag{15}$$

Finally, the number of such counts is summed from the largest plus or minus value toward the smallest to produce the cumulative counts per nautical mile.

4.4 DATA REDUCTION CRITERIA.

To process the measured data into statistical flight loads format, specific data reduction criteria were established for each parameter. These criteria are discussed in this section.

4.4.1 Phases of Flight.

Each flight was divided into nine phases—four ground phases (taxi out, takeoff roll, landing roll with and without thrust reverser, and taxi in), and five airborne phases (departure, climb, cruise, descent, and approach). Figure 3 shows these nine phases of a typical flight. The phases of flight were not defined by the airline but had to be determined from the data. Table 5 lists the conditions for determining the starting times for each phase. It should be noted that an airborne phase can occur several times per flight because it is determined by the rate of climb and the position of the flaps. When this occurs the flight loads data are combined and presented in a single flight phase. The UDRI software creates a file which chronologically lists the phases of flight and their corresponding starting times.

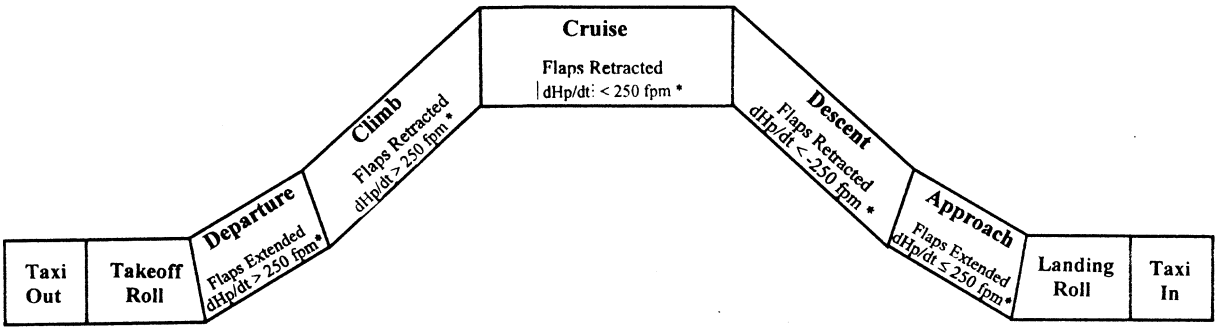

*Climb rate must be maintained for at least one minute before transition into another phase of flight takes place

FIGURE 3. DESCRIPTION OF PHASES OF FLIGHT

TABLE 5. PHASE OF FLIGHT STARTING CRITERIA

Phase of Flight	Conditions at Start of Phase
Taxi Out	Initial condition
Takeoff Roll	Acceleration > 4 kts/sec for a minimum of 12 seconds
Departure	Time at liftoff; flaps extended (squat switch off)
Climb	Flaps retracted; rate of climb ≥ 250 ft/min. for at least 1 minute
Cruise	Flaps retracted; rate of climb ≤ 250 ft/min. for at least 1 minute
Descent	Flaps retracted; rate of descent ≤ -250 ft/min. for at least 1minute
Approach	Flaps extended; rate of descent < 250 ft/min. for at least 1 minute
Landing Roll	Touchdown; (squat switch on)
Taxi In	Magnetic heading change greater than 13.5 degrees after touchdown or deviation from runway centerline greater than 100 feet

The criteria for the start of the takeoff roll have been redefined from those used in reference 3. In reference 3, the start of takeoff roll was defined as the time when the calibrated airspeed exceeded 50 knots and the longitudinal acceleration exceeded 0.15 g. It was found that in most cases when these criteria were met, the airplane had already been accelerating for 6 to 8 seconds and the initial portion of the takeoff roll was lost. The present criteria better defines the initial start of takeoff roll. When the acceleration remains above 4 knots per second for a minimum of 12 seconds, the takeoff roll phase begins.

The criteria for the start of taxi in has also been redefined from the criteria used in reference 3. In reference 3 the start of taxi in was defined as the time when thrust reversers were stowed after initial deployment on landing. This definition did not account for cases when the thrust reversers are not deployed during the landing roll or the thrust reversers are stowed before or after the airplane turns off the active runway. In the new criteria, the start of taxi in has been redefined as the time when the aircraft turns off the active runway. The primary method for detecting turnoff is to monitor magnetic heading change for a change greater than 13.5 degrees from the landing

magnetic heading. The time when the heading starts to change in the turnoff direction is then identified as the start of the turn or the beginning of the taxi in phase. This method can fail to detect a shallow turnoff onto a parallel taxiway. In such cases a substitute criteria that identifies a lateral deviation greater than 100 feet from the landing centerline is used to detect the turnoff point.

The criteria for determining the pitch angle at takeoff has been changed from that used in reference 3. In reference 3 the pitch angle at takeoff was defined as the maximum pitch angle occurring between 5 seconds before and 10 seconds after the squat switch moved from the closed to the open position. Using this time increment for selection of the pitch angle at takeoff results in pitch angles at the instant of takeoff that would cause the aircraft aft fuselage to strike the ground. For this report the pitch angle is defined as the angle occurring just prior to the squat switch change.

4.4.2 Flight Distance.

The flight distance can be obtained either by determining the stage length of the flight or by integrating the range with respect to changes in aircraft velocity as a function of time.

The stage length is defined as the distance from departure airport to destination airport and is determined as the great circle distance in nautical miles between the point of liftoff (departure) and the point of touchdown (destination). Appendix B describes the calculation of great circle distance. The time histories of longitude and latitude are matched against the UDRI generated phase of flight file to determine the geographical location of the aircraft at the point of liftoff and the point of touchdown.

The integrated flight distance D is obtained by the numerical integration from the time at liftoff (t_0) to the time of touchdown (t_n), and V is the average velocity during Δt.

$$D = \sum_{t_0}^{t_n} \Delta t \cdot V \tag{16}$$

4.4.3 Sign Convention.

Acceleration data are recorded in three directions: normal (*z*), lateral (*y*), and longitudinal (x*)*. As shown in figure 4, the positive *z* direction is up; the positive *y* direction is airplane starboard; and the positive *x* direction is forward.

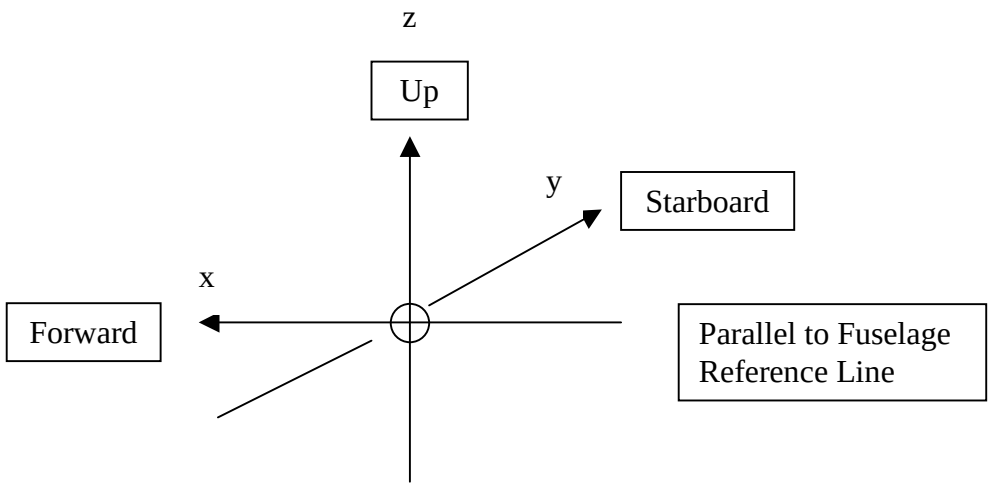

FIGURE 4. SIGN CONVENTION FOR AIRPLANE ACCELERATIONS

4.4.4 Peak-Valley Selection.

The peak-between-means method presented in reference 2 was used to select the peaks and valleys in the acceleration data. This method is consistent with past practices and pertains to all accelerations (n_x, n_y, Δn_z, $\Delta n_{z_{man}}$, $\Delta n_{z_{gust}}$). Figure 5 depicts an example of the peak-between-mean criteria. This method counts upward events as positive and downward events as negative. Only one peak or one valley is counted between two successive crossings of the mean. A threshold zone is used in the data reduction to ignore irrelevant loads variations around the mean. For the normal accelerations Δn_z, $\Delta n_{z_{gust}}$, and $\Delta n_{z_{man}}$, the threshold zone is ±0.05 g; for lateral acceleration n_y, the threshold zone is ±0.005 g; and for longitudinal accelerations n_x, the threshold zone is ±0.0025 g.

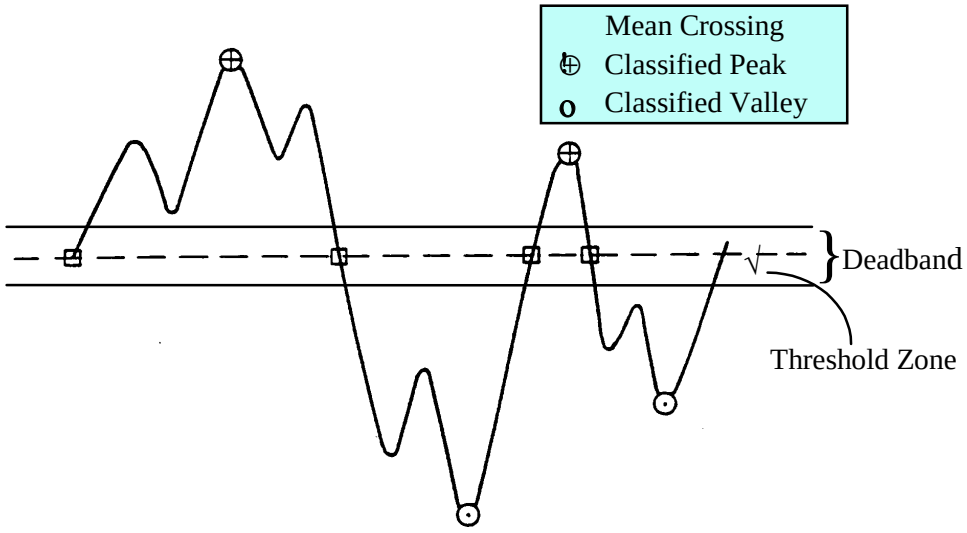

FIGURE 5. THE PEAK-BETWEEN-MEANS CLASSIFICATION CRITERIA

A peak is generated only when the acceleration data cross into or through the deadband. Two situations must be considered: the position of the current acceleration value relative to the deadband and the position of the previous acceleration value relative to the deadband. In the peak-between-means counting algorithm, the previous acceleration value is that value in a consecutive set of values all of which lie either above the deadband or below the deadband. The previous value is established as a peak when the current value has crossed into or through the deadband. Figures 6a and 6b demonstrate the concept of current and previous acceleration values. In figure 6a the current acceleration value passes into the deadband, whereas in figure 6b the current value passes through the deadband.

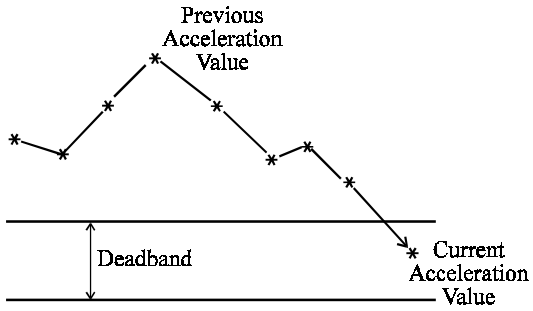

FIGURE 6a. CURRENT ACCELERATION VALUE PASSES INTO DEADBAND

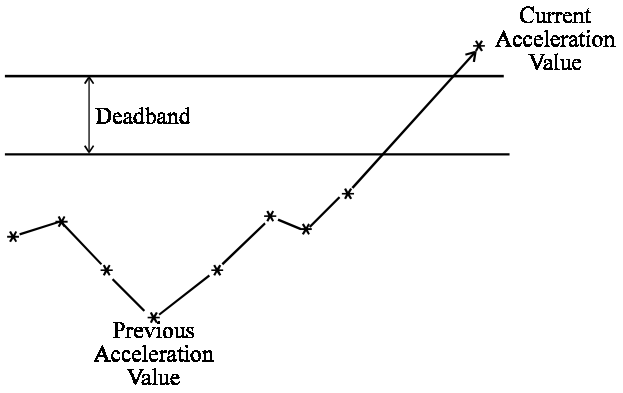

FIGURE 6b. CURRENT ACCELERATION VALUE PASSES THROUGH DEADBAND

Italicized text in table 6 summarizes the action(s) taken when the various possibilities occur. Note that when a previous acceleration value is retained as a potential peak, its coincident time is also retained.

4.4.5 Separation of Maneuver and Gust Load Factors.

The recorded normal acceleration (n_z) values included the 1 g flight condition. The 1 g condition was removed from each n_z reading which was then recorded as Δn_z. In order to avoid the inclusion of peaks and valleys associated with nonsignificant small load variations, a threshold zone of $\Delta n_z = \pm 0.05$ g was established. An algorithm was then developed to extract the acceleration peaks and valleys.

For each flight, the maximum and minimum total accelerations were determined from just after liftoff to just before touchdown. For the five in-flight phases, the Δn_z cumulative occurrences were determined as cumulative counts per nautical mile and cumulative counts per 1000 hours using the peak-between-means counting method of reference 2 explained in section 4.4.4.

The incremental acceleration measured at the center of gravity (c.g.) of the aircraft may be the result of either maneuvers or gusts or a combination of both. In order to derive gust statistics, the maneuver induced acceleration is separated from the total acceleration history. Most maneuver induced loads are associated with turning maneuvers.

TABLE 6. PEAK CLASSIFICATION CRITERIA

Previous Acceleration Value Relative to Deadband	Current Acceleration Value Relative to Deadband		
	Below	Within	Above
Above Previous value is potential positive peak	Current acceleration passes through deadband. *Previous value classified as a positive peak.* *Current value retained as a potential negative peak.*	Current acceleration passes into deadband. *Previous value classified as a positive peak.* *Acceleration value flagged as being in deadband.*	Current acceleration is on same side of deadband as previous. *If current > previous value, retain current value as potential positive peak and release previous.*
Within At start of processing, or a peak was established but current acceleration value has not since gone outside of deadband	Current acceleration passes downward out of deadband. *Current value is retained as a potential negative peak.*	*No Action Required*	Current acceleration passes upward out of deadband. *Current value retained as potential positive peak.*
Below Previous value is potential negative peak	Current acceleration is on same side of deadband as previous. *If current value < previous value, retain current value as potential negative peak and release previous value.*	Current acceleration passes into deadband. *Previous value is established as a negative peak.* *Acceleration value flagged as being in deadband.*	Current acceleration passes through deadband. *Previous value is classified as a negative peak.* *Current value retained as potential positive peak.*

The increment due to a turning maneuver (Δm) is determined using the bank angle method discussed in reference 2 to calculate the maneuver acceleration $\Delta n_{z_{man}}$ as

$$\Delta n_{z_{man}} = (\sec \varphi - 1) \tag{17}$$

where φ is the bank angle. The remaining peaks and valleys are assumed to be gust induced, where gust normal acceleration ($\Delta n_{z_{gust}}$) is calculated as

$$\Delta n_{z_{gust}} = \Delta n_z - \Delta n_{z_{man}} \tag{18}$$

This approach does not separate the pitching maneuvers induced by pilot control inputs. In reference 2, J.B. de Jonge suggests that accelerations resulting from pitch maneuvers induced by pilot input to counteract turbulence can be considered as part of the aircraft system response to the turbulence. Accelerations that are induced by the pitch maneuver at the specific points of rotation and flare during takeoff and climb and approach and touchdown have not been removed during this initial data reduction effort. Since turbulence is a more dominant loading input on commercial aircraft than maneuvers, correcting for pitch maneuvers at a later time will not substantially alter the statistics presented herein.

Once calculated, the measurements of Δn_z, $\Delta n_{z_{gust}}$, and $\Delta n_{z_{man}}$ are maintained as three unique data streams. The $\Delta n_{z_{gust}}$ and $\Delta n_{z_{man}}$ data are plotted as cumulative occurrences of a given acceleration fraction per nautical mile and per 1000 flight hours. Separate plots are provided for each phase of flight and all phases combined. The Δn_z fraction is the recorded incremental

normal load factor (airplane limit load factor minus 1.0 g). As a result of the threshold zone, only accelerations greater than ±0.05 g (measured from a 1.0 g base) are counted for data presentation.

4.4.6 Flap Detents.

When flaps are extended, the effective deflection is considered to be that of the applicable detent, as indicated in table 7. The flap deflection ranges and placard speeds reflect the flap design and cockpit placards.

TABLE 7. FLAP DETENTS (B-737-400)

Flap Detent	Minimum Flap Setting	Maximum Flap Setting	Design Placard Speed (KIAS)	Cockpit Placard Speed (KIAS)
1	> 0	≤ 0.5	250	250
5	> 0.5	≤ 5	250	250
10	> 5	≤ 10	218	215
15	> 10	≤ 15	213	205
25	> 15	≤ 25	206	190
30	> 25	≤ 30	199	185
40	> 30	≤ 40	162	162
45	>40		162	162

5. DATA PRESENTATION.

Table 8 lists the statistical data presentation formats for which data was processed and included in appendix A of this report. Similar statistical loads data, but of a reduced scope and based on fewer flights for a single aircraft, were previously presented in reference 3. To facilitate comparisons of the present data formats with this earlier data, the data formats available in reference 3 are identified by an asterisk in the listings of table 8.

Figures A-1 through A-83 present the processed data. It will be noted that the data presented in these figures are not always based on an identical number of flights. During data reduction it was found that the acceleration measurements in certain flights exhibited random errors and were unreliable. When this occurred, those flights were eliminated from the statistical data for any parameters associated, directly or indirectly, with the unreliable acceleration measurements. As a result, not all figures are based on data from identical numbers of flights, hours, or nautical miles.

5.1 AIRCRAFT OPERATIONAL USAGE DATA.

The aircraft usage data include flight profile statistics such as weights, altitudes, speeds, and flight distance information. This information is useful in the derivation of typical flight profiles and in defining ground-air-ground cycles for structural durability, damage tolerance analyses, future design criteria, and for use in the analysis of airline operating economics. Aircraft usage data are presented in figures A-1 through A-12.

TABLE 8. STATISTICAL DATA FORMATS

Data Description	Figure
AIRCRAFT USAGE DATA	
WEIGHT DATA	
Cumulative Probability of Takeoff Gross Weight	A-1
Cumulative Probability of Takeoff Fuel Weight	A-2
Cumulative Probability of Landing Gross Weight	A-3
Correlation of Takeoff Fuel Weight and Flight Distance, Percent of Flights	A-4
Correlation of Takeoff Gross Weight and Flight Distance, Percent of Flights	A-5
Correlation of Gross Weight at Liftoff and Touchdown, Percent of Flights *	A-6
ALTITUDE DATA	
Correlation of Maximum Altitude and Flight Distance, Percent of Flights	A-7
Percent of Total Distance in Altitude Bands	A-8
Coincident Altitude at Maximum Mach Number, Cruise Phase	A-9a
Coincident Altitude at Maximum Equivalent Airspeed, Cruise Phase	A-9b
Coincident Altitude at Maximum Mach Number, All Flight Phases	A-10a
Coincident Altitude at Maximum Equivalent Airspeed, All Flight Phases	A-10b
FLIGHT DISTANCES	
Cumulative Probability of Flight Distances	A-11
AUTOPILOT OPERATION *	
Cumulative Probability of Percent of Flight Time on Autopilot	A-12
GROUND LOADS DATA	
LATERAL LOAD FACTOR, n_y	
Cumulative Frequency of Maximum Side Load Factor During Ground Turns	A-13
LONGITUDINAL LOAD FACTOR, n_x	
Cumulative Frequency of Longitudinal Load Factor During Ground Taxi	A-14
Cumulative Frequency of Longitudinal Load Factor During Landing Roll	A-15
Cumulative Probability of Maximum Longitudinal Load Factor During Takeoff	A-16
Cumulative Probability of Minimum Longitudinal Load Factor During Landing	A-17
VERTICAL LOAD FACTOR, n_z	
Cumulative Frequency of Incremental Vertical Load Factor During Taxi Operations	A-18
Cumulative Frequency of Incremental Vertical Load Factor During Takeoff Roll	A-19
Cumulative Frequency of Incremental Vertical Load Factor During Landing Roll	A-20
Cumulative Probability of Minimum and Maximum Incremental Vertical Load Factor at Touchdown and Spoiler Deployment *	A-21
Coincident Incremental Vertical Load Factor and Touchdown Gross Weight	A-22
GROUND SPEED DATA	
Cumulative Probability of Ground Speed During Taxi	A-23
Cumulative Probability of Airspeed at Liftoff and Touchdown *	A-24
FLARE DATA	
Cumulative Probability of Airspeed at Flare	A-25
PITCH/ROTATION DATA	
Cumulative Probability of Pitch Angle at Liftoff and Touchdown *	A-26
Cumulative Probability of Maximum Pitch Rate at Takeoff Rotation *	A-27
Cumulative Probability of Pitch Angle at Touchdown Peak Vertical Load Factor *	A-28

*Denotes data formats from reference 3.

TABLE 8. STATISTICAL DATA FORMATS (Continued)

Data Description	Figure
FLIGHT LOADS DATA	
GUST LOADS DATA	
Cumulative Occurrences of Vertical Gust Load Factor per 1000 Hours by Flight Phase	A-29
Cumulative Occurrences of Incremental Vertical Gust Load Factor per 1000 Hours, Combined Flight Phases	A-30
Cumulative Occurrences of Vertical Gust Load Factor per Nautical Mile by Flight Phase	A-31
Cumulative Occurrences of Incremental Vertical Gust Load Factor per Nautical Mile, Combined Flight Phases	A-32
Cumulative Occurrences of Derived Gust Velocity per Nautical Mile, < 500 Feet	A-33
Cumulative Occurrences of Derived Gust Velocity per Nautical Mile, 500-1,500 Feet	A-34
Cumulative Occurrences of Derived Gust Velocity per Nautical Mile, 1,500-4,500 Feet	A-35
Cumulative Occurrences of Derived Gust Velocity per Nautical Mile, 4,500-9,500 Feet	A-36
Cumulative Occurrences of Derived Gust Velocity per Nautical Mile, 9,500-19,500 Feet	A-37
Cumulative Occurrences of Derived Gust Velocity per Nautical Mile, 19,500-29,500 Feet	A-38
Cumulative Occurrences of Derived Gust Velocity per Nautical Mile, 29,500-39,500 Feet	A-39
Cumulative Occurrences of Derived Gust Velocity per Nautical Mile, Flaps Extended	A-40
Cumulative Occurrences of Derived Gust Velocity per Nautical Mile, Flaps Retracted	A-41
Cumulative Occurrences of Continuous Gust Intensity per Nautical Mile, Flaps Extended	A-42
Cumulative Occurrences of Continuous Gust Intensity per Nautical Mile, Flaps Retracted	A-43
MANEUVER LOADS DATA	
Cumulative Occurrences of Incremental Maneuver Load Factor per 1000 Hours During Departure by Altitude	A-44
Cumulative Occurrences of Incremental Maneuver Load Factor per 1000 Hours During Climb by Altitude	A-45
Cumulative Occurrences of Incremental Maneuver Load Factor per 1000 Hours During Cruise by Altitude	A-46
Cumulative Occurrences of Maneuver Load Factor per 1000 Hours During Descent by Altitude	A-47
Cumulative Occurrences of Maneuver Load Factor per 1000 Hours During Approach by Altitude	A-48
Cumulative Occurrences of Maneuver Load Factor per Nautical Mile During Departure by Altitude	A-49
Cumulative Occurrences of Maneuver Load Factor per Nautical Mile During Climb by Altitude	A-50
Cumulative Occurrences of Maneuver Load Factor per Nautical Mile During Cruise by Altitude	A-51
Cumulative Occurrences of Maneuver Load Factor per Nautical Mile During Descent by Altitude	A-52
Cumulative Occurrences of Maneuver Load Factor per Nautical Mile During Approach by Altitude	A-53
Cumulative Occurrences of Maneuver Load Factor per 1000 Hours by Flight Phase	A-54
Cumulative Occurrences of Maneuver Load Factor per 1000 Hours, Combined Flight Phases	A-55
Cumulative Occurrences of Maneuver Load Factor per Nautical Mile by Flight Phase	A-56
Cumulative Occurrences of Maneuver Load Factor per Nautical Mile, Combined Flight Phases	A-57
COMBINED MANEUVER AND GUST LOADS DATA *	
Cumulative Occurrences of Combined Maneuver and Gust Vertical Load Factor per 1000 Hours by Flight Phase	A-58
Cumulative Occurrences of Vertical Load Factor per 1000 Hours, Combined Flight Phases	A-59
Cumulative Occurrences of Vertical Load Factor per Nautical Mile by Flight Phase	A-60
Cumulative Occurrences of Vertical Load Factor per Nautical Mile, Combined Flight Phases	A-61
Cumulative Occurrences of Lateral Load Factor per 1000 Hours, Combined Flight Phases	A-62
Coincident Maneuvers Load Factor and Speed Versus V-n Diagram for Flaps Retracted	A-63
Coincident Maneuvers Load Factor and Speed Versus V-n Diagram for Flaps Extended	A-64
Coincident Gust Load Factor and Speed Versus V-n Diagram for Flaps Retracted	A-65
Coincident Gust Load Factor and Speed Versus V-n Diagram for Flaps Extended	A-66

*Denotes data formats from reference 3.

TABLE 8. STATISTICAL DATA FORMATS (Continued)

Data Description	Figure
MISCELLANEOUS OPERATIONAL DATA	
FLAP USAGE DATA	
Cumulative Probability of Maximum Airspeed in Flap Detent During Departure	A-67
Cumulative Probability of Maximum Airspeed in Flap Detent During Approach	A-68
Percent of Time in Flap Detent During Departure	A-69
Percent of Time in Flap Detent During Approach	A-70
Cumulative Probability of Maximum Dynamic Pressure in Flap Detent During Departure	A-71
Cumulative Probability of Maximum Dynamic Pressure in Flap Detent During Approach	A-72
SPEED BRAKE/FLIGHT SPOILER DATA	
Cumulative Probability of Maximum Speed During Speed Brake Deployment	A-73
Cumulative Frequency of Speed at Speed Brake Deployment	A-74
Cumulative Frequency of Altitude at Speed Brake Deployment	A-75
Cumulative Probability of Maximum Deployment Angle During Speed Brake Deployment, Flaps Retracted	A-76
THRUST REVERSER DATA	
Cumulative Probability of Time With Thrust Reversers Deployed	A-77
Cumulative Probability of Speed at Thrust Reverser Deployment and Stowage	A-78
LANDING GEAR EXTENSION/RETRACTION DATA	
Cumulative Probability of Time With Landing Gear Extended After Liftoff	A-79
Cumulative Probability of Time With Landing Gear Extended Prior to Touchdown	A-80
Cumulative Probability of Maximum Airspeed With Gear Extended	A-81
PROPULSION SYSTEM DATA	
Cumulative Probability of Percent of N_1 at Takeoff	A-82
Cumulative Probability of Percent of N_1	A-83

*Denotes data formats from reference 3.

5.1.1 Weight Data.

Statistical data on operational takeoff gross weights, landing gross weights, and fuel weights are presented in this section. These weights are also correlated to flight distance. The cumulative probabilities of takeoff gross weight, takeoff fuel weight, and landing weight are presented in figures A-1 through A-3 respectively. The correlation between fuel weight at takeoff and the flight distance is presented in figure A-4. A similar correlation for takeoff gross weight and flight distance is shown in figure A-5. The flight distances in figures A-4 and A-5 are based on the great circle distance between departure and arrival points. It is interesting to note that the small difference in the number of flights between figures A-4 and A-5 has an insignificant impact on the flight distance distribution as indicated by a comparison of the numbers in the right end columns of these figures. Figure A-6 provides the correlation between the takeoff gross weight and the landing gross weight. The correlation shows that for most flights with light takeoff weights (less than 100,000 pounds) the landing weight is within 10,000 pounds of the takeoff weight. For the medium takeoff weights from 100,000-130,000 pounds the landing weights are from 10,000-20,000 pounds below takeoff weight. For the heavy weight takeoffs from 130,000-150,000 pounds the landing weights are from 20,000-30,000 pounds below the takeoff weight.

5.1.2 Altitude Data.

Measured operational altitudes and their correlation to flight distance and maximum speed are presented. Figure A-7 shows the correlation between the maximum altitude attained in flight and the flight distance flown in percent of flights. The data show that for short flights of less than 250 nautical miles, the maximum altitude is generally below 30,000 feet with the most flights occurring from 20,000-25,000 feet. For flights from 250-500 nautical miles the altitude may range from 25,000 to 40,000 feet, while for flights above 500 nautical miles the maximum altitude can be considered above 30,000 feet. Figure A-8 presents the percent of total flight distance spent in various altitude bands as a function of flight distance. The flight distances in figure A-7 reflect the stage lengths, whereas the flight distances in figure A-8 are based on the numerical integration approach mentioned in paragraph 4.4.2. The combined information in figures A-7 and A-8 provide a comprehensive picture of the flight profile distribution. Figures A-9a and A-9b show the coincident altitude at the maximum Mach number and the maximum equivalent airspeed attained in the cruise phase of the flights respectively. Figures A-10a and A-10b show the maximum Mach number or the maximum equivalent airspeed with respect to the design cruise limit regardless of flight phase. In other words, the speed that most closely approached the speed limit in a flight was identified as the maximum speed. As an example, in one flight the maximum speed with respect to the limit might have been attained in the climb phase, while in another flight the maximum speed with respect to the limit speed might have occurred in the cruise phase. The data in figures A-10a and A-10b are fairly evenly distributed between the climb, cruise, and descent phases with only a single occurrence in the departure and approach phases. The design speed limits are also shown in the figures. It should be noted that maximum Mach number and maximum equivalent airspeed do not necessarily occur simultaneously.

5.1.3 Flight Distance Data.

Flight distance statistics useful in the generation of flight profiles were derived and are presented here. The cumulative probability of flight distances flown is presented in figure A-11. The great circle distance reflects the ground distance between two points as obtained from the great circle distance calculation, but does not necessarily reflect the actual distance flown. Deviation from direct flight between departure and arrival points resulting from traffic control requirements will increase the actual distance flown by some unknown amount. To a much lesser extent, the climb and descent distances are slightly larger than the level flight distance. Head or tail winds also are unknown contributors. The integrated distance accounts for such variables. The figure provides a graphical presentation of the differences in flight distance obtained by the two approaches.

5.1.4 Autopilot Usage.

Autopilot usage is determined by the operational procedures employed. Figure A-12 shows the cumulative probability of percent flight time flown on autopilot. Comparison with the autopilot data presented in reference 3 shows that autopilot usage has increased significantly.

5.2 GROUND LOADS DATA.

The ground loads data include frequency and probability information on vertical, lateral, and longitudinal accelerations, speeds, and pitch rotation associated with takeoff, landing, and ground operations. These data are of primary importance to landing gear and landing gear backup structure and to a lesser extent to the wing, fuselage, and empennage.

5.2.1 Lateral Load Factor Data.

Lateral load factor statistics resulting from ground turning during taxi were derived and are presented. Figure A-13 shows the cumulative frequency of maximum side load factor during ground turns. The information is presented for preflight and postflight taxi, as well as, left and right turns. The turning load factors during taxi in are shown to be more severe than those experienced during turning while taxiing out. This is likely the result of higher taxi in speed as shown in figure A-23. There is no significant difference between the number of left and right turns.

5.2.2 Longitudinal Load Factor Data.

Longitudinal load factor statistics were derived for all phases of ground operation, including preflight and postflight taxi, and takeoff and landing roll. Figures A-14 and A-15 present the cumulative frequency of longitudinal load factor during ground operations. Figure A-14 shows the data for pre- and postflight taxi. The higher number of occurrences of negative longitudinal load factor less than –0.15 g during the taxi in phase are possibly due to braking action occurring at the higher taxi in speeds. Figure A-15 shows the landing rollout with and without thrust reverser deployment. Figures A-16 and A-17 present the cumulative probability of the maximum longitudinal load factor measured during the takeoff and landing rolls respectively.

5.2.3 Vertical Load Factor Data.

Vertical load factor statistics during all phases of ground operation with and without thrust reverser were derived and are presented. Figure A-18 presents the cumulative frequency of incremental vertical load factor during preflight and postflight taxi. Figure A-19 presents the cumulative frequency of incremental vertical load factor during the takeoff roll, while Figure A-20 presents the cumulative frequency of incremental vertical load factor during the landing roll for operation with and without thrust reverser. As can be seen there is little difference in the frequency of vertical load factor occurrences resulting from taxi, takeoff roll, and landing roll except for positive occurrences during landing without thrust reverser. It is noteworthy (see figure A-15) that there is also increased longitudinal load factor activity during landing without thrust reversers. Figure A-21 presents the cumulative probability of the minimum and maximum incremental vertical load factors associated with touchdown and ground spoiler deployment. As can be seen the minimum load factors measured at spoiler deployment remain positive. Figure A-22 shows the coincident incremental vertical load factor and gross weight at touchdown for all flights.

5.2.4 Ground Speed Data.

The cumulative probabilities of ground speed for taxi in and taxi out operations are presented in figure A-23. The taxi in speeds are seen to be considerably higher than the taxi out speeds. There can be several reasons for this difference. First, the airplane may still be moving at a fairly high speed shortly after turning off the active runway. Departure from the active runway has been used as the criterion for start of taxi in. Second, movement of inbound traffic to the terminal after landing is generally accomplished faster than similar movement from the terminal to the takeoff position. Figure A-24 shows the cumulative probabilities of airspeed at liftoff and touchdown rotation. The liftoff speeds are approximately 20 knots higher than the touchdown speeds. The figure indicates that a considerable number of touchdowns are performed at speeds well above published stall speeds.

5.2.5 Flare Data.

Figure A-25 presents the cumulative probability of airspeed at flare. Since the actual instant of flare is difficult to determine with any great accuracy, the start of flare was assumed to occur 3 seconds prior to main gear squat switch closure.

5.2.6 Pitch/Rotation Data.

The cumulative probability of maximum pitch angle at takeoff and landing is presented in figure A-26. The pitch angles for takeoff presented in this figure are considerably lower than those previously reported in reference 3. It has been determined that the time increment previously used for selecting the pitch angle at takeoff was too long, resulting in pitch angles at the instant of takeoff that would have resulted in the aircraft aft fuselage striking the ground. This increment was reduced for the present data reduction effort as discussed in section 4.4.1. Figure A-27 presents the cumulative probability of maximum takeoff pitch rate at takeoff rotation. Figure A-28 presents the cumulative probability of pitch angle that occurs at touchdown peak vertical load factor.

5.3 FLIGHT LOADS DATA.

The flight loads data include the statistical data that describe the gust and maneuver environment. The gust environment is presented in the form of cumulative occurrences of derived gust velocity, continuous gust intensity, and vertical load factor. The derived gust velocity and continuous gust intensity are computed values as described in section 4.3. Since the 1950's, it has been common practice to present flight loads data as cumulative occurrences. Data that were previously recorded on the B-737 are reported in references 4 and 5 as cumulative occurrences per 1000 hours. To compare to data from different references, the normal acceleration data are plotted two ways, as cumulative occurrences per 1000 hours and as cumulative occurrences per nautical mile.

5.3.1 Gust Loads Data.

The gust data are presented in the form of derived gust velocity U_{de} and continuous gust intensities U_{σ}. Figure A-29 presents the cumulative occurrences of incremental vertical gust

load factor per 1000 hours. The data are presented by phase of flight. Figure A-30 shows cumulative occurrences of incremental vertical gust load factor for the total combined airborne phases per 1000 hours. Figure A-31 presents the cumulative occurrences of incremental vertical gust load factor per nautical mile by phase of flight, and figure A-32 shows the cumulative occurrences of incremental vertical gust load factor for the total combined airborne phases per nautical mile. In figures A-33 through A-39 the derived gust velocity U_{de} is plotted as cumulative counts per nautical mile for altitudes from sea level to 39,500 feet. Figures A-40 and A-41 present the derived gust velocity U_{de} as cumulative counts per nautical mile with flaps extended and retracted respectively.

5.3.2 Maneuver Loads Data.

The technique used to identify maneuvers assumes that maneuvers are associated primarily with turning conditions and that the impact of pitch maneuvers is insignificant and can be ignored. As a result, maneuvers resulting from push down or pull up maneuvers are ignored and only positive maneuver load factors resulting from banked turns are identified.

Figures A-44 through A-48 present the cumulative occurrences of maneuver load factor per 1000 hours by altitude for each of the airborne flight phases, i.e., departure, climb, cruise, descent, and approach. Figures A-49 through A-53 present the cumulative occurrences of maneuver load factor by altitude per nautical mile in the airborne phases of flight. Figure A-54 presents the total cumulative occurrences of incremental maneuver load factor per 1000 hours for each phase of flight, regardless of altitude. Figure A-55 presents the total cumulative occurrences of incremental maneuver load factor per 1000 hours for all flight phases combined. Figure A-56 presents the total cumulative occurrences of incremental maneuver load factor per nautical mile for each phase of flight regardless of altitude. Figure A-57 presents the total cumulative occurrences of incremental maneuver load factor per nautical mile for all flight phases combined. The maneuver data presented in this report extend beyond load factor magnitudes available in reference 3. However, at identical load factor levels, the data trends between this report and reference 3 are quite similar.

5.3.3 Combined Maneuver and Gust Loads Data.

For the data presented in this section, the maneuver and gust load factors were not separated, but the total load factor occurrences regardless of the cause were used in the derivation of the figures. Figure A-58 shows the cumulative occurrences of total combined maneuver and gust normal load factor per 1000 hours by phases of flight, and figure A-59 shows the occurrences for all phases combined. Figures A-60 and A-61 show the data of figures A-58 and A-59 as occurrences per nautical mile.

Federal Aviation Regulation (FAR) 25.333 requires that airplane structural operating limitations be established at each combination of airspeed and load factor on and within the boundaries of maneuvering and gust load envelopes (V-n diagrams). For purposes of displaying the coincident maneuver or gust accelerations, four representative V-n diagrams were developed from the FAR requirements.

The required limit load factors for maneuvers are specified in FAR 25.337. The positive limit maneuvering load factor (n) may not be less than 2.5, and the negative limit maneuvering load factor may not be less than -1.0 at speeds up to V_C , varying linearly with speed to zero at V_D. FAR 25.345 specifies that the positive limit maneuver load factor is 2.0 g when the flaps are extended. The stall curve on the left side of the envelopes is determined by the maximum lift coefficient. The curve was estimated by using the 1 g stall speed to estimate $C_{L_{\max}}$.

The required limit load factors for gusts result from gust velocities as specified in FAR 25.341. The FAR specifies positive (up) and negative (down) air gust design requirements for three different aircraft design speeds: maximum gust intensity (V_B), cruising speed (V_C), and dive speed (V_D). Between sea level and 20,000 feet, the gust requirement is constant, varying linearly to the value given for 50,000 feet. FAR 25.345 sets a requirement of positive, negative, and head-on for 25 fps gusts when flaps are extended. These gust design requirements are shown in table 9.

TABLE 9. FAR REQUIREMENTS FOR DERIVED DISCRETE GUST VELOCITIES

Aircraft Design Speed	Gust Velocity	
	0-20,000 Feet Altitude	50,000 Feet Altitude
V_B	66 fps	38 fps
V_C	50 fps	25 fps
V_D	25 fps	12.5 fps
Flaps Extended	25 fps	—

Sufficient data to generate V-n diagrams for all weight and altitude conditions were not available. Therefore, sea level data were used to develop the representative diagrams, and all of the recorded maneuvers and gusts were plotted on these. A weight of 90,000 lbs., the lowest recorded weight, was used for the calculations required in developing these diagrams.

Figure A-63 through A-66 shows the V-n diagrams for maneuver and for gust with flaps retracted and extended. Coincident acceleration and speed measurements are also plotted on the V-n diagrams. As can be seen in figure A-66, a large number of gust accelerations occurred outside the gust V-n diagram for the flaps extended case.

5.4 MISCELLANEOUS OPERATIONAL DATA.

The miscellaneous operational data includes statistical usage information for flaps, speed brake/spoilers, thrust reversers, and landing gear operations. Although aileron and rudder deflection information was available it was not processed because it was deemed that the slow sampling rates prevented the reduction of reliable statistical usage information for these components.

5.4.1 Flap Usage Data.

Flap usage statistics of value in the design of flap structure, backup structure, and other flap components were reduced from the measured data. Figure A-67 presents the cumulative probability of maximum airspeed encountered in various flap detents during the departure phase of the flights. The flap detents are defined in table 7. The single points for detents 40 and 45 at 160 knots indicate a single occurrence of these settings during departure. Figure A-68 presents similar data for the approach phase of the flights. Figures A-69 and A-70 present the percent of time spent in various flap detents during the departure and approach phases of flight, respectively. As shown in figure A-69, flap detent 5 was the detent used in almost all cases during departure. Previous data presented in reference 6 showed that detent 1 was used approximately one-third of the total time. Discussion with the airline confirmed that a change in flap operating procedure for departure had occurred between the two reporting periods. Comparison of the data in figure A-70 with similar data in reference 5 shows that although changes in flap usage for approach had occurred, these changes were not as dramatic as those seen for the departure phase. Figures A-71 and A-72 show the cumulative probability of maximum dynamic pressure encountered while in different flap detents for the departure and approach phases respectively. The single points for detents 40 and 45 in figure A-71 indicate a single occurrence of these settings during departure.

5.4.2 Speed Brake/Spoiler Usage Data.

Information on speed brake operations during flight was determined to be of primary interest to various users of the data. Therefore, statistics on speed brake usage as a function of speed, altitude, and deflection angle were derived from the measured data. To be counted as a deployment cycle the speed brake had to deflect more than 7 degrees for a period of 3 seconds. Data on spoiler operations occurring during the landing roll are available, but were not reduced into statistical format. Figure A-73 presents the cumulative occurrences of maximum speed encountered while the speed brakes were deployed, while figure A-74 presents the cumulative occurrences of speed at the moment of speed brake deployment. Figure A-75 presents the cumulative occurrences of altitude at the moment of speed brake deployment. Figure A-76 presents the cumulative probability of maximum deployment angle reached during the time that the speed brakes were deployed for the flaps retracted configuration. As can be seen in figures A-73 through A-76 speed brake cycles occur on average less than once per flight. Speed brake cycles occurred but were not counted for the conditions of flaps deflected in various detents.

5.4.3 Thrust Reverser Data.

Cumulative probabilities of duration and speed associated with thrust reverser operations were derived from the measured data. Figure A-77 presents the cumulative probability of total time that thrust reversers are deployed. Figure A-78 presents the cumulative probability of the speed at the time when the thrust reversers were deployed or stowed. Although normally the thrust reversers are deployed and stowed a single time for each landing, the measured data showed two cycles of thrust reverser operation on a few occasions. This accounts for the rare occurrence of thrust reverser deployment at speeds as low as 45 knots in figure A-78. The data processing did not evaluate the engine power lever angles existing at these specific low-speed thrust reverser

deployments. However, at such low speeds, exhaust gas re-ingesting becomes a concern. Normally the engine manufacturer specifies a thrust reverser cutoff speed, typically about 50 knots, below which thrust reversers should not be used.

5.4.4 Landing Gear Extension/Retraction Data.

Landing gear operating statistics were reduced from the measured data. The information can be used to support design, evaluation, and monitoring of the landing gear and associated structure. Figure A-79 shows the cumulative probability of total time with the landing gear extended after liftoff. Figure A-80 shows the cumulative probability of time with the landing gear extended prior to touchdown. As is expected, the time with gear extended during approach is considerably longer than the time after liftoff when the pilot retracts the gear within seconds after liftoff. Figure A-81 presents the cumulative probability of the maximum airspeed during the time that the gear is extended for both the departure and approach phases of flight.

5.5 PROPULSION SYSTEM DATA.

The cumulative probability of engine fan speed N_1 associated with thrust reverser operations was derived from the measured N_1 engine parameter. Figure A-82 presents the cumulative probability of engine fan speed N_1 at takeoff, at thrust reverser deployment, and the maximum fan speed N1 encountered during the time that the thrust reverser is deployed.

6. CONCLUSIONS.

Incorporation of the additional data formats provides new and informative statistical information to the aircraft manufacturers, airlines, and the FAA.

Comparison of the gust load factor occurrence data of this report based on 13,916 hours with the same data based on 817.7 hours in reference 3 shows general agreement for incremental load factor levels to plus or minus 0.5 g. At higher load factors the new data shows reduced occurrence levels, indicating that the extrapolation of limited data samples may lead to erroneous results. An identical conclusion is drawn when comparing the maneuver load factor results. The FAA goal is to collect a minimum of recorded flight hours equal to one design life to provide a reliable database. It would seem prudent to continue the data gathering for some time, until a stable database is obtained.

The autopilot and flap usages presented in this report differ significantly from earlier usages presented in reference 3. This suggests that the operational procedures employed change over time. Changes in operational procedures would be expected to apply to all identical aircraft in the airline fleet. To track the impact of such changes a single representative aircraft should remain installed with a flight loads recorder throughout its life.

The data in figure A-66 shows that the measured gust load factors for the flaps extended configuration often occur outside the design V-n diagram. The data suggests that the present gust design requirements for the flaps extended configuration may need to be reviewed for adequacy. An assessment of the appropriateness of the continued use of U_{de} values specified in FAR 25.345 for high-lift devices appears to be justified. Derived gust velocity, U_{de}, values

obtained from this effort show deviation from the data presented in reference 6. In general, for altitudes below 1,500 feet the B-737–400 data show higher levels of occurrences for the upward gusts and fewer for the downward gusts than presented in reference 6. For the altitude range from 1,500-9,500 feet the occurrences from the B-737-400 compare very well with the reference 6 data. For levels above 9,500 feet the B-737-400 occurrences are below those predicted by reference 6. In as much as reference 6 represented a rather preliminary effort to define atmospheric turbulence in power spectral format, the B-737-400 data should also be compared to other study results to provide a more complete assessment of the B-737-400 data and its influence on future design requirements.

Furthermore, calculation of turbulence field parameters, P and b values, based on the B-737-400 data is considered desirable and should be included in future data reduction efforts. The resulting values should be compared with turbulence field parameters specified in reference 6 and Appendix G to Part 25 of the FAR.

The technique used in this report to separate gust and maneuver accelerations results in positive maneuver occurrences only. The most common method previously used to separate maneuver and gust accelerations has been the so called 2-second rule. From reviews of measured data and studies of aircraft response to elevator motion it was determined that for larger aircraft essentially all of the maneuver load factor peaks can be expected to be counted if a time between zero crossings greater than 2 seconds is used. Load factor peaks with zero crossings less than 2 seconds will mostly all be gusts. This approach resulted in the identification of both positive and negative maneuver occurrences. A cursory review of the B-737-400 acceleration data shows that pitching maneuvers resulting in both positive and negative accelerations do occur with some frequency and magnitude in the climb phase. Unfortunately these occurrences are counted as gusts. A study to evaluate the impact of different maneuver and gust separation criteria is very important and should be done before much is made of the differences in the gust frequencies noted and before turbulence field parameters are derived.

Statistical information on flight control surface activity is a valuable input to the design requirements for these surfaces and their associated components. Flight control surface deflections are recorded at two samples per second (2 sps) and can easily be reduced to provide the desired information. Unfortunately, there are doubts about the adequacy of the sampling rates to provide reliable results. For this reason the flight control surface deflection data were not processed. A study to determine the sampling rates as a function of control surface deflection rate necessary to provide acceptable statistical surface deflection information would be invaluable.

7. REFERENCES.

1. Crabill, Norman L., "FAA/NASA Prototype Flight Loads Program Systems Requirements, B737-400 Aircraft," Eagle Aerospace Inc., Contract NAS1-19659, unpublished report, November 1994.

2. de Jonge, B., "Reduction of Incremental Load Factor Acceleration Data to Gust Statistics," DOT/FAA/CT-94/57, August 1994.

3. "Flight Loads Data for a Boeing 737-400 in Commercial Operation," Department of Transportation Report DOT/FAA/AR-95/21, April 1996.

4. "Data From Unusual Events Recording System in a Commercial 737 Aircraft," Technology Incorporated Instruments and Controls Division, Dayton OH, Report No. FAA-RD-72-113, November 1972.

5. Clay, Larry E., DeLong, Robert C., and Rockafellow, Ronald I., "Airline Operational Data From Unusual Events Recording Systems in 707, 727, and 737 Aircraft," Report No. FAA-RD-71-69, September 1971.

6. Press, Harry and Steiner, Roy, "An Approach to the Problem of Estimating Severe and Repeated Gust Loads for Missile Operations," National Advisory Committee for Aeronautics Technical Note 4332, September 1958, Langley Aeronautical Laboratory, Langley Field, Va.

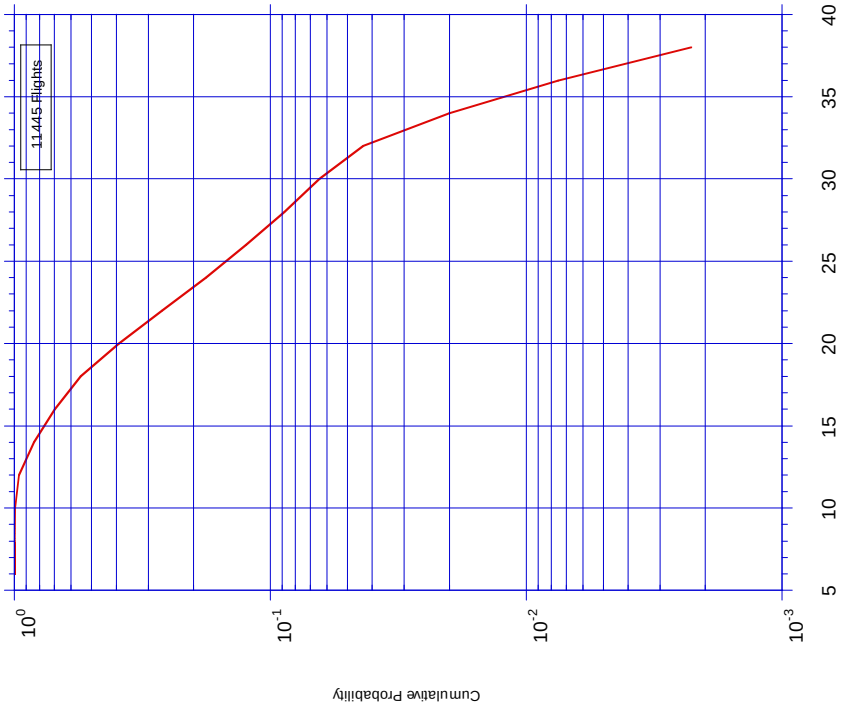

FIGURE A-2. CUMULATIVE PROBABILITY OF TAKEOFF FUEL WEIGHT

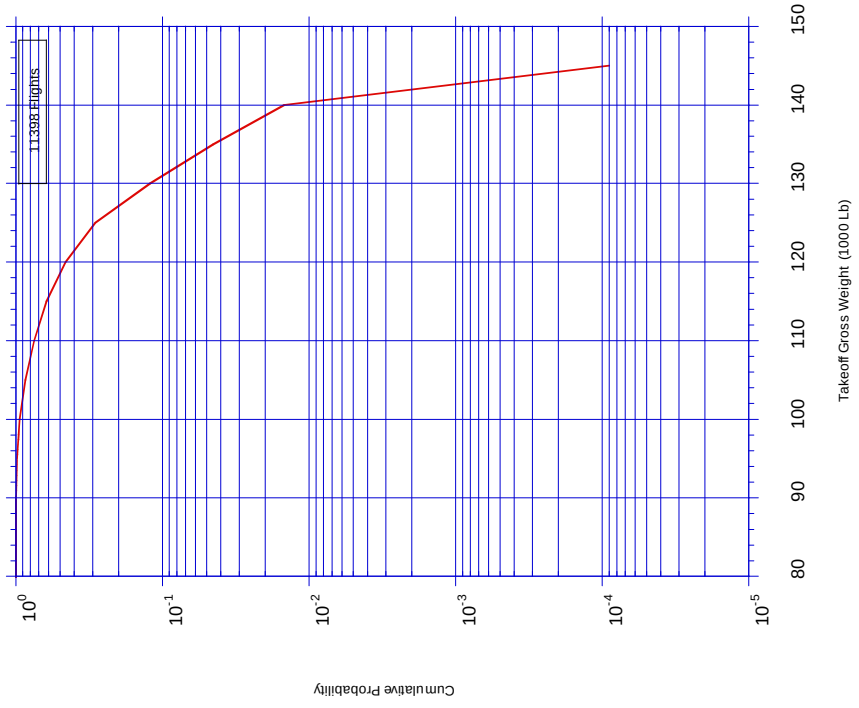

FIGURE A-1. CUMULATIVE PROBABILITY OF TAKEOFF GROSS WEIGHT

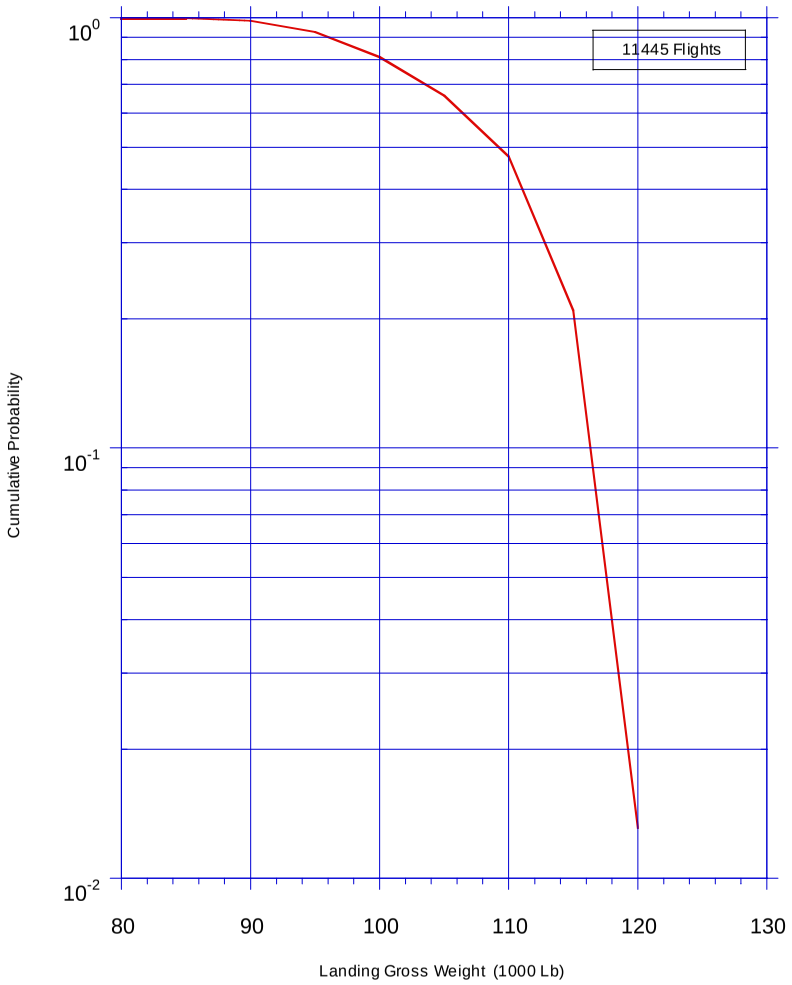

FIGURE A-3. CUMULATIVE PROBABILITY OF LANDING GROSS WEIGHT

Takeoff Fuel Weight (1000 Lb)

Flight Distance (NM)

11445 Flts	5-10	10-15	15-20	20-25	25-30	30-35	35-40	Total
0-250	0.367	9.891	5.618	0.664	0.079	0.07		16.689
250-500		12.46	19.056	3.862	0.14	0.009		35.526
500-750		0.358	9.567	6.317	1.145	0.384	0.009	17.781
750-1000	0.009		3.032	11.691	3.093	0.498	0.192	18.515
1000-1250	0.009		0.079	2.08	2.665	0.647	0.035	5.513
1250-1500				0.096	0.629	0.682	0.061	1.468
1500-1750				0.017	0.507	2.149	0.323	2.997
1750-2000					0.052	0.821	0.446	1.319
2000-2250						0.026	0.166	0.192
Total	0.384	22.709	37.353	24.727	8.309	5.286	1.232	100

FIGURE A-4. CORRELATION OF TAKEOFF FUEL WEIGHT AND FLIGHT DISTANCE, PERCENT OF FLIGHTS

Takeoff Gross Weight (1000 Lb)

Flight Distance (NM) 11398 Flts	80-90	90-100	100-110	110-120	120-130	130-140	140-150	Total
0-250	0.14	2.343	6.413	5.782	2			16.678
250-500	0.044	2.676	9.203	13.397	10.177	0.035		35.533
500-750		0.132	1.904	5.027	9.589	1.105	0.009	17.766
750-1000		0.079	1.237	3.834	9.037	4.343	0.009	18.538
1000-1250			0.149	0.886	2.062	2.316	0.105	5.519
1250-1500			0.026	0.307	0.404	0.658	0.07	1.465
1500-1750				0.053	0.518	1.5	0.912	2.983
1750-2000			0.009	0.035	0.123	0.842	0.316	1.325
2000-2250					0.018	0.088	0.088	0.193
Total	0.184	5.229	18.942	29.321	33.927	10.888	1.509	100

FIGURE A-5. CORRELATION OF TAKEOFF GROSS WEIGHT AND FLIGHT DISTANCE, PERCENT OF FLIGHTS

Gross Weight at Liftoff (1000 Lb)

Gross Weight at Touchdown (1000 Lb) 11398 Flts	80-90	90-100	100-110	110-120	120-130	130-140	140-150	Total
80-90	0.184	1.193	0.132					1.509
90-100		4.036	11.046	1.939	0.114			17.135
100-110			7.765	19.635	4.834	1.044	0.035	33.313
110-120				7.747	28.356	9.116	1.43	46.649
120-130					0.623	0.728	0.044	1.395
Total	0.184	5.229	18.942	29.321	33.927	10.888	1.509	100

FIGURE A-6. CORRELATION OF GROSS WEIGHT AT LIFTOFF AND TOUCHDOWN, PERCENT OF FLIGHTS

Maximum Altitude (1000 Feet)

Flight Distance (NM) 11723 Flts	0-5	5-10	10-15	15-20	20-25	25-30	30-35	35-40	Total
0-250	0.051	0.563	1.638	2.602	9.068	2.269	0.392	0.136	16.719
250-500				0.017	1.689	14.911	10.663	8.249	35.528
500-750					0.068	0.768	8.462	8.436	17.734
750-1000					0.06	0.478	9.733	8.317	18.587
1000-1250					0.034	0.094	3.062	2.32	5.511
1250-1500						0.026	0.631	0.793	1.45
1500-1750						0.026	1.467	1.476	2.969
1750-2000						0.026	0.887	0.384	1.297
2000-2250							0.171	0.034	0.205
Total	0.051	0.563	1.638	2.619	10.919	18.596	35.469	30.146	100

FIGURE A-7. CORRELATION OF MAXIMUM ALTITUDE AND FLIGHT DISTANCE, PERCENT OF FLIGHTS

Total Flight Distance (NM)

Altitude Band (Feet) 11723 Flts	0-250	250-500	500-750	750-1000	1000-1250	1250-1500	1500-1750	1750-2000	2000-2250	2250-2500
29,500-39,500	0.09	20.03	51.4	64.46	70.11	76.33	80.4	81.79	81.63	83.56
19,500-29,500	28.14	42.66	26.6	20.27	17.95	14.44	11.6	11.32	12.54	12.17
9,500-19,500	42.13	22.02	12.76	8.69	6.94	5.67	4.71	3.99	3.44	2.4
4,500-9,500	16.73	8.6	5.26	3.66	2.91	2.05	2.13	1.77	1.25	0.92
1,500-4,500	10.31	5.24	3.09	2.18	1.6	1.19	0.93	0.93	0.89	0.71
500-1,500	2.04	1.07	0.68	0.49	0.34	0.23	0.18	0.17	0.18	0.16
0-500	0.56	0.38	0.21	0.24	0.16	0.08	0.05	0.04	0.06	0.08
Total	100	100	100	100	100	100	100	100	100	100

FIGURE A-8. PERCENT OF TOTAL DISTANCE IN ALTITUDE BANDS

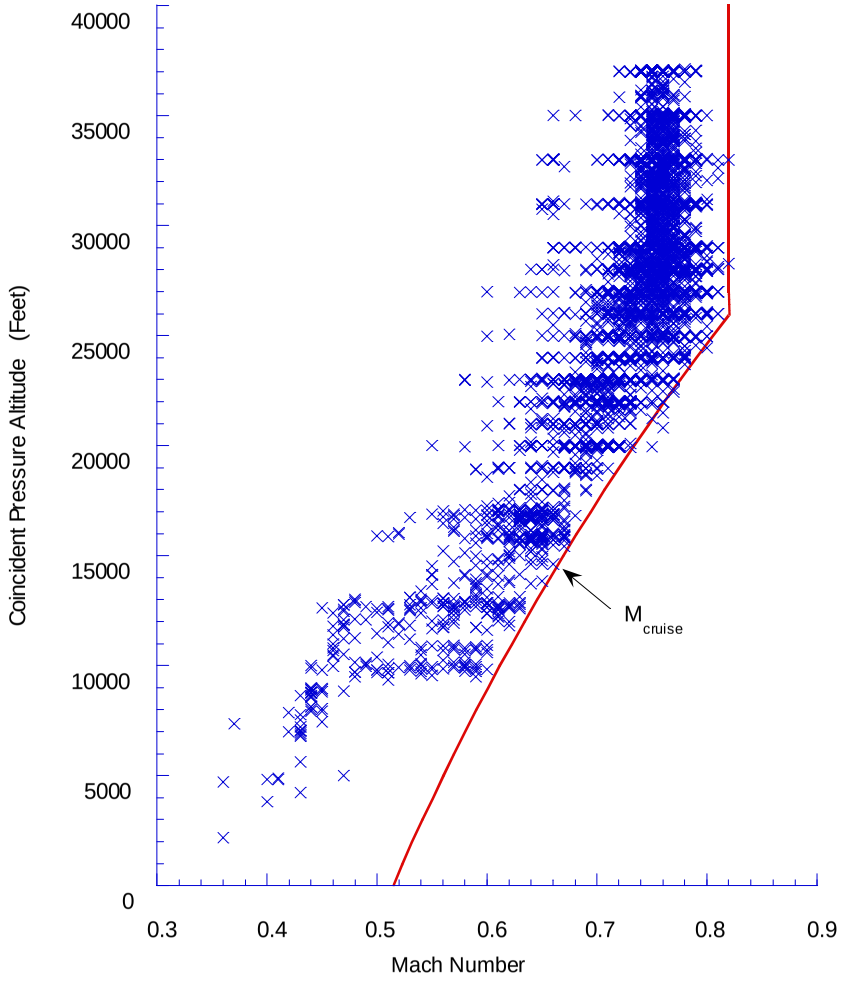

FIGURE A-9a. COINCIDENT ALTITUDE AT MAXIMUM MACH NUMBER, CRUISE PHASE

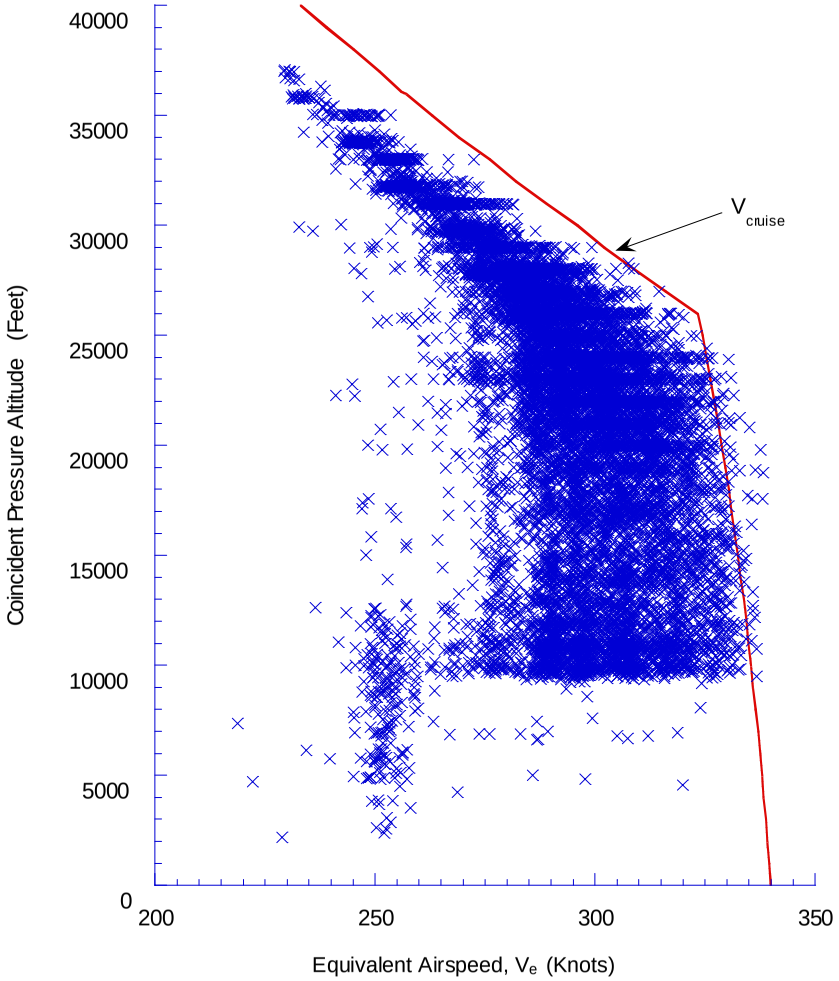

FIGURE A-9b. COINCIDENT ALTITUDE AT MAXIMUM EQUIVALENT AIRSPEED, CRUISE PHASE

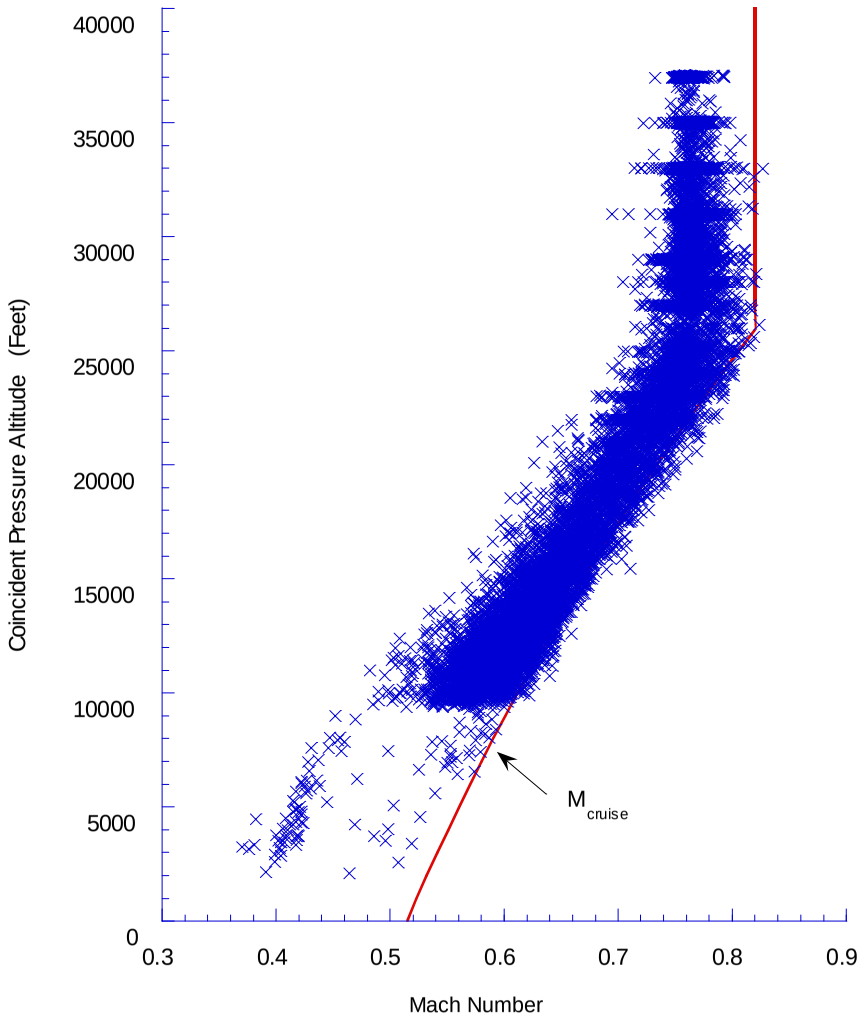

FIGURE A-10a. COINCIDENT ALTITUDE AT MAXIMUM MACH NUMBER, ALL FLIGHT PHASES

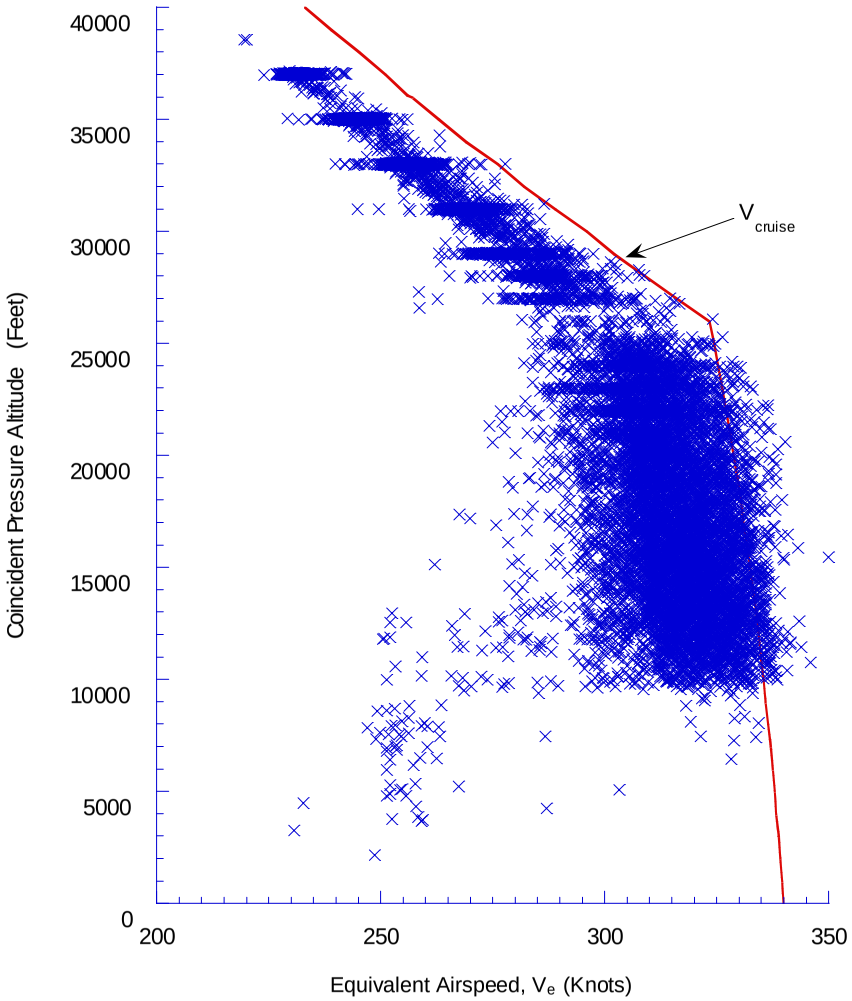

FIGURE A-10b. COINCIDENT ALTITUDE AT MAXIMUM EQUIVALENT AIRSPEED, ALL FLIGHT PHASES

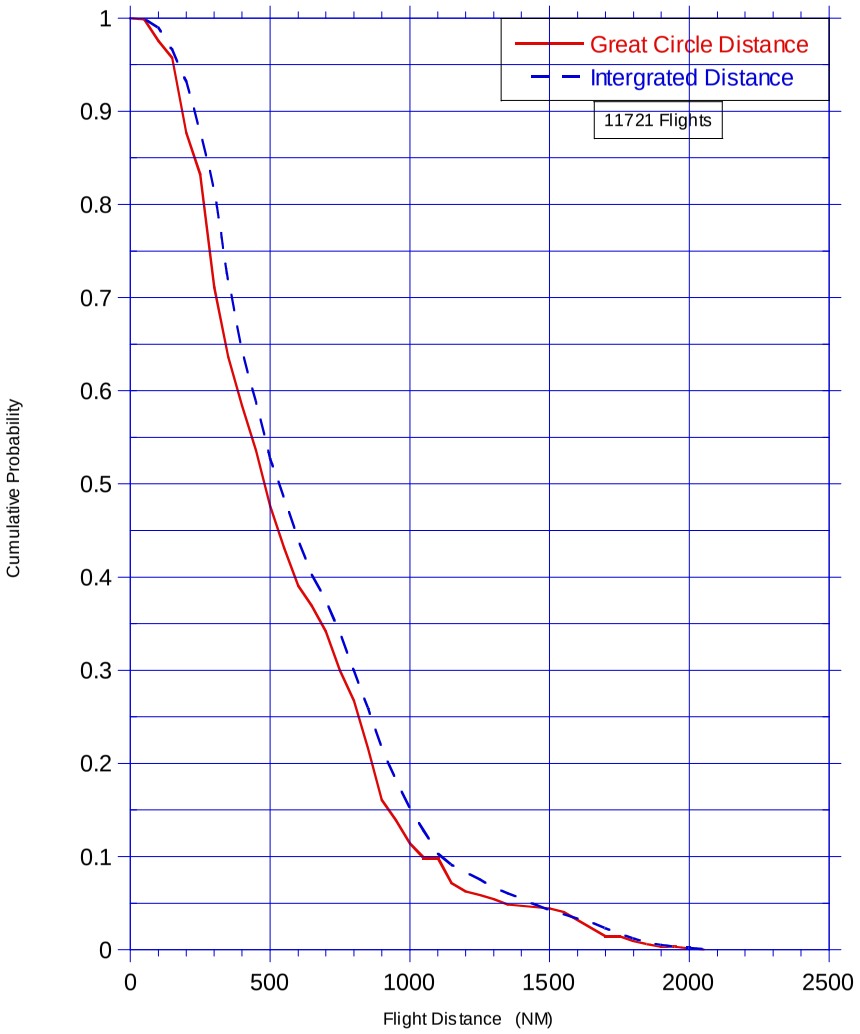

FIGURE A-11. CUMULATIVE PROBABILITY OF FLIGHT DISTANCES

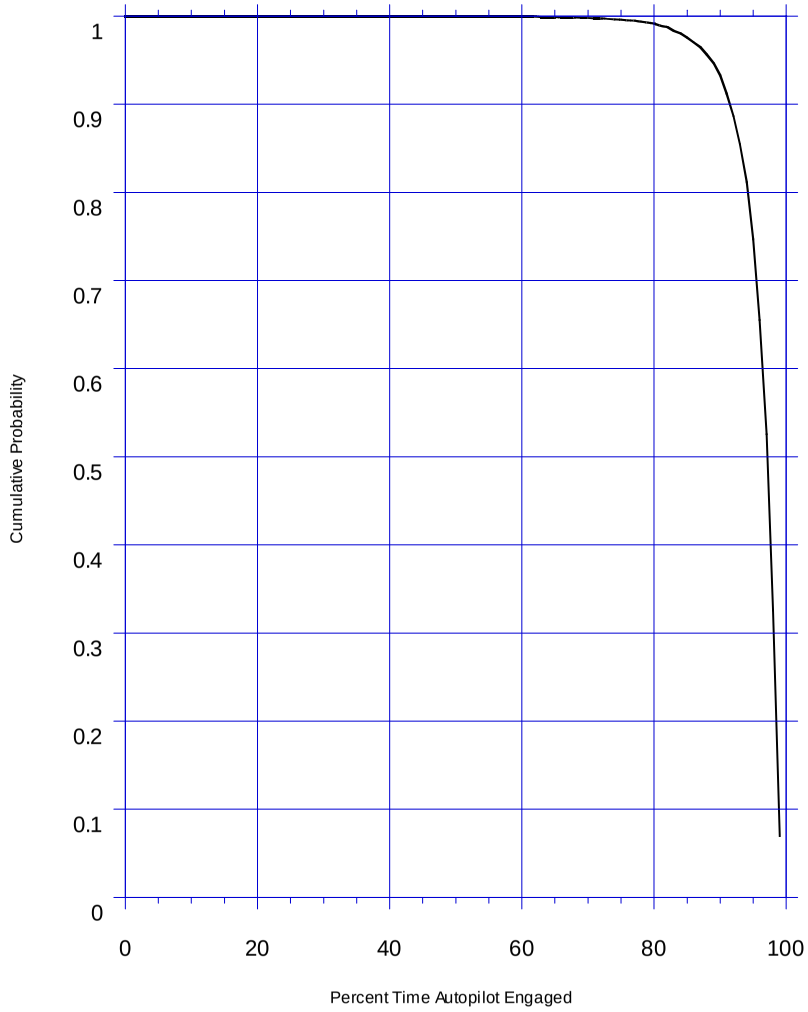

FIGURE A-12. CUMULATIVE PROBABILITY OF PERCENT OF FLIGHT TIME ON AUTOPILOT

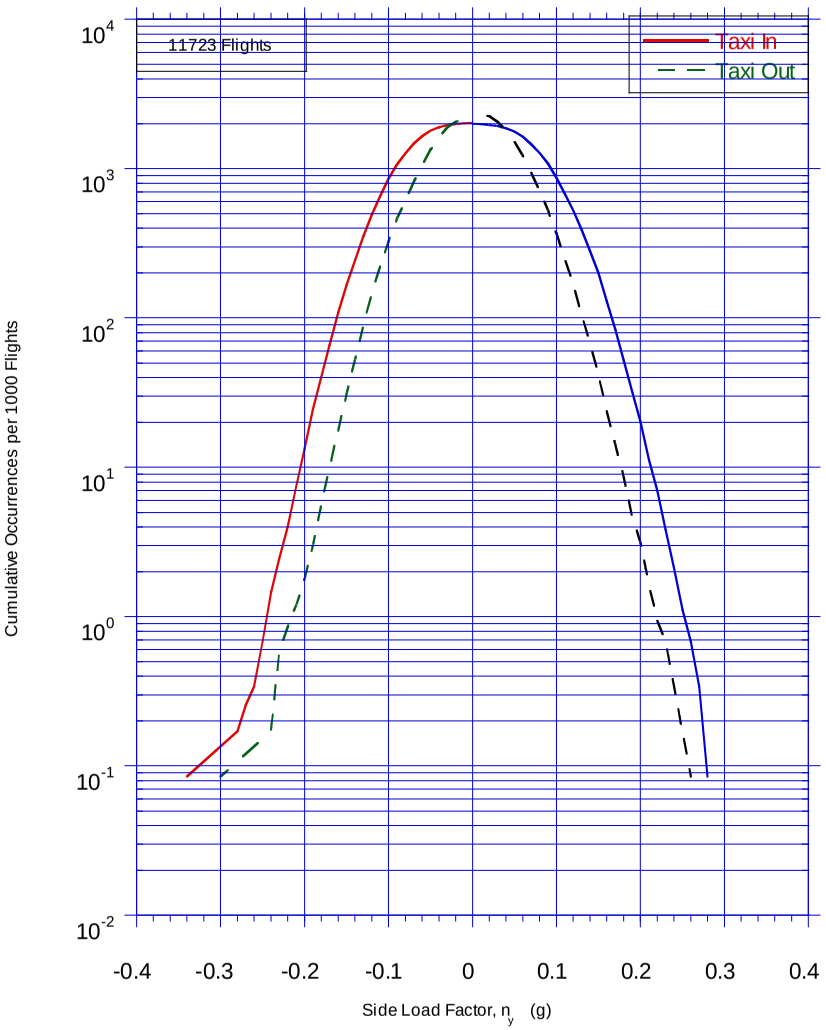

FIGURE A-13. CUMULATIVE FREQUENCY OF MAXIMUM SIDE LOAD FACTOR DURING GROUND TURNS

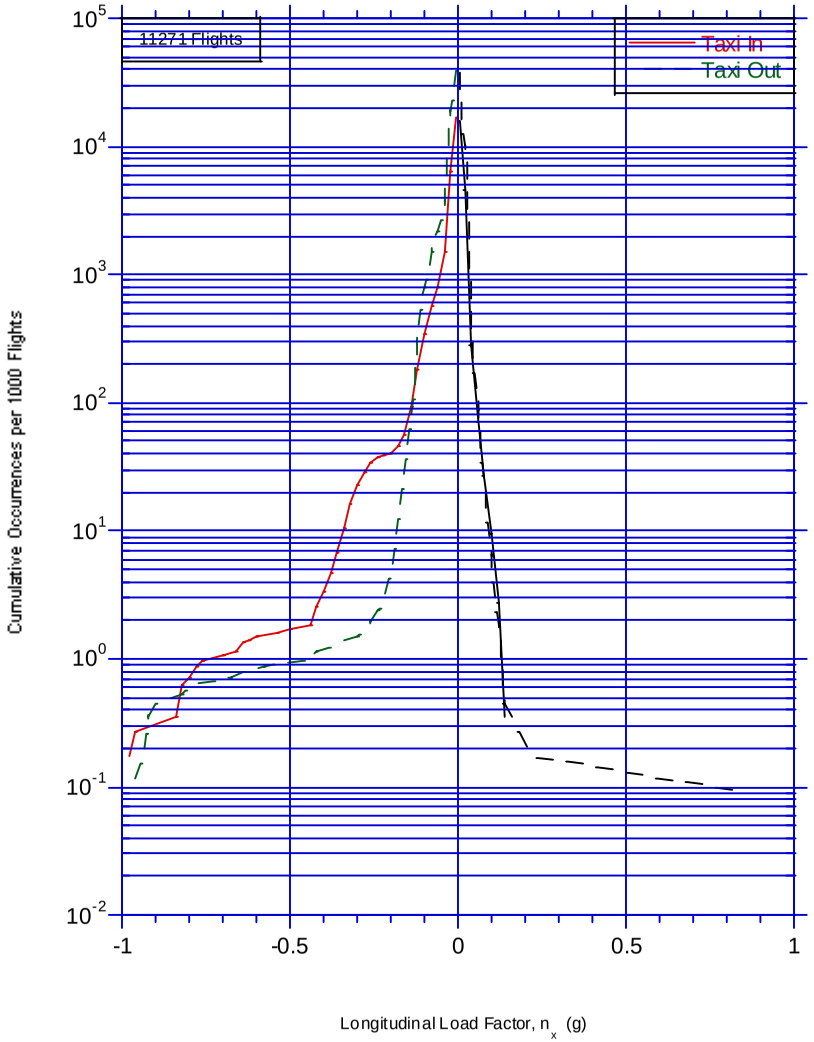

FIGURE A-14. CUMULATIVE FREQUENCY OF LONGITUDINAL LOAD FACTOR DURING GROUND TAXI

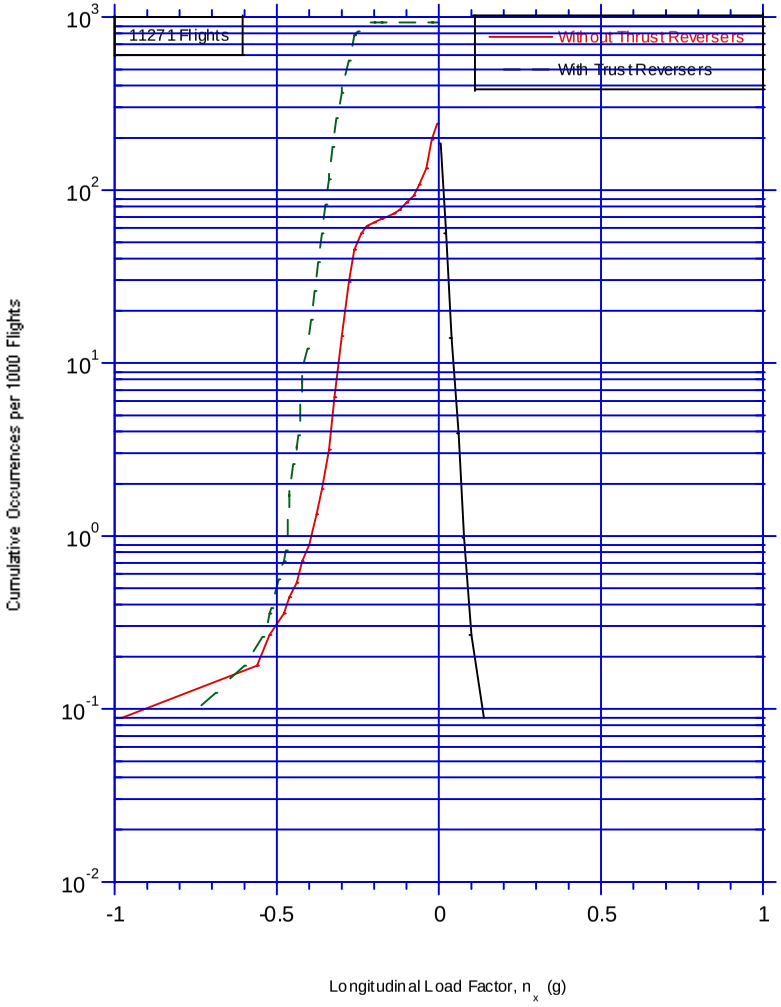

FIGURE A-15. CUMULATIVE FREQUENCY OF LONGITUDINAL LOAD FACTOR DURING LANDING ROLL

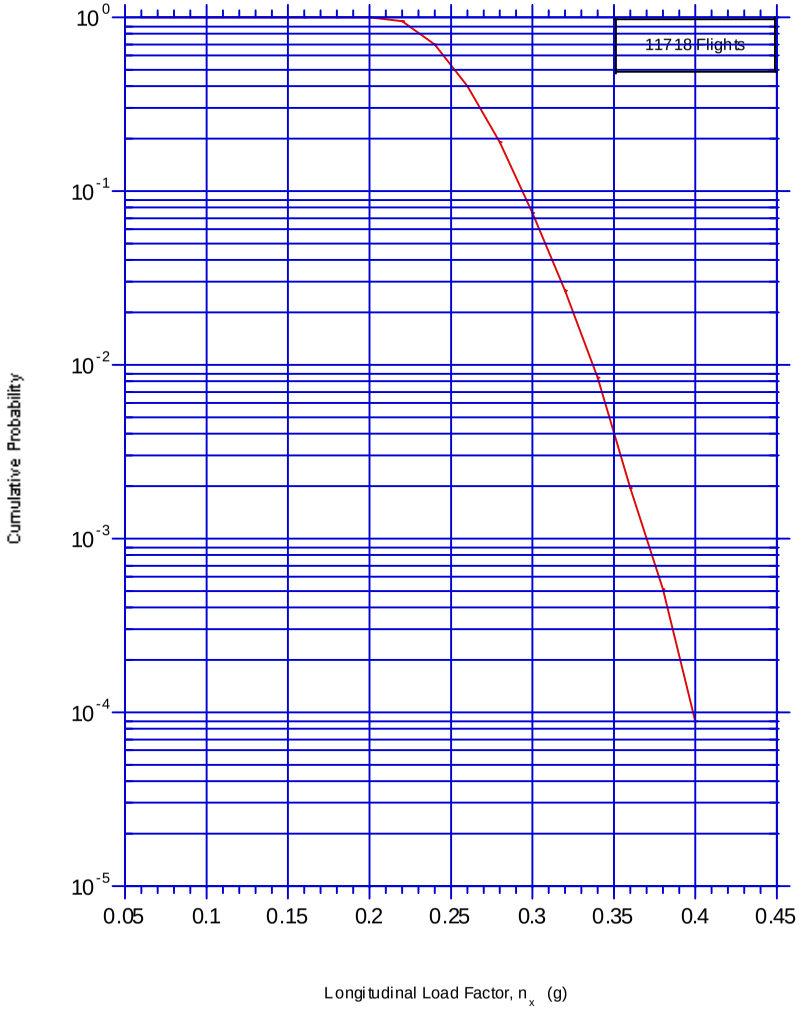

FIGURE A-16. CUMULATIVE PROBABILITY OF MAXIMUM LONGITUDINAL LOAD FACTOR DURING TAKEOFF

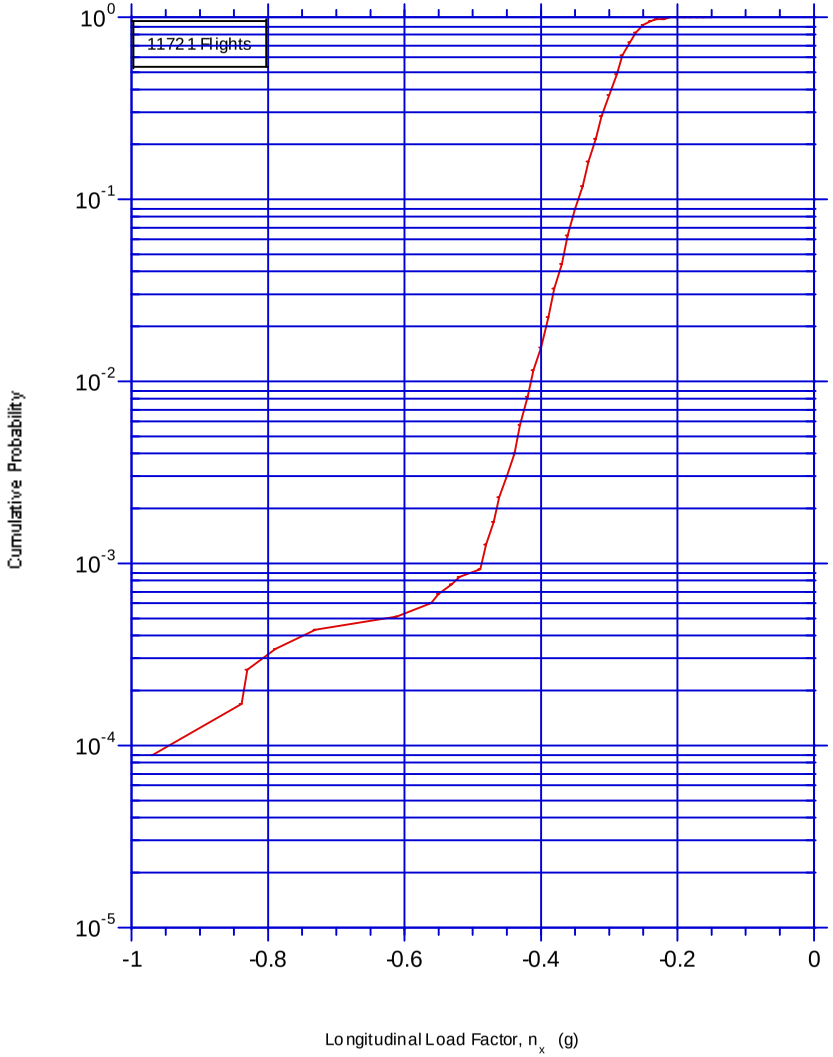

FIGURE A-17. CUMULATIVE PROBABILITY OF MINIMUM LONGITUDINAL LOAD FACTOR DURING LANDING

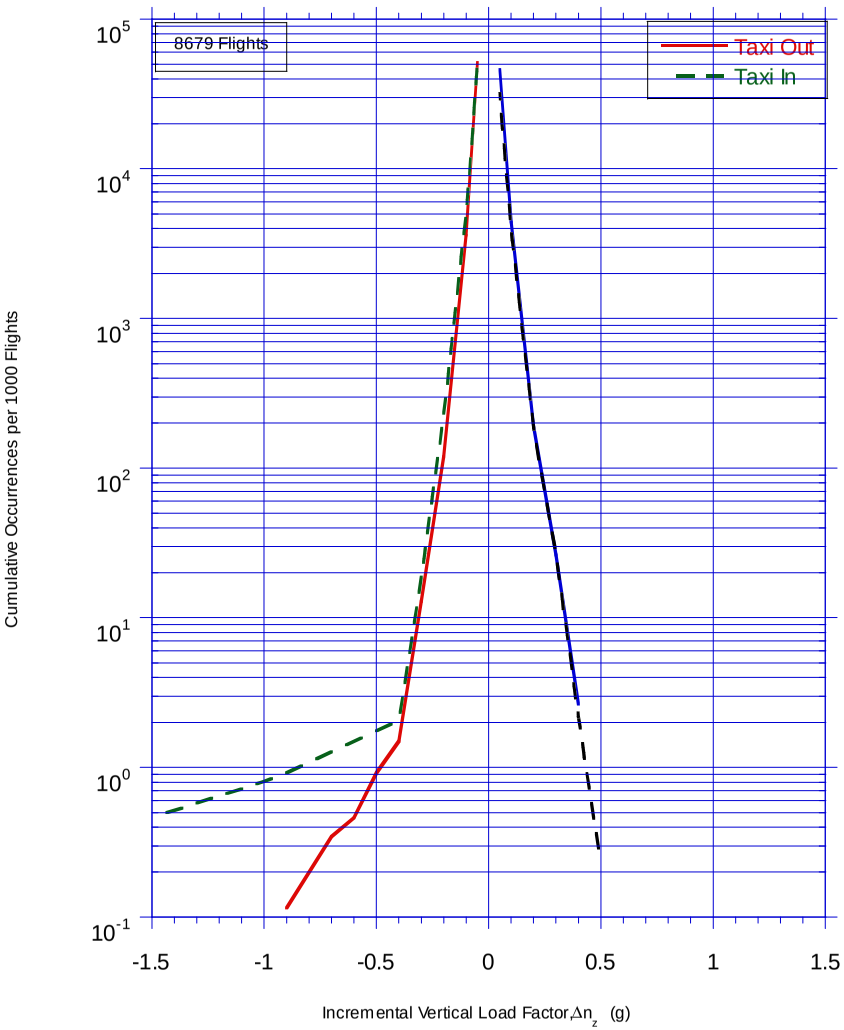

FIGURE A-18. CUMULATIVE FREQUENCY OF INCREMENTAL VERTICAL LOAD FACTOR DURING TAXI OPERATIONS

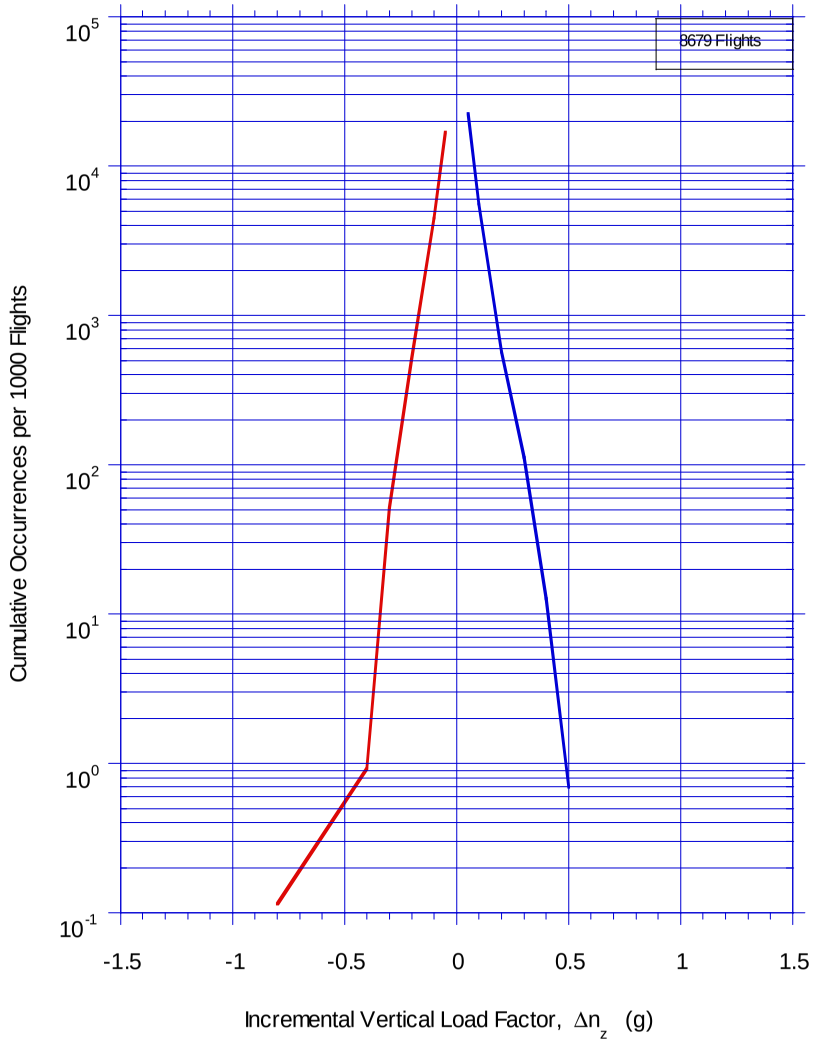

FIGURE A-19. CUMULATIVE FREQUENCY OF INCREMENTAL VERTICAL LOAD FACTOR DURING TAKEOFF ROLL

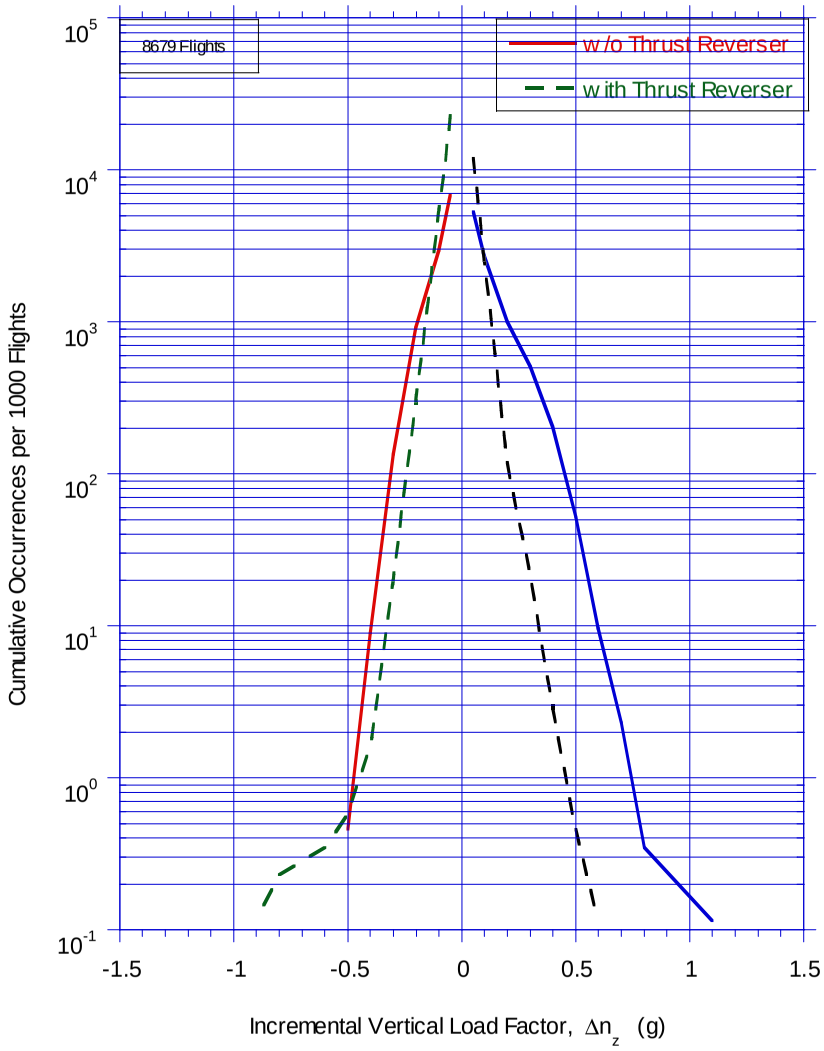

FIGURE A-20. CUMULATIVE FREQUENCY OF INCREMENTAL VERTICAL LOAD FACTOR DURING LANDING ROLL

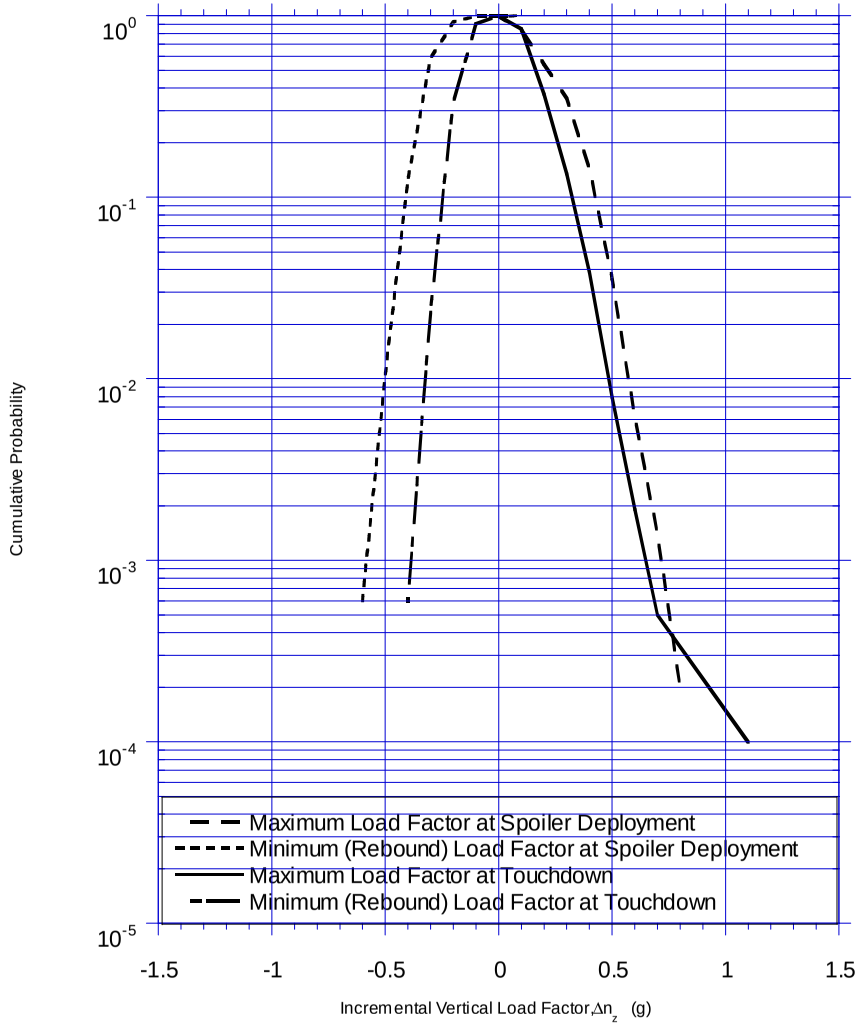

FIGURE A-21. CUMULATIVE PROBABILITY OF MINIMUM AND MAXIMUM INCREMENTAL VERTICAL LOAD FACTOR AT TOUCHDOWN AND SPOILER DEPLOYMENT

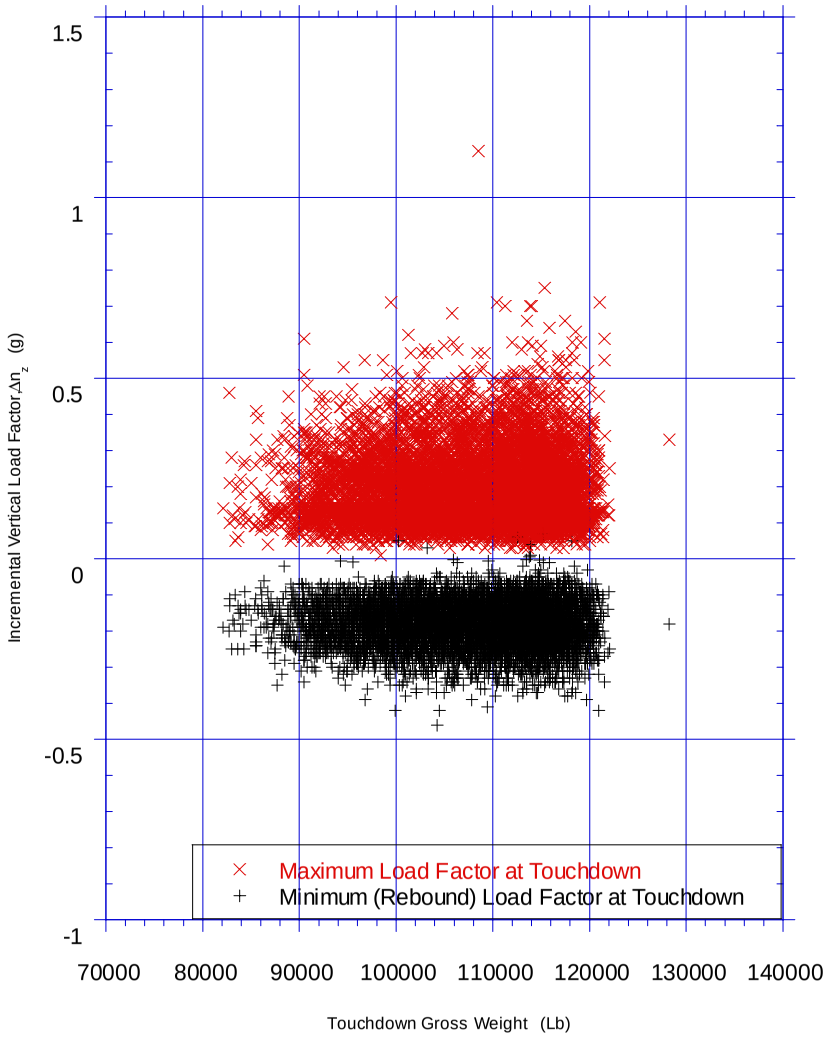

FIGURE A-22. COINCIDENT INCREMENTAL VERTICAL LOAD FACTOR AND TOUCHDOWN GROSS WEIGHT

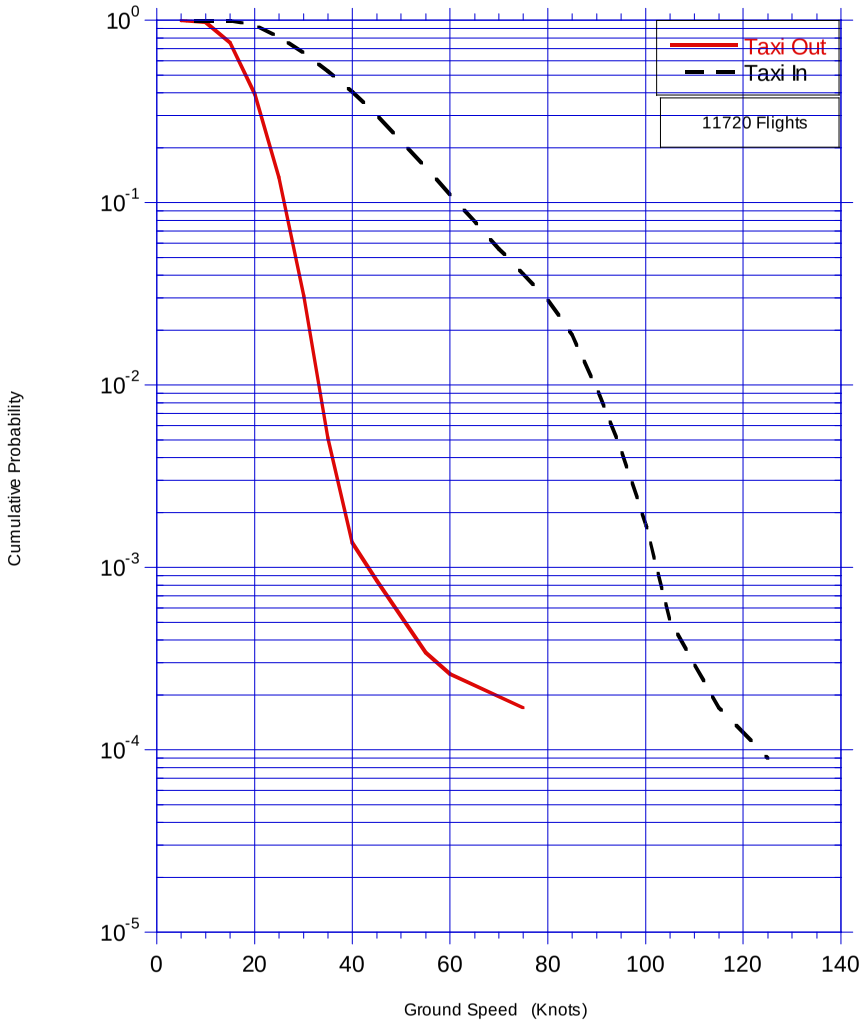

FIGURE A-23. CUMULATIVE PROBABILITY OF GROUND SPEED DURING TAXI

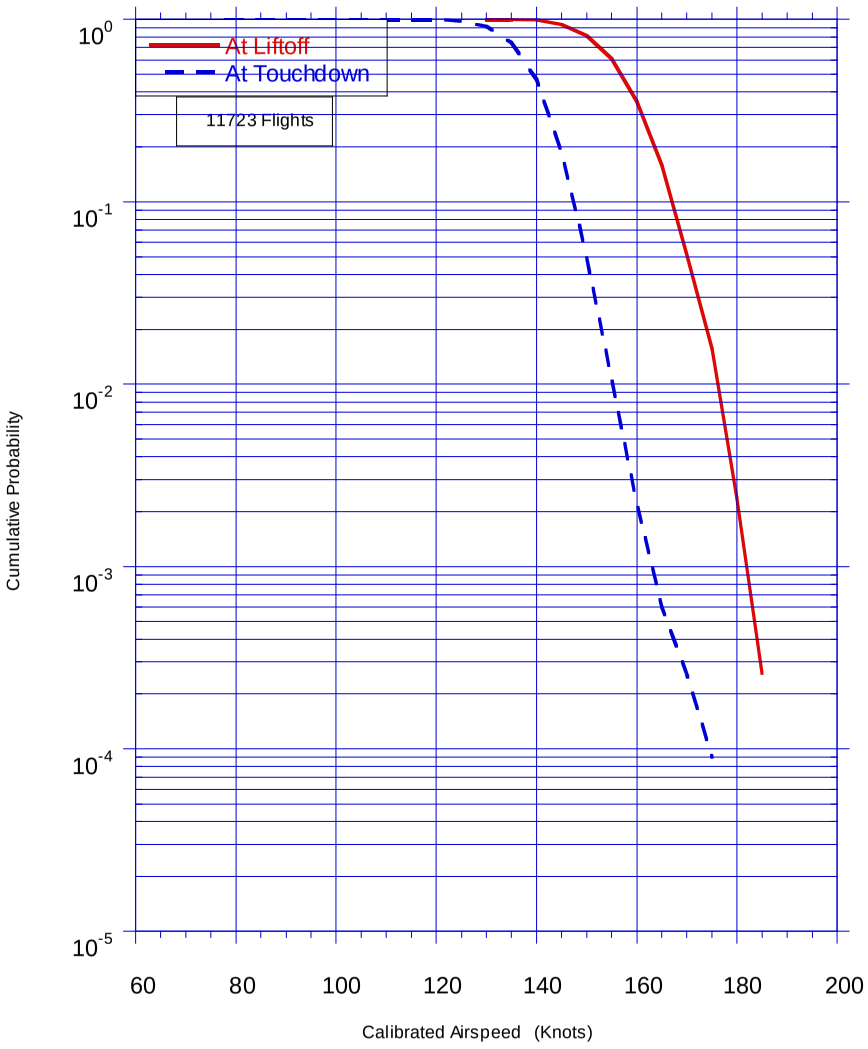

FIGURE A-24. CUMULATIVE PROBABILITY OF AIRSPEED AT LIFTOFF AND TOUCHDOWN

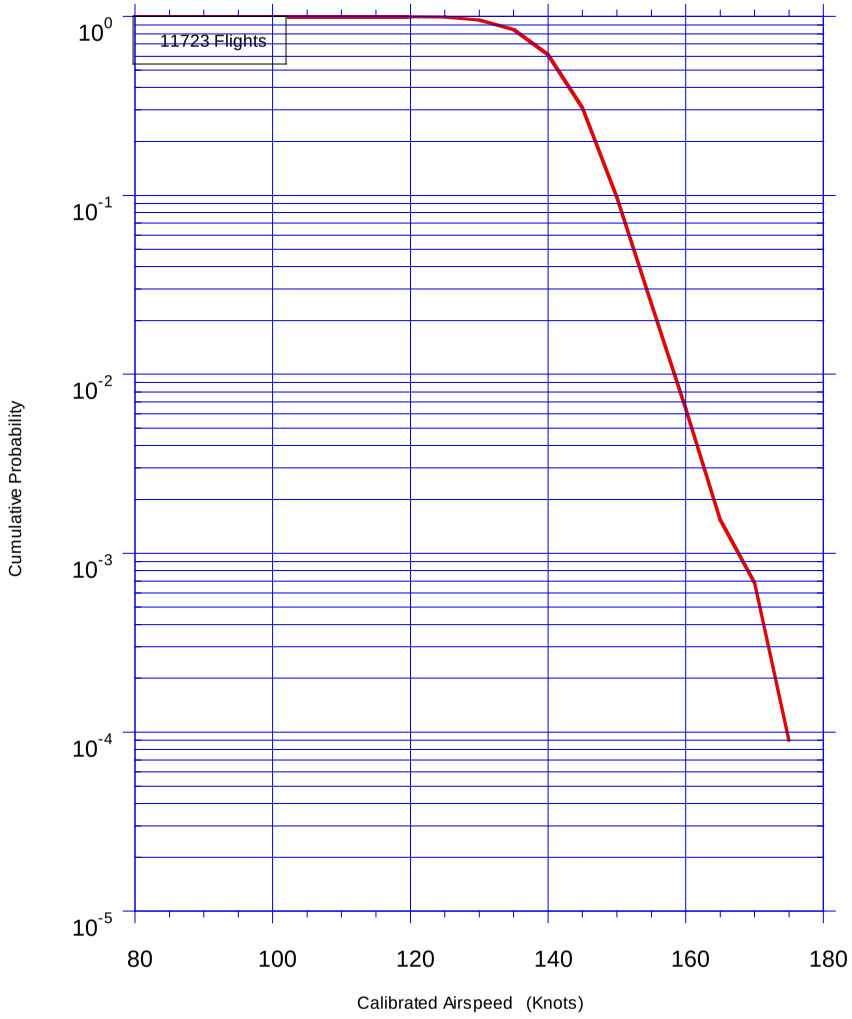

FIGURE A-25. CUMULATIVE PROBABILITY OF AIRSPEED AT FLARE

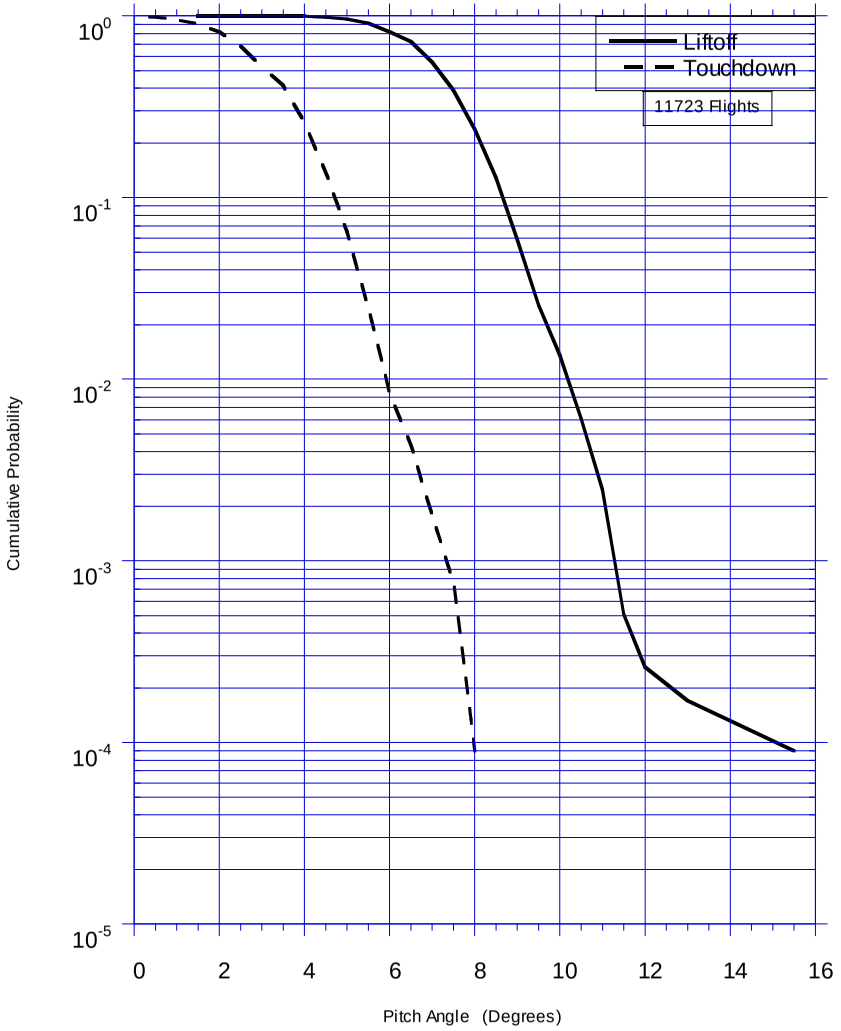

FIGURE A-26. CUMULATIVE PROBABILITY OF PITCH ANGLE AT LIFTOFF AND TOUCHDOWN

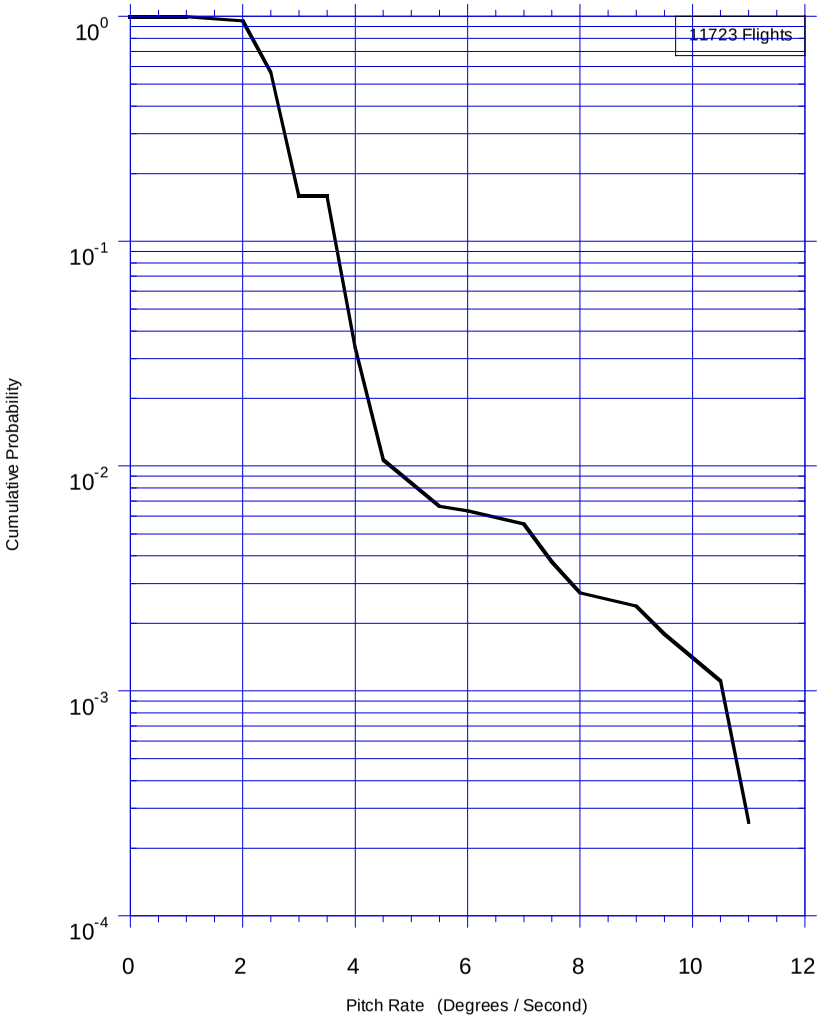

FIGURE A-27. CUMULATIVE PROBABILITY OF MAXIMUM PITCH RATE AT TAKEOFF ROTATION

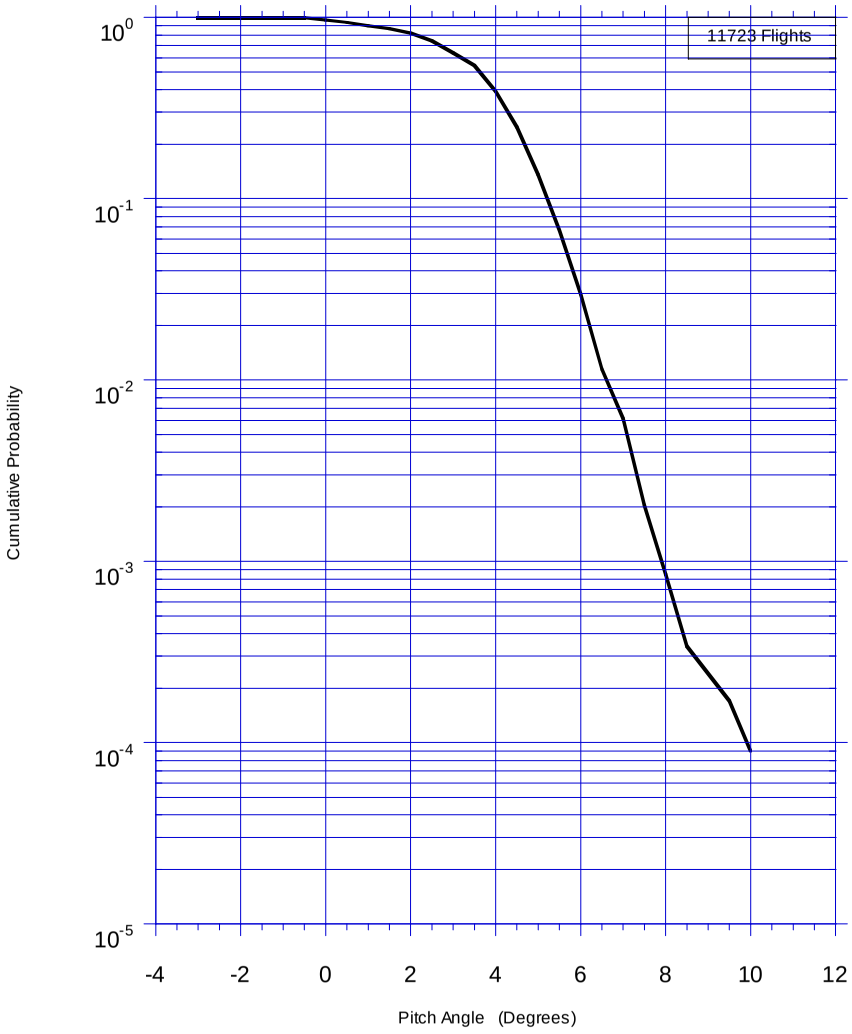

FIGURE A-28. CUMULATIVE PROBABILITY OF PITCH ANGLE AT TOUCHDOWN PEAK VERTICAL LOAD FACTOR

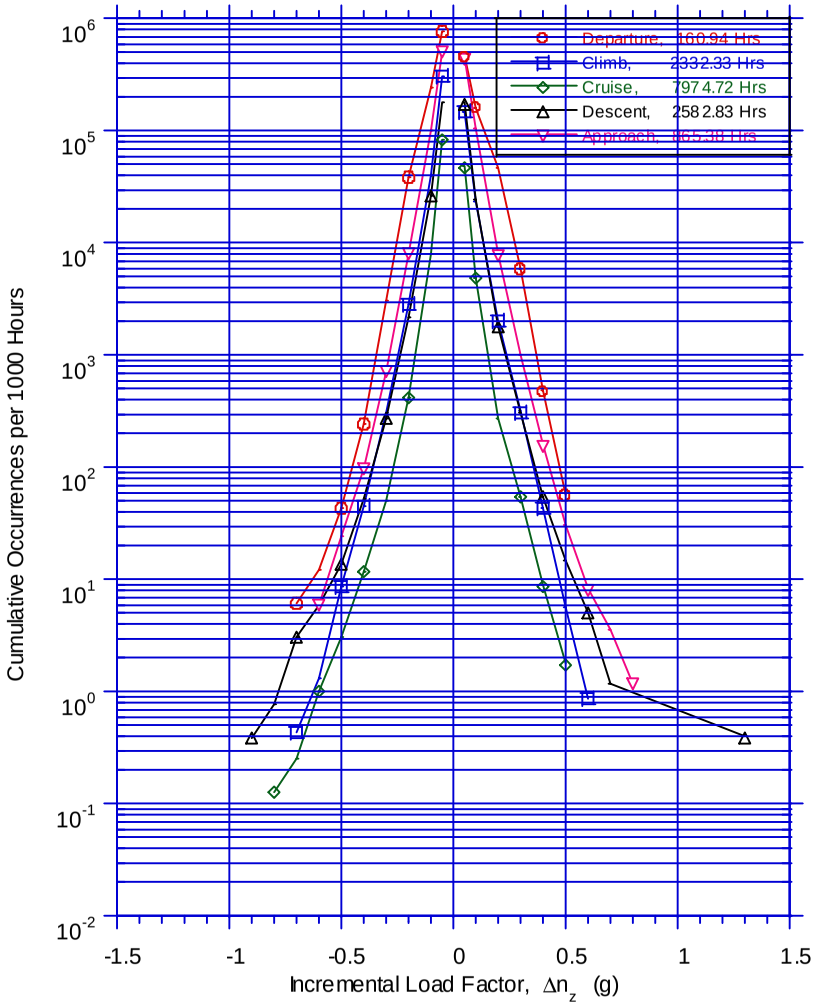

FIGURE A-29. CUMULATIVE OCCURRENCES OF VERTICAL GUST LOAD FACTOR PER 1000 HOURS BY FLIGHT PHASE

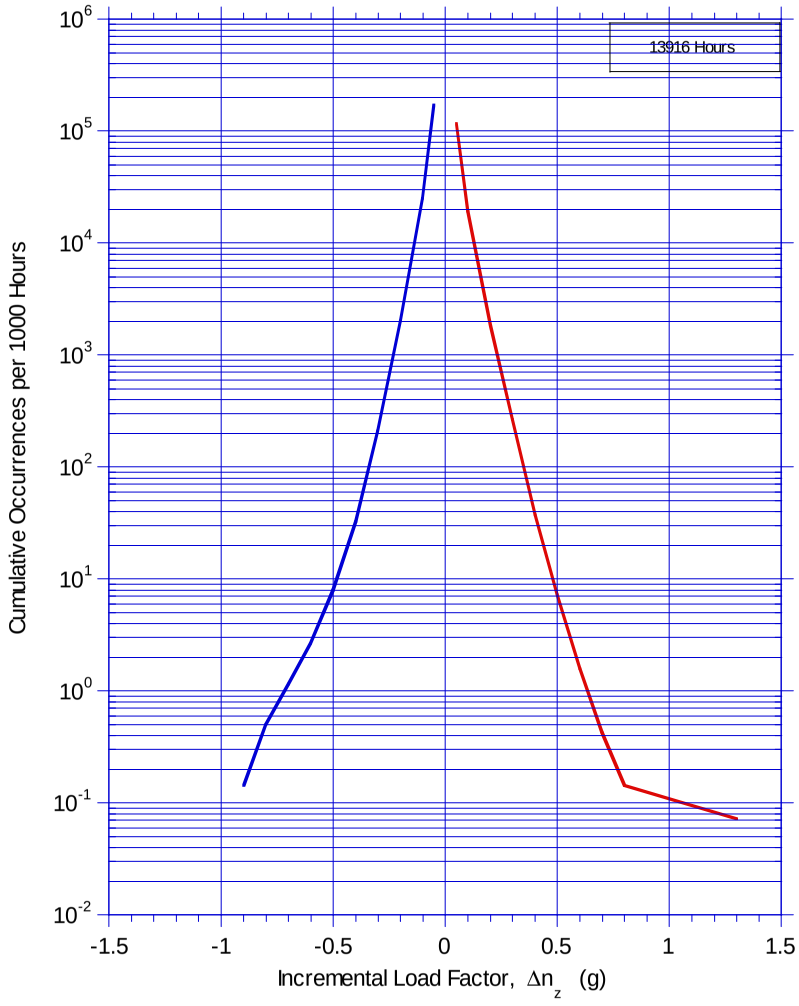

FIGURE A-30. CUMULATIVE OCCURRENCES OF INCREMENTAL VERTICAL GUST LOAD FACTOR PER 1000 HOURS, COMBINED FLIGHT PHASES

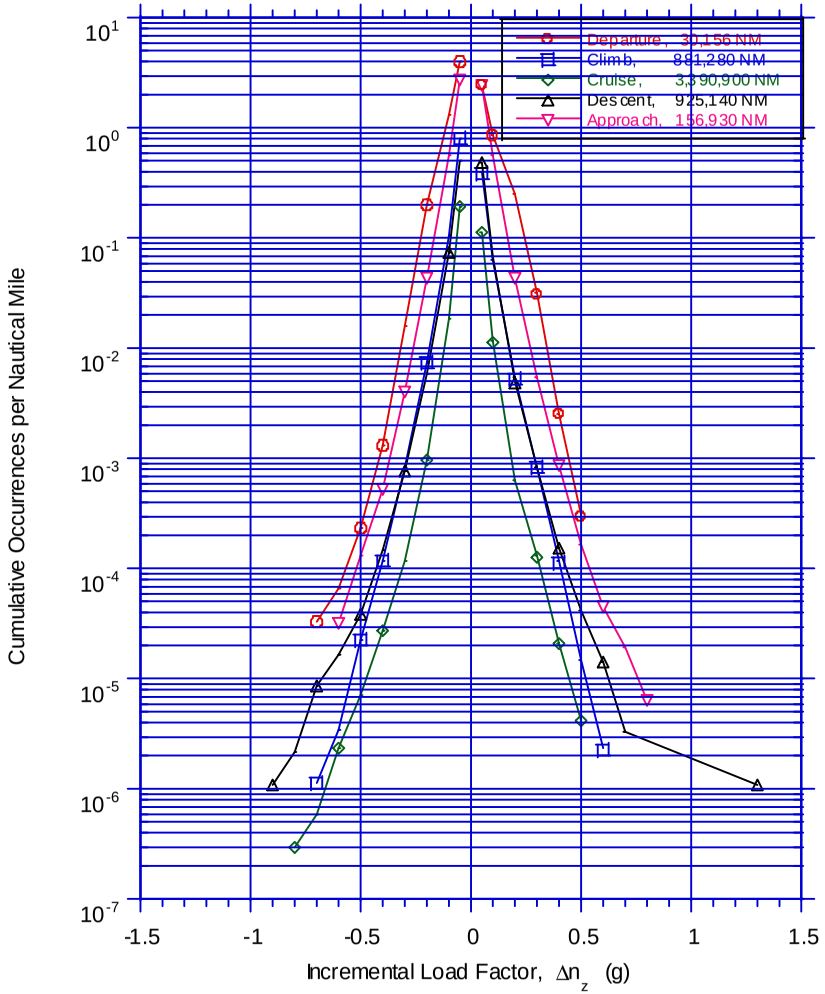

FIGURE A-31. CUMULATIVE OCCURRENCES OF VERTICAL GUST LOAD FACTOR PER NAUTICAL MILE BY FLIGHT PHASE

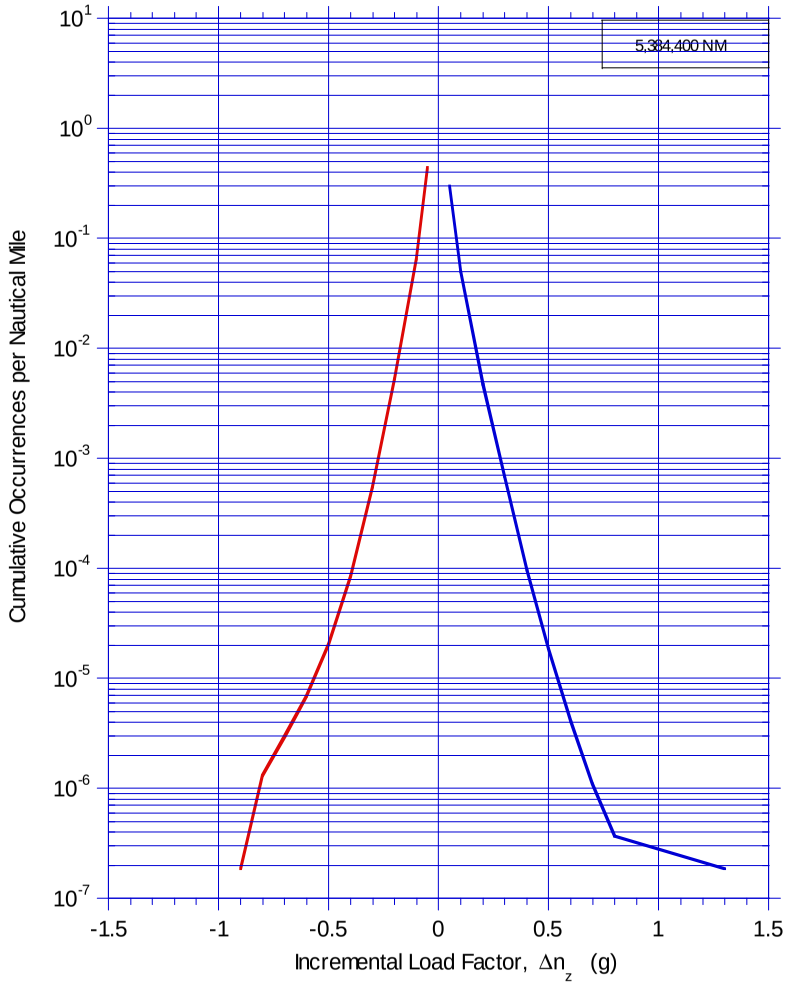

FIGURE A-32. CUMULATIVE OCCURRENCES OF INCREMENTAL VERTICAL GUST LOAD FACTOR PER NAUTICAL MILE, COMBINED FLIGHT PHASES

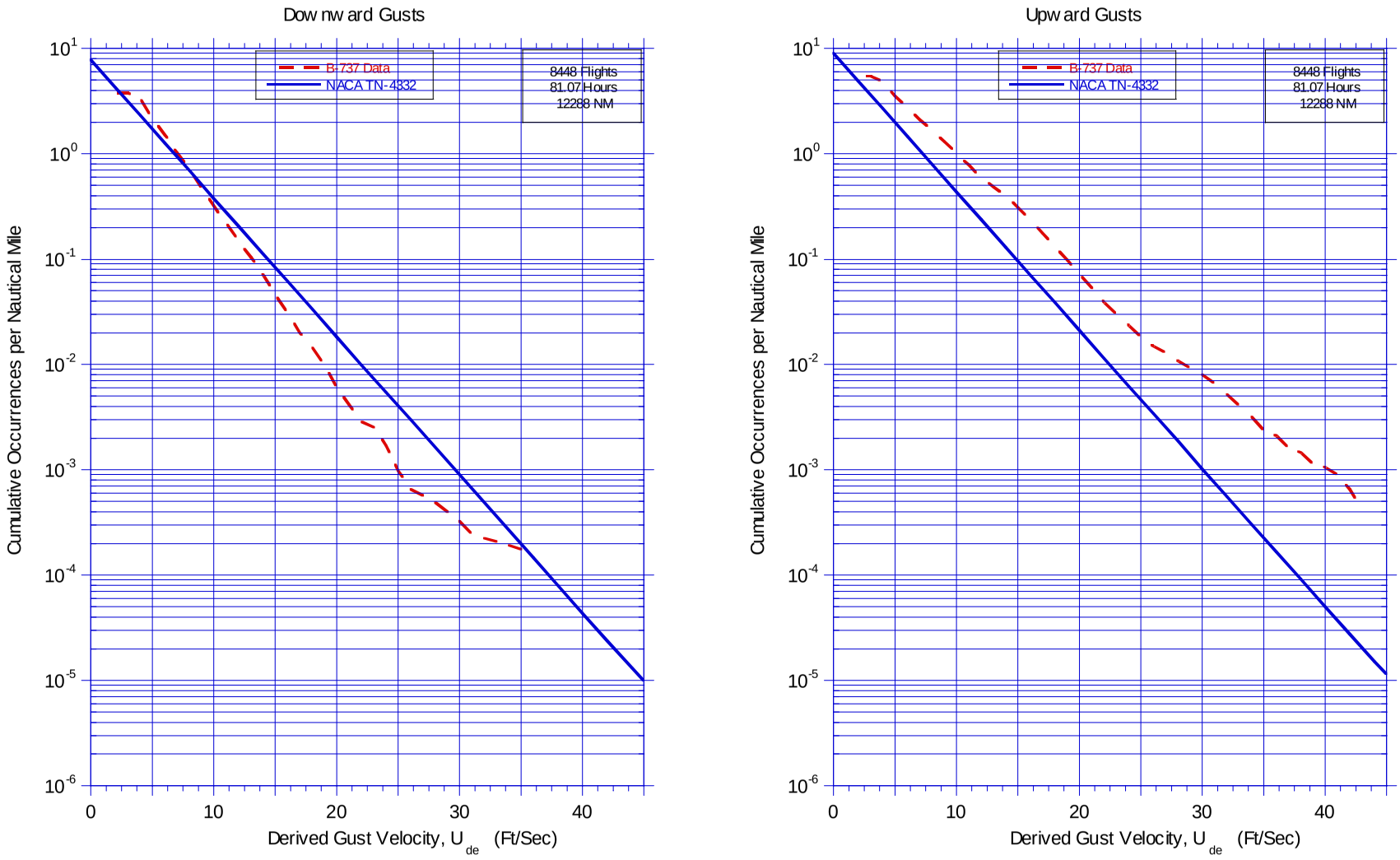

FIGURE A-33. CUMULATIVE OCCURRENCES OF DERIVED GUST VELOCITY PER NAUTICAL MILE, < 500 FEET

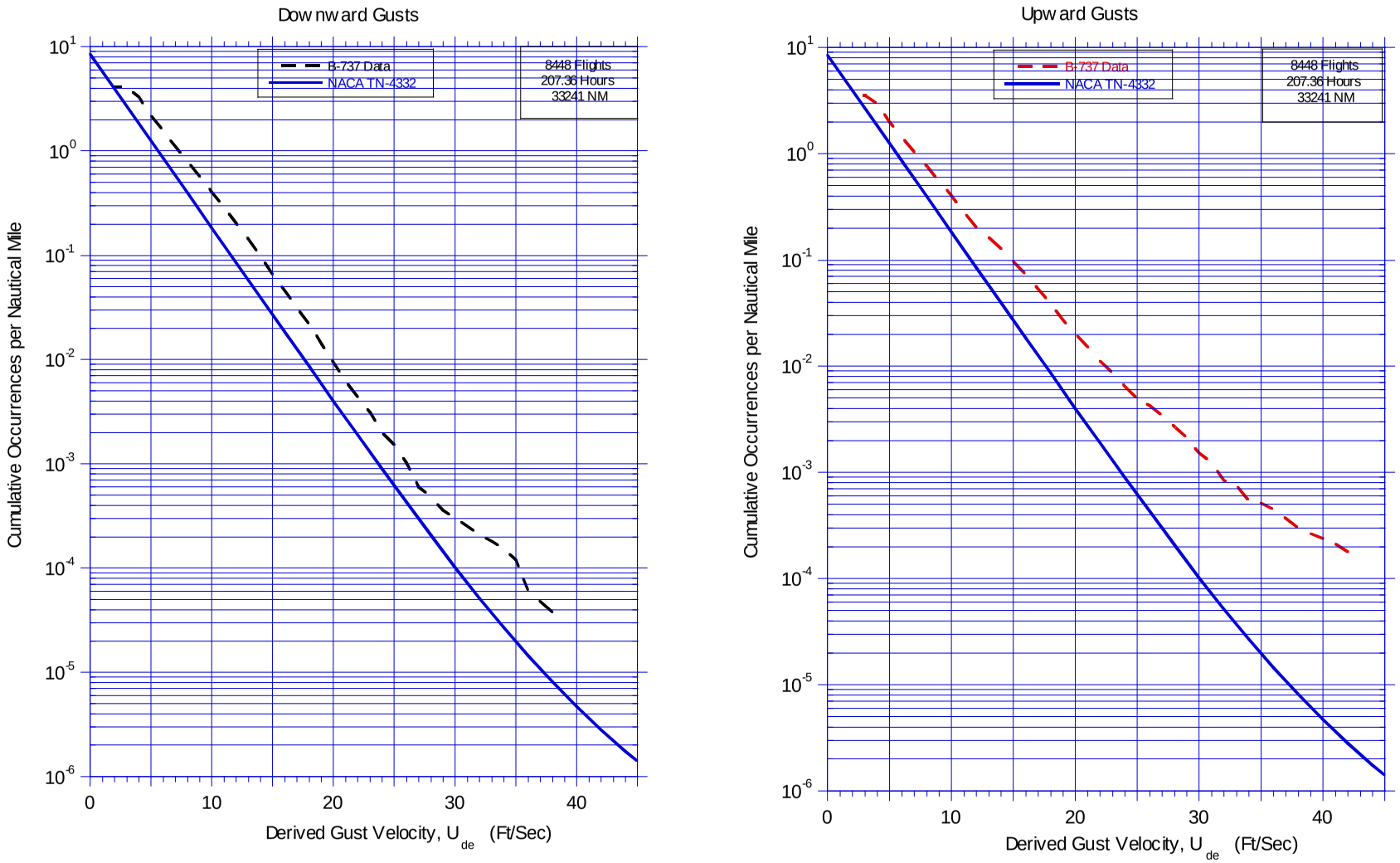

FIGURE A-34. CUMULATIVE OCCURRENCES OF DERIVED GUST VELOCITY PER NAUTICAL MILE, 500-1,500 FEET

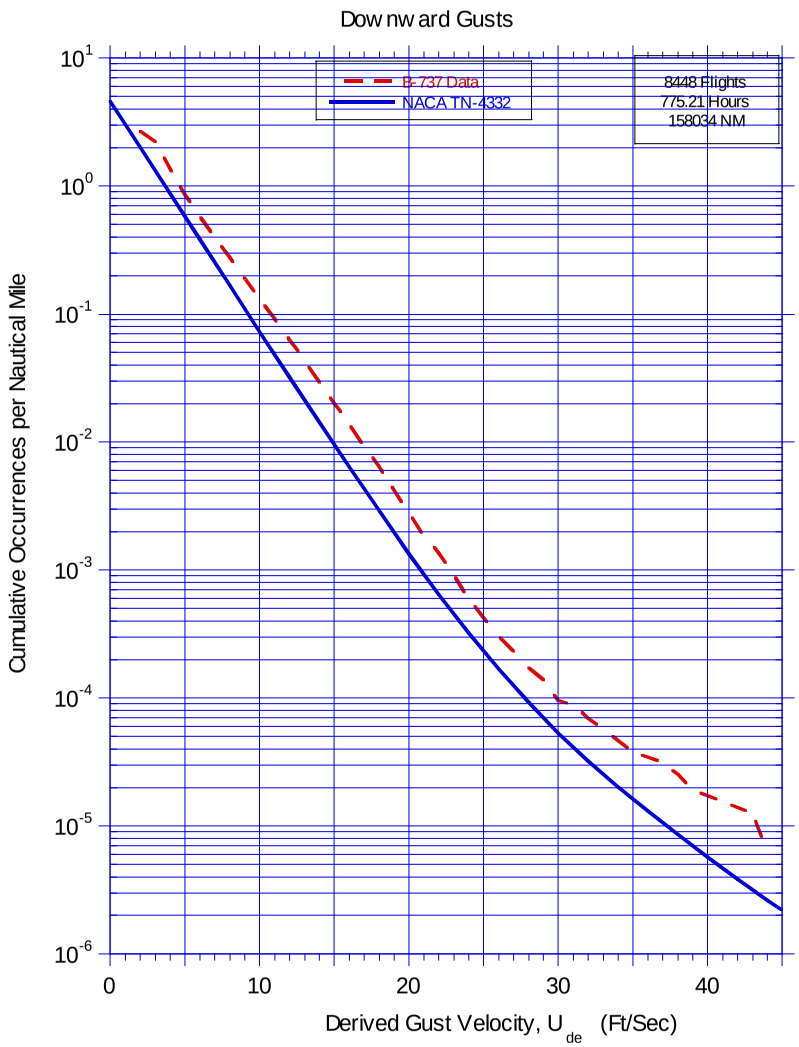

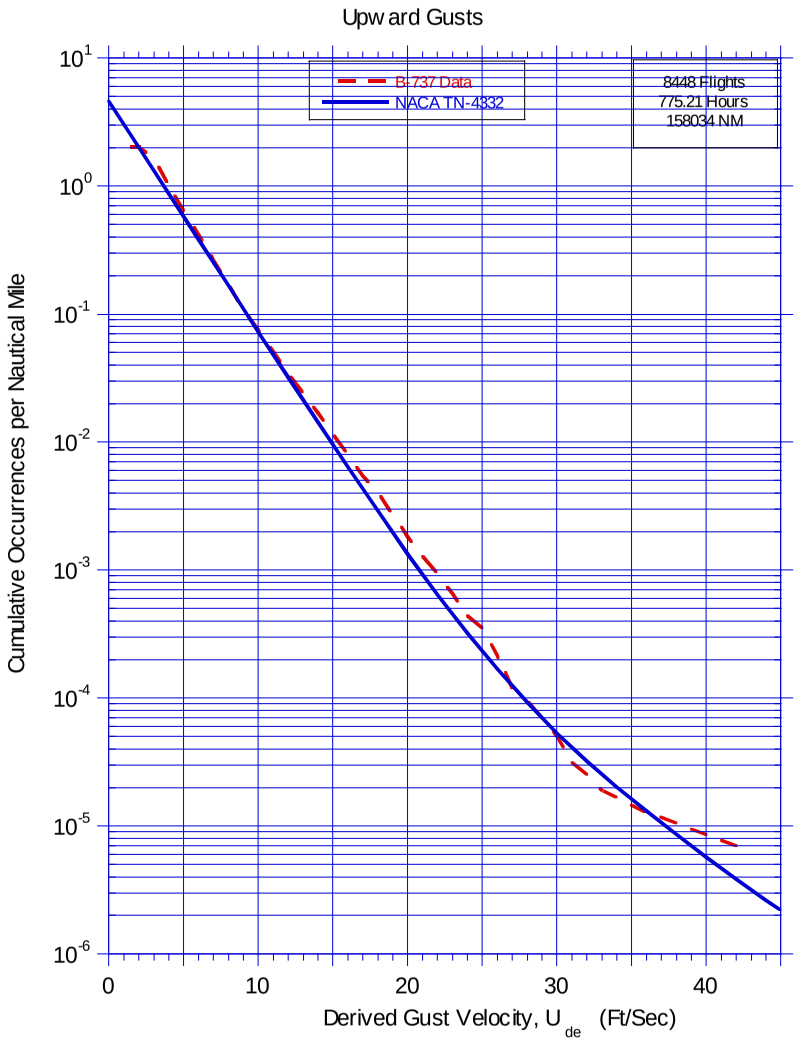

FIGURE A-35. CUMULATIVE OCCURRENCES OF DERIVED GUST VELOCITY PER NAUTICAL MILE, 1,500-4,500 FEET

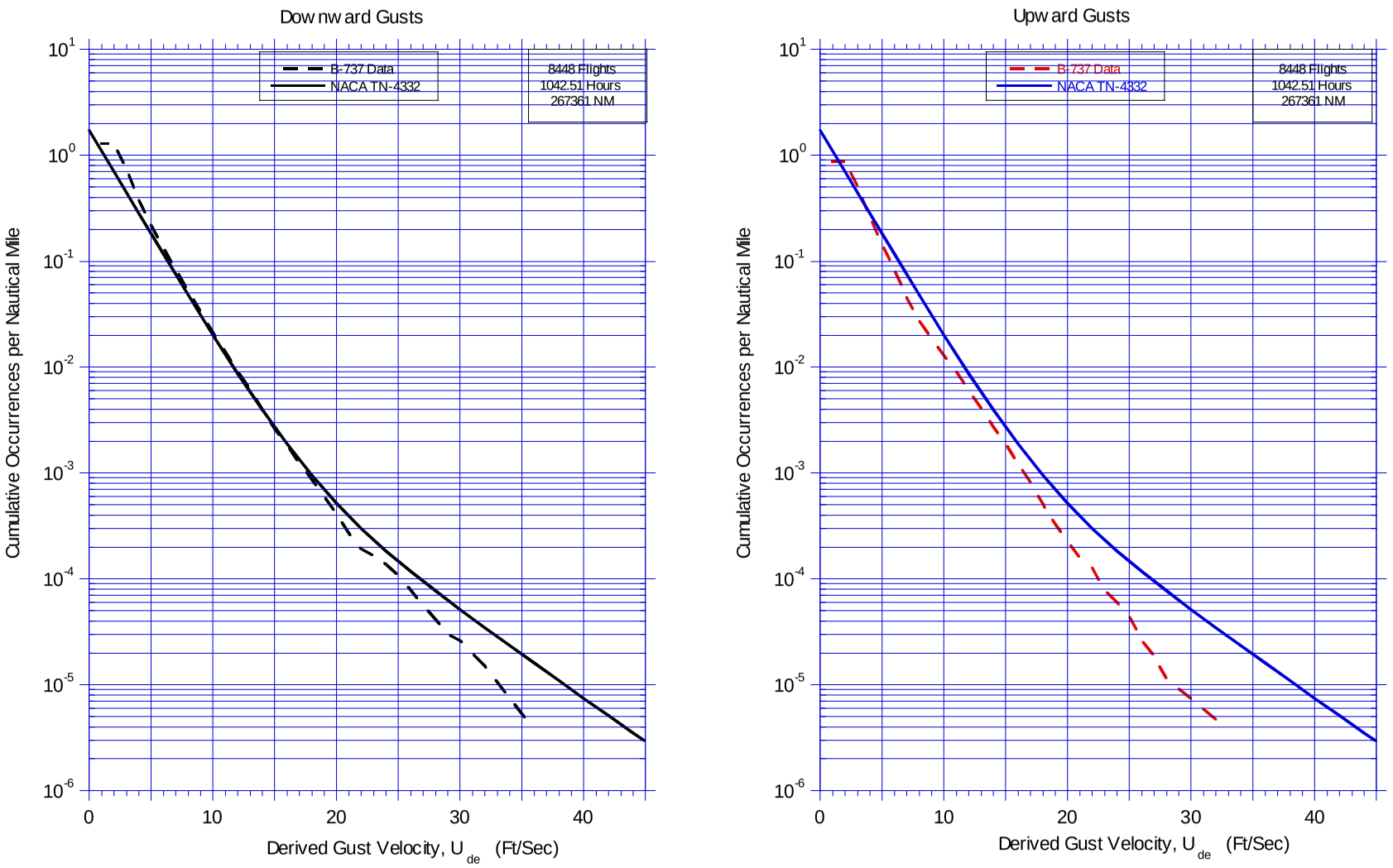

FIGURE A-36. CUMULATIVE OCCURRENCES OF DERIVED GUST VELOCITY PER NAUTICAL MILE, 4,500-9,500 FEET

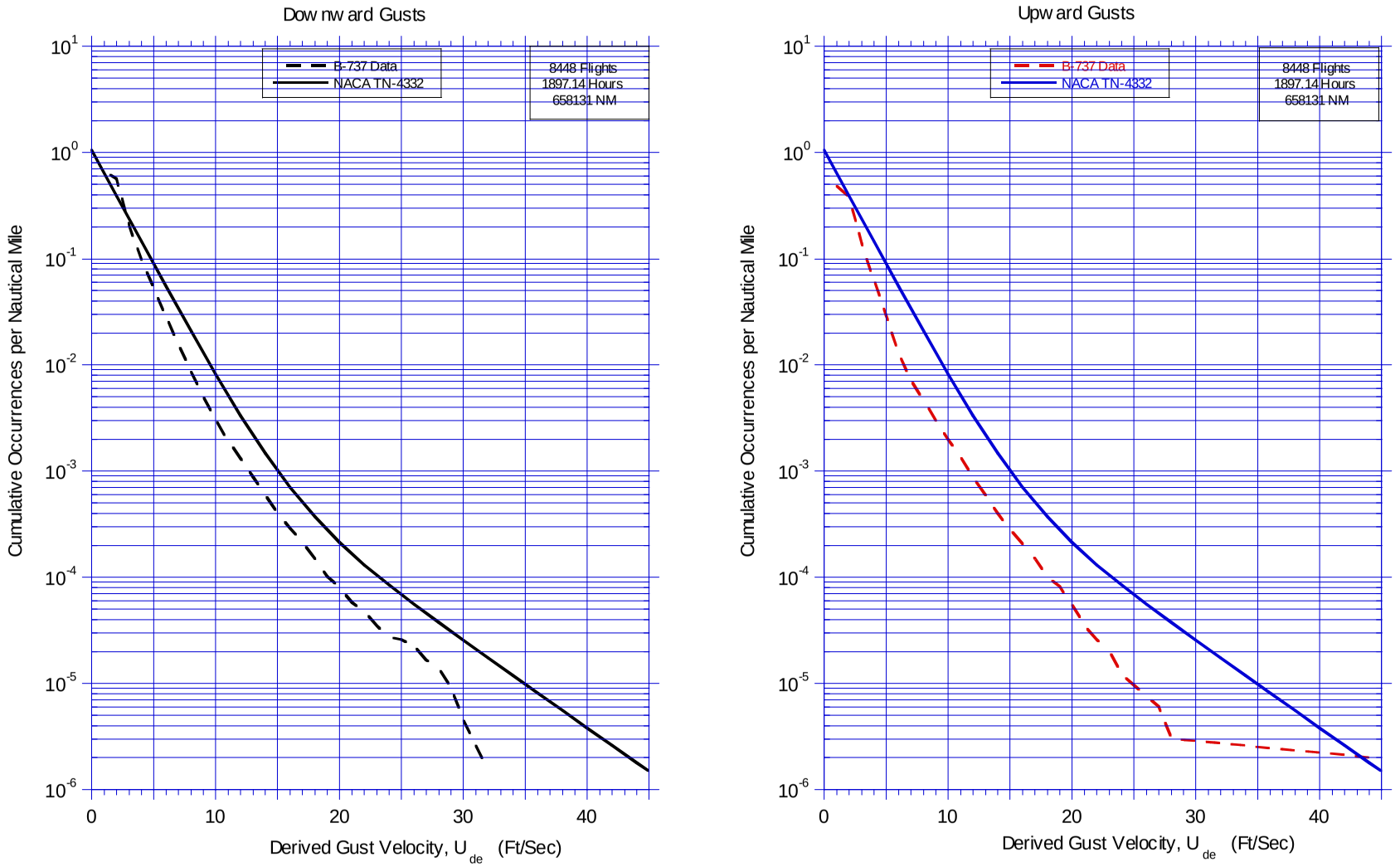

FIGURE A-37. CUMULATIVE OCCURRENCES OF DERIVED GUST VELOCITY PER NAUTICAL MILE, 9,500-19,500 FEET

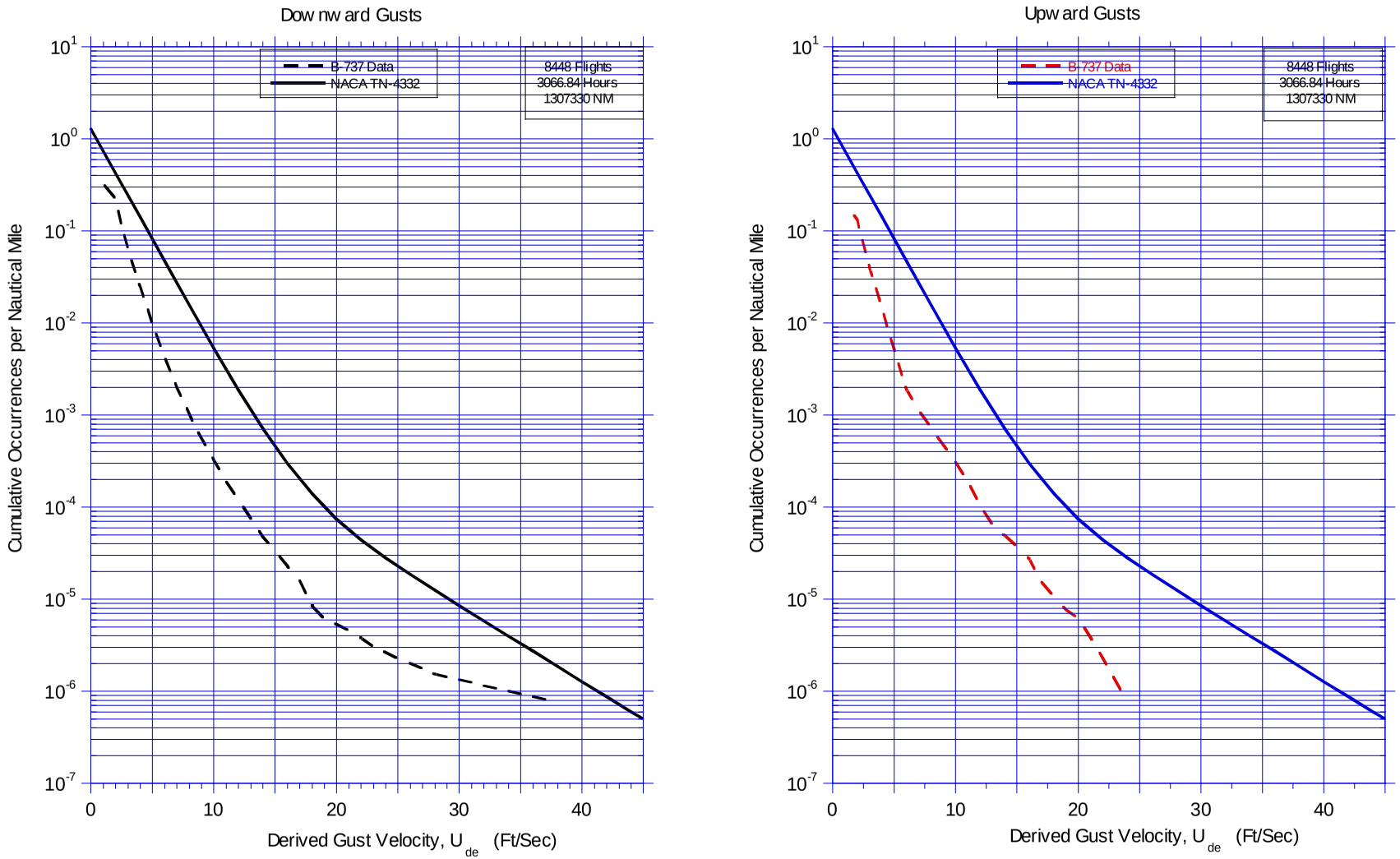

FIGURE A-38. CUMULATIVE OCCURRENCES OF DERIVED GUST VELOCITY PER NAUTICAL MILE, 19,500-29,500 FEET

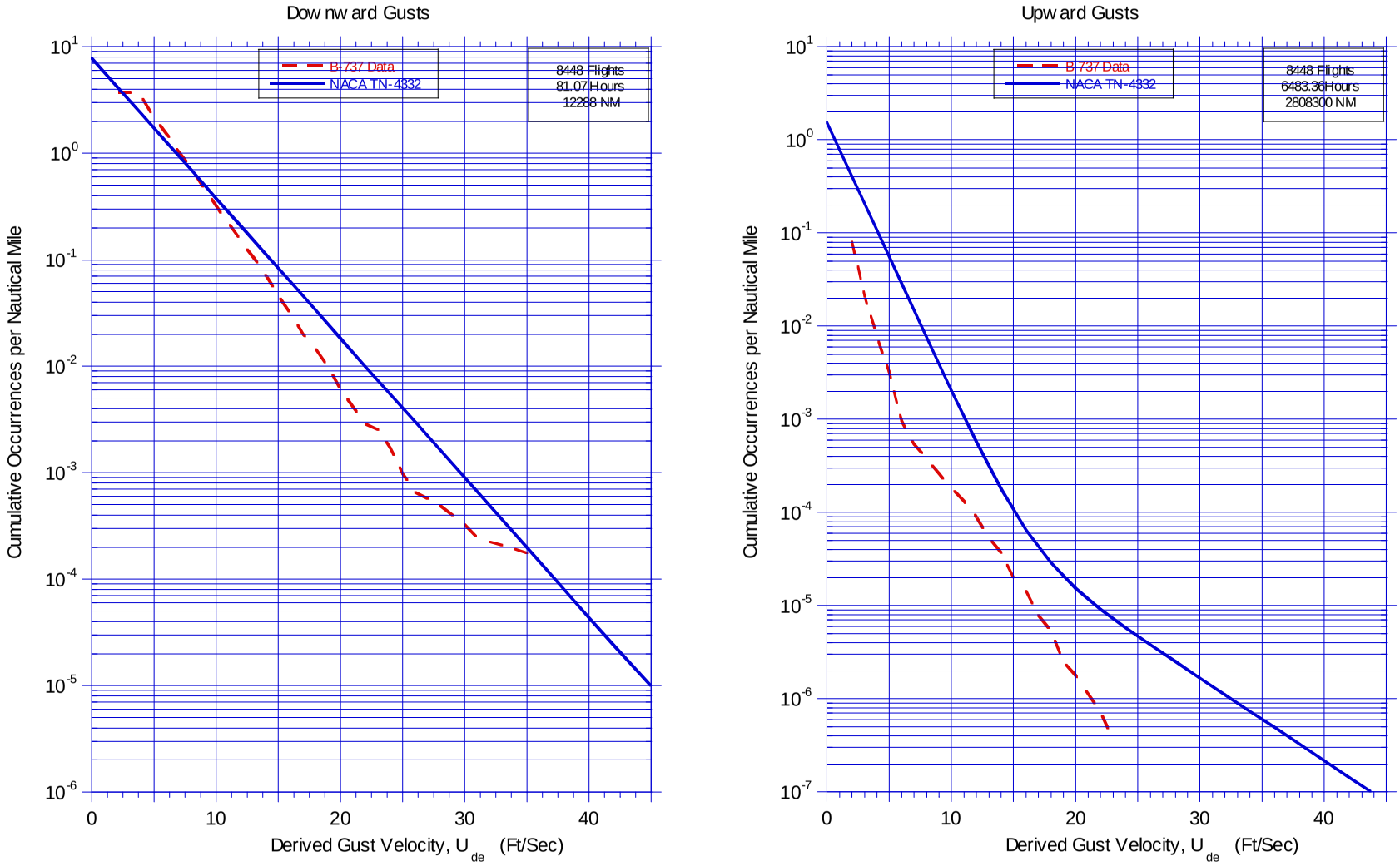

FIGURE A-39. CUMULATIVE OCCURRENCES OF DERIVED GUST VELOCITY PER NAUTICAL MILE, 29,500-39,500 FEET

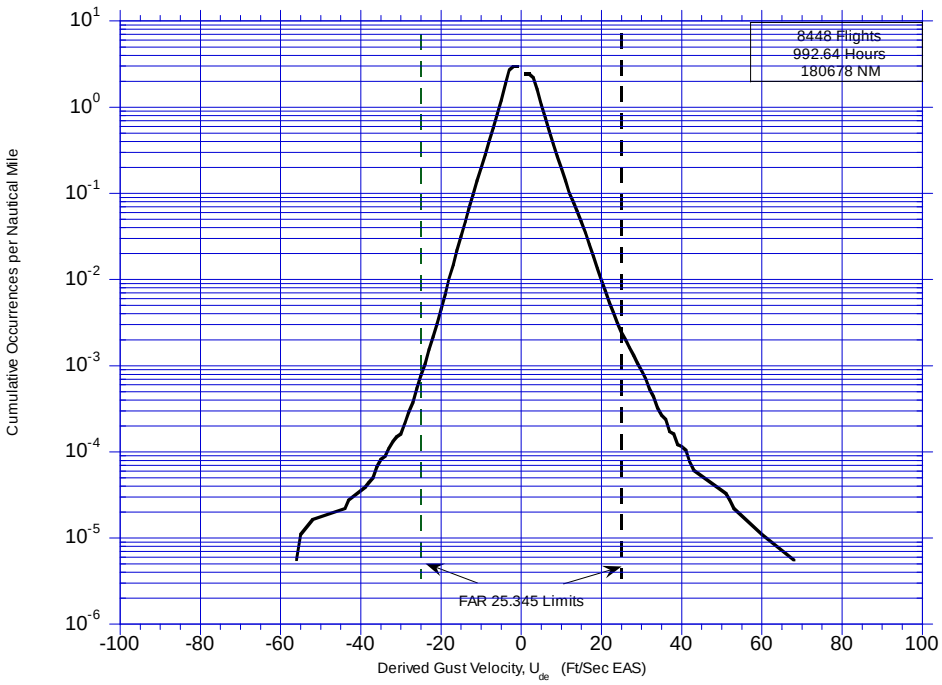

FIGURE A-40. CUMULATIVE OCCURRENCES OF DERIVED GUST VELOCITY PER NAUTICAL MILE, FLAPS EXTENDED

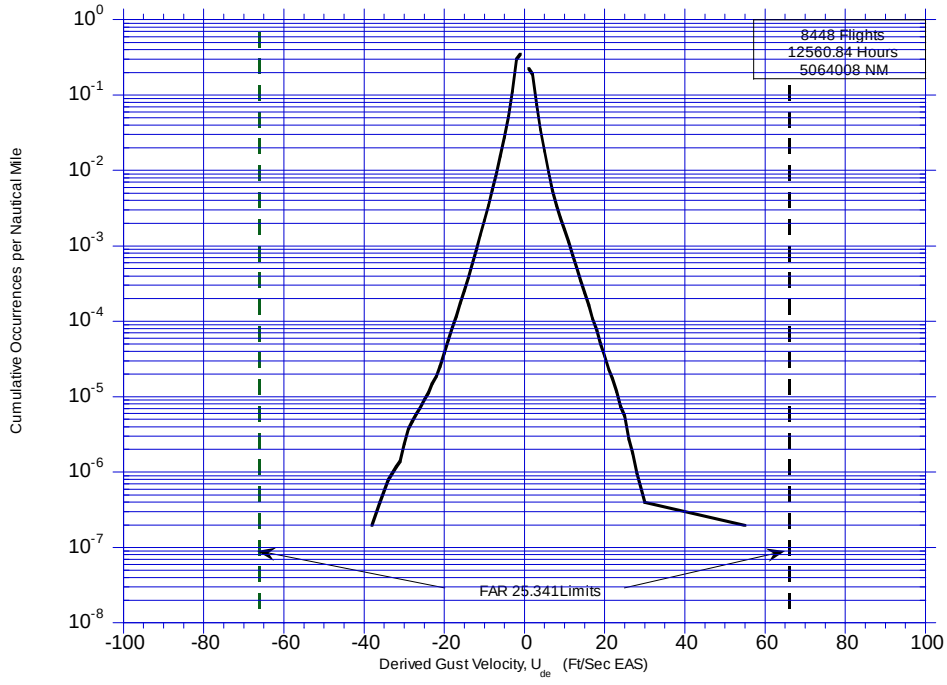

FIGURE A-41. CUMULATIVE OCCURRENCES OF DERIVED GUST VELOCITY PER NAUTICAL MILE, FLAPS RETRACTED

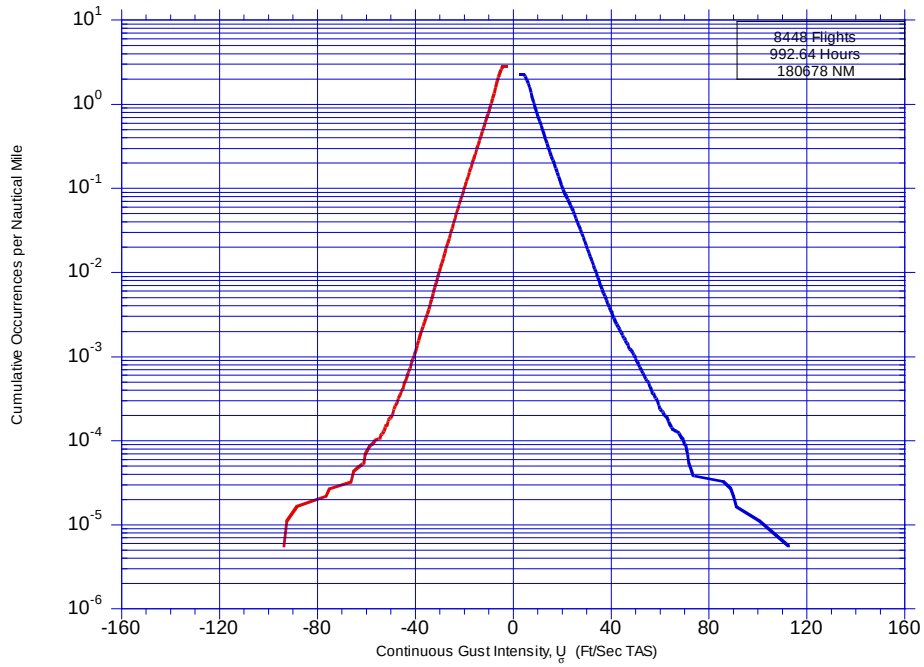

FIGURE A-42. CUMULATIVE OCCURRENCES OF CONTINUOUS GUST INTENSITY PER NAUTICAL MILE, FLAPS EXTENDED

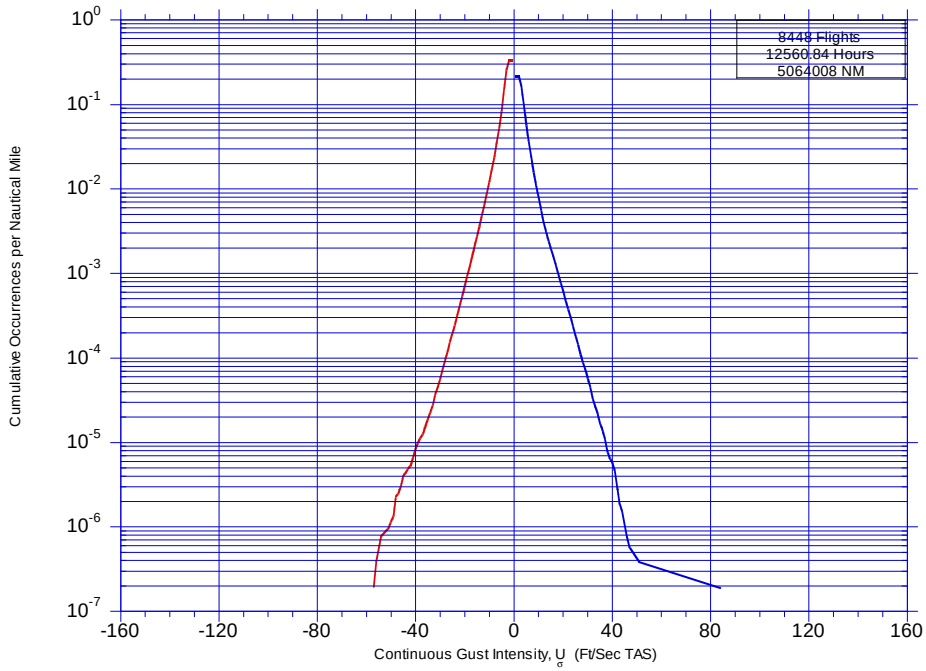

FIGURE A-43. CUMULATIVE OCCURRENCES OF CONTINUOUS GUST INTENSITY PER NAUTICAL MILE, FLAPS RETRACTED

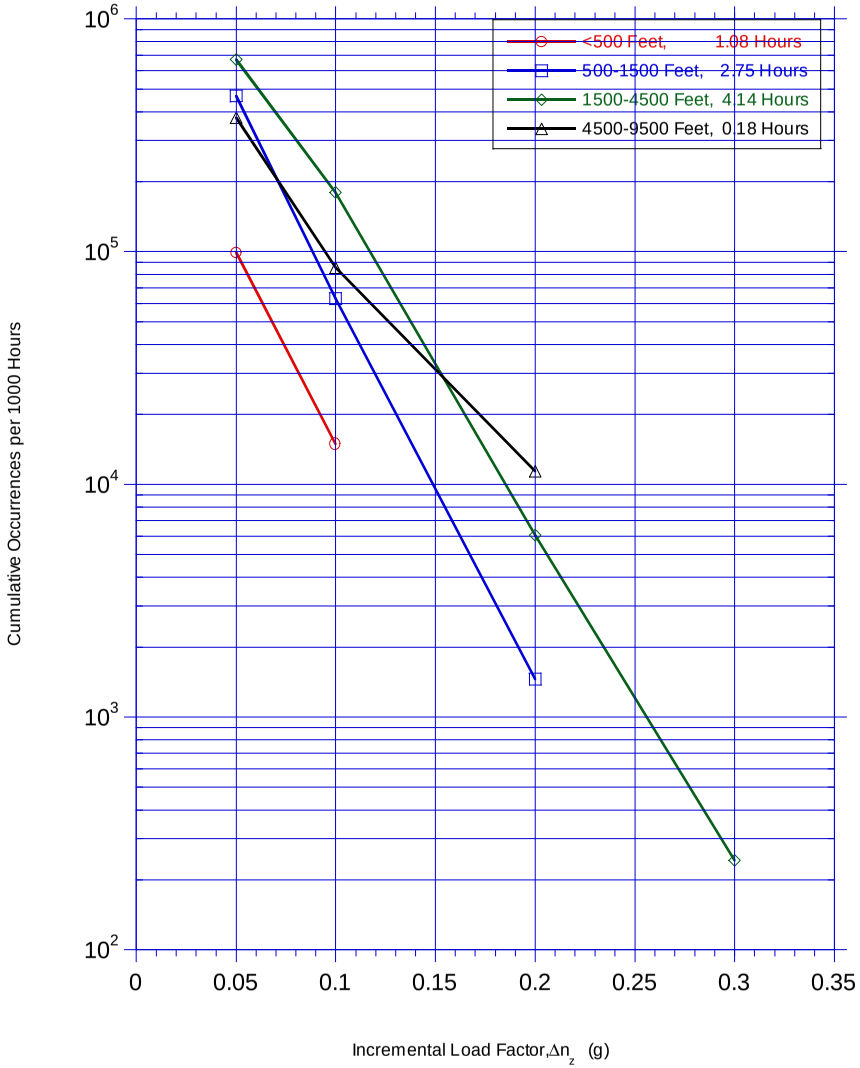

FIGURE A-44. CUMULATIVE OCCURRENCES OF INCREMENTAL MANEUVER LOAD FACTOR PER 1000 HOURS DURING DEPARTURE BY ALTITUDE

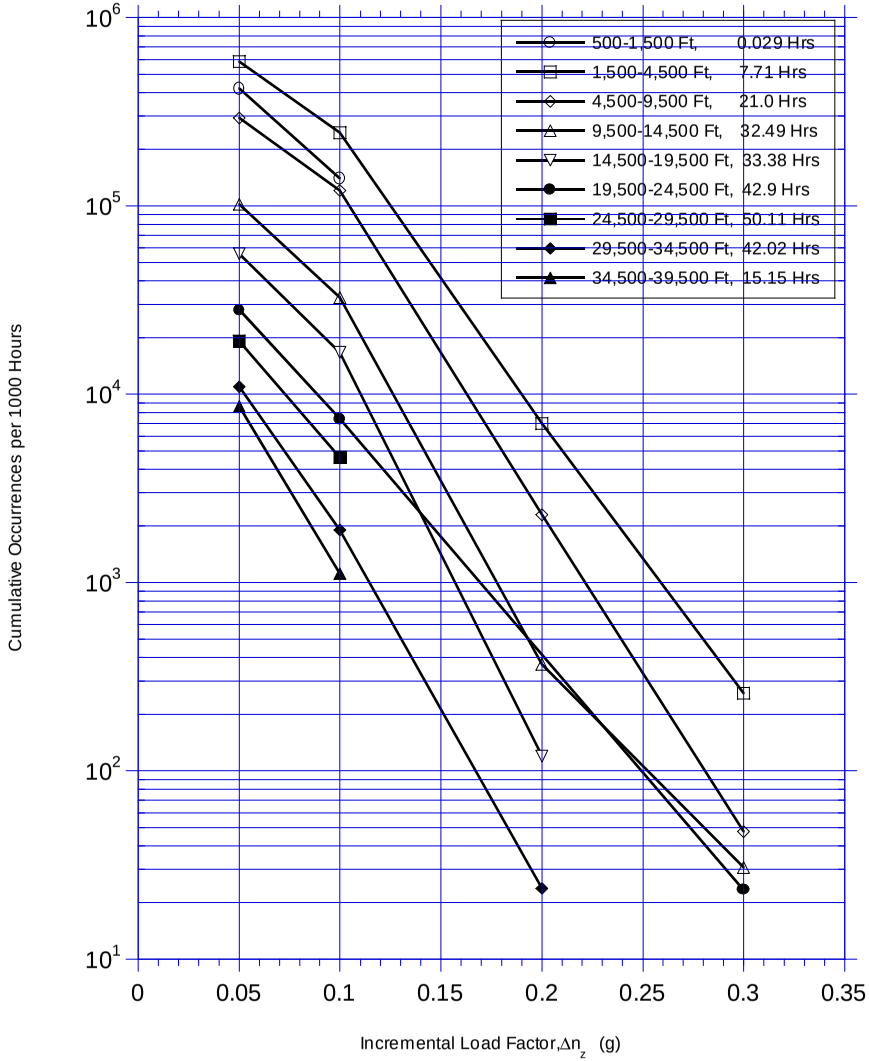

FIGURE A-45. CUMULATIVE OCCURRENCES OF INCREMENTAL MANEUVER LOAD FACTOR PER 1000 HOURS DURING CLIMB BY ALTITUDE

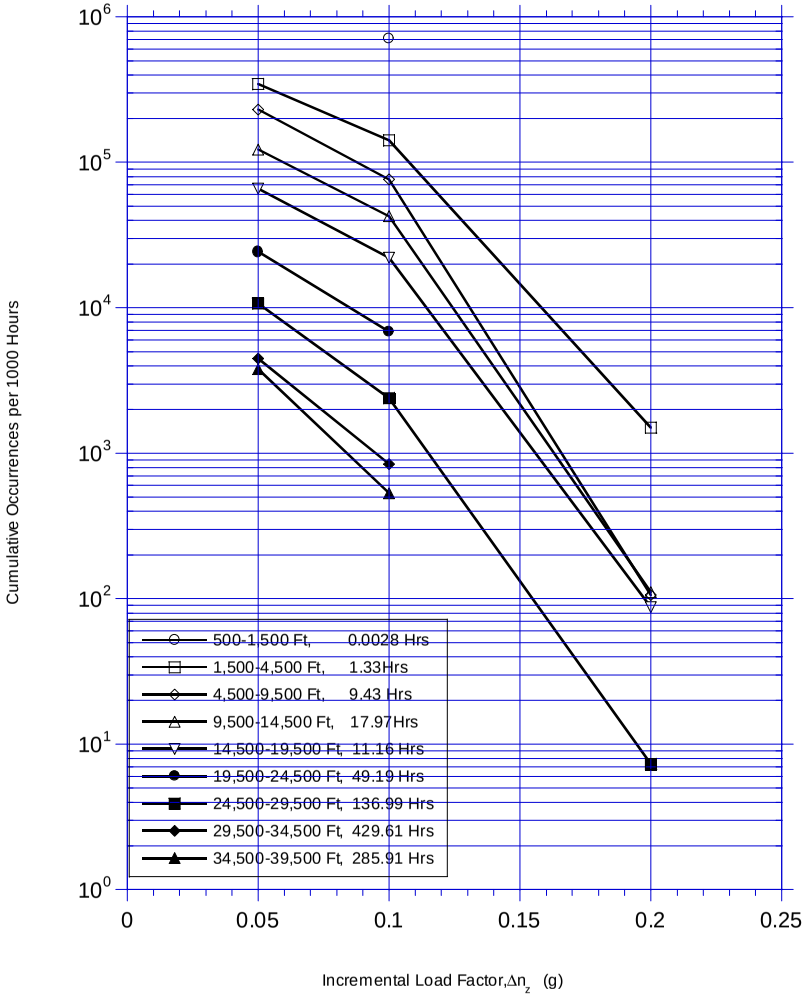

FIGURE A-46. CUMULATIVE OCCURRENCES OF INCREMENTAL MANEUVER LOAD FACTOR PER 1000 HOURS DURING CRUISE BY ALTITUDE

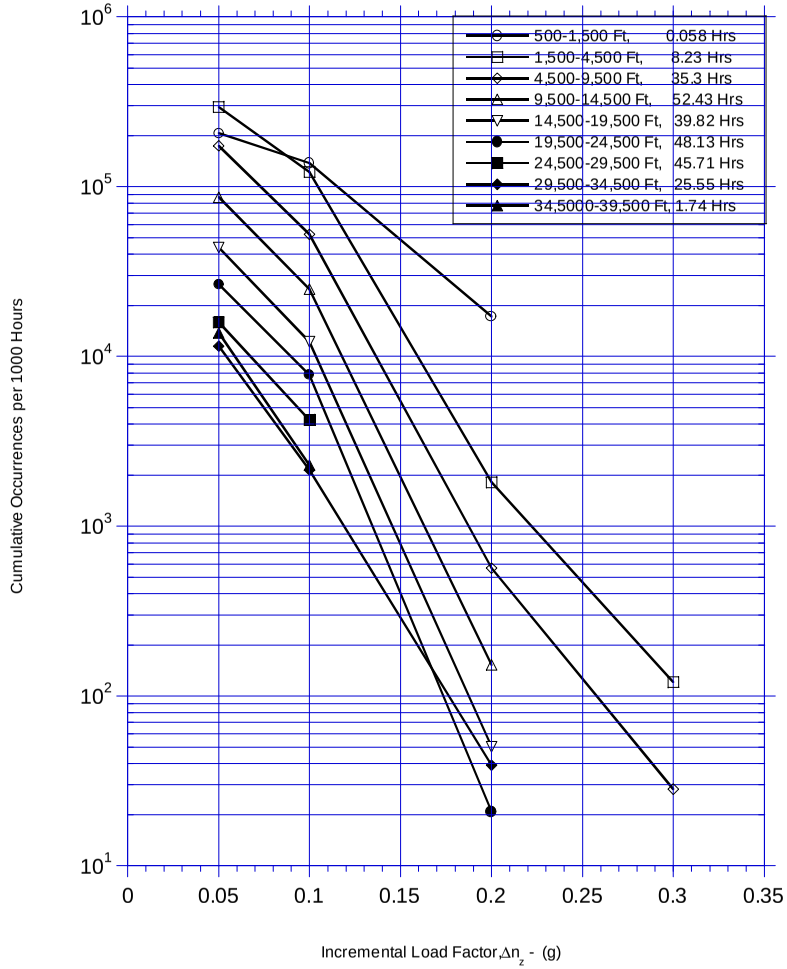

FIGURE A-47. CUMULATIVE OCCURRENCES OF MANEUVER LOAD FACTOR PER 1000 HOURS DURING DESCENT BY ALTITUDE

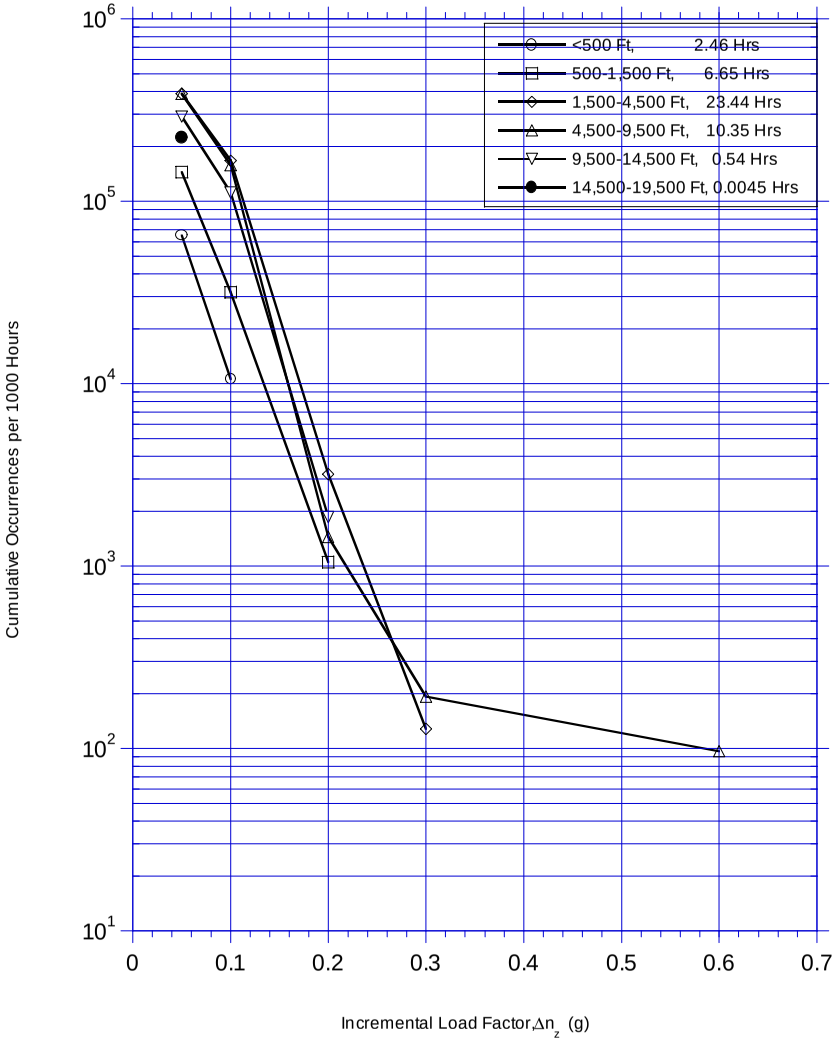

FIGURE A-48. CUMULATIVE OCCURRENCES OF MANEUVER LOAD FACTOR PER 1000 HOURS DURING APPROACH BY ALTITUDE

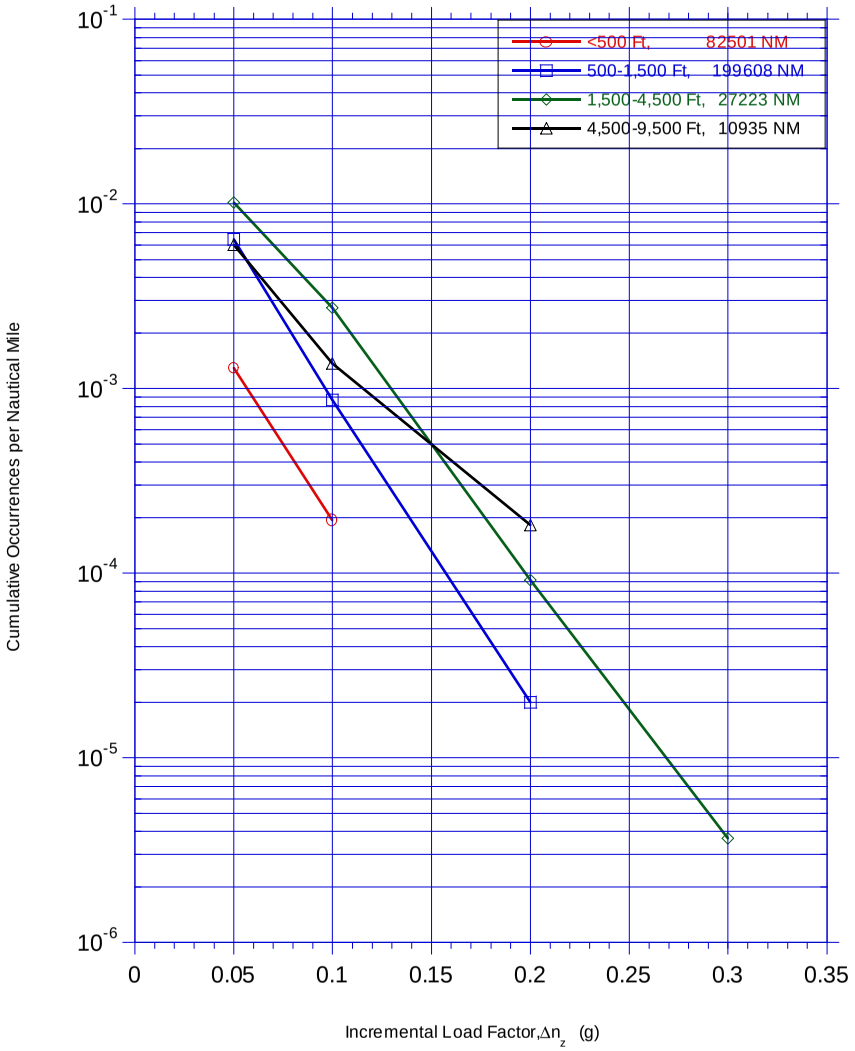

FIGURE A-49. CUMULATIVE OCCURRENCES OF MANEUVER LOAD FACTOR PER NAUTICAL MILE DURING DEPARTURE BY ALTITUDE

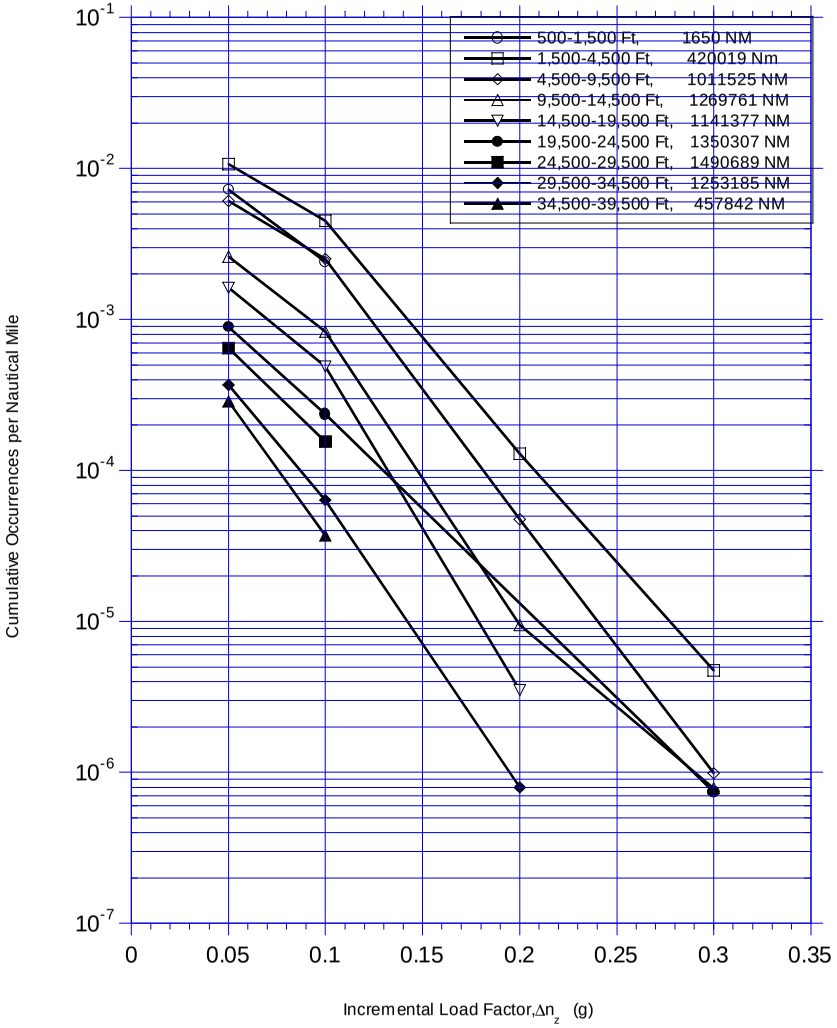

FIGURE A-50. CUMULATIVE OCCURRENCES OF MANEUVER LOAD FACTOR PER NAUTICAL MILE DURING CLIMB BY ALTITUDE

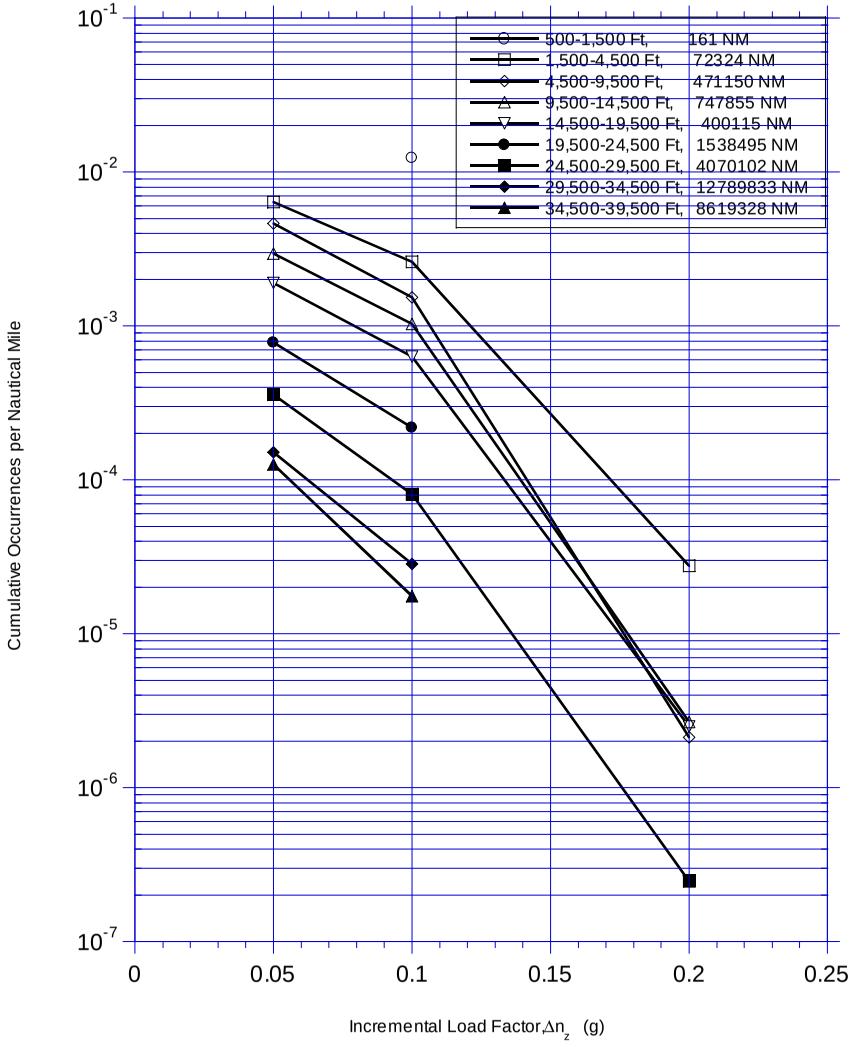

FIGURE A-51. CUMULATIVE OCCURRENCES OF MANEUVER LOAD FACTOR PER NAUTICAL MILE DURING CRUISE BY ALTITUDE

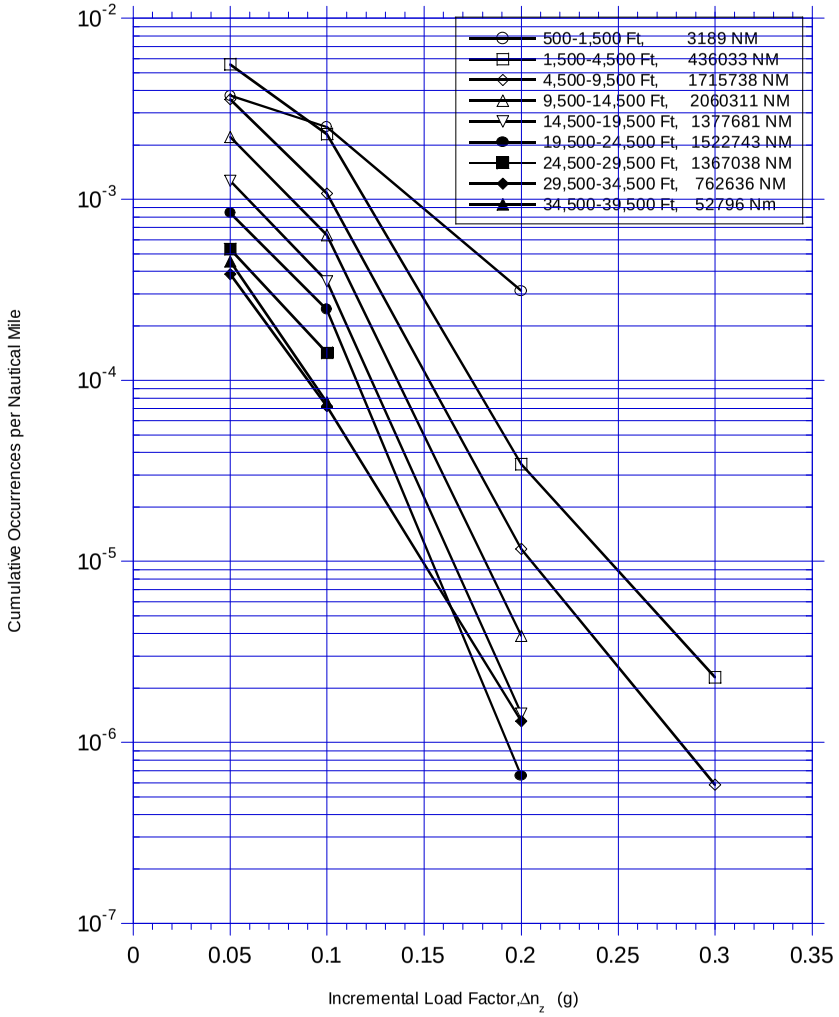

FIGURE A-52. CUMULATIVE OCCURRENCES OF MANEUVER LOAD FACTOR PER NAUTICAL MILE DURING DESCENT BY ALTITUDE

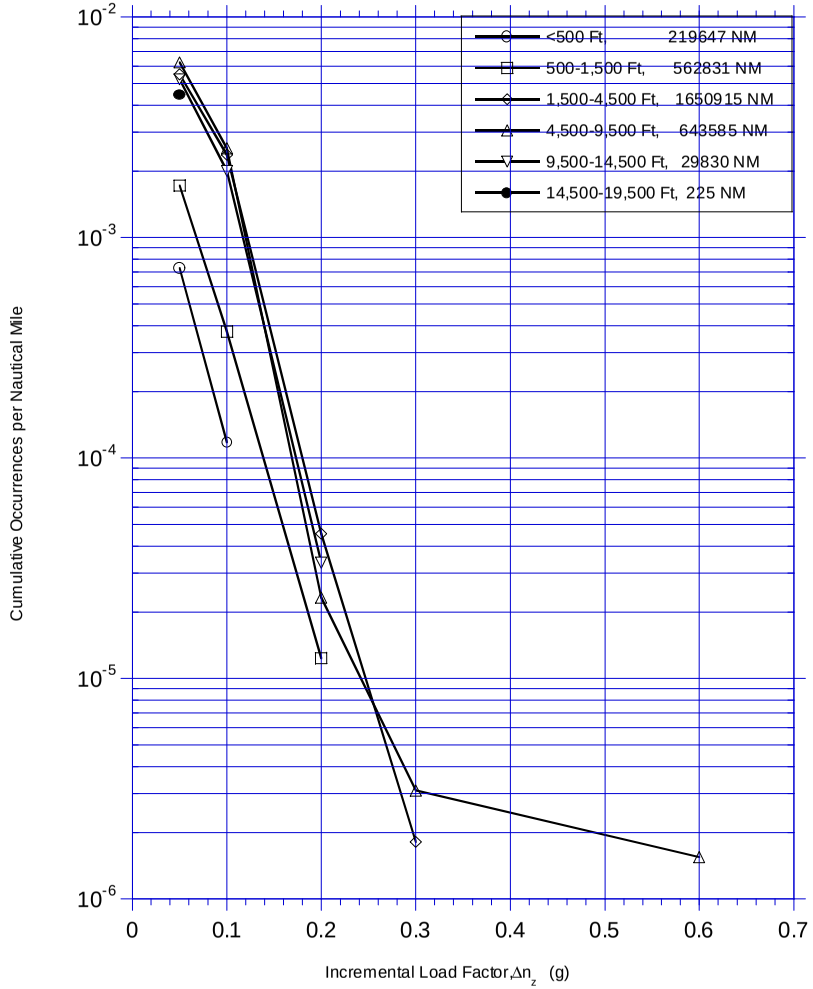

FIGURE A-53. CUMULATIVE OCCURRENCES OF MANEUVER LOAD FACTOR PER NAUTICAL MILE DURING APPROACH BY ALTITUDE

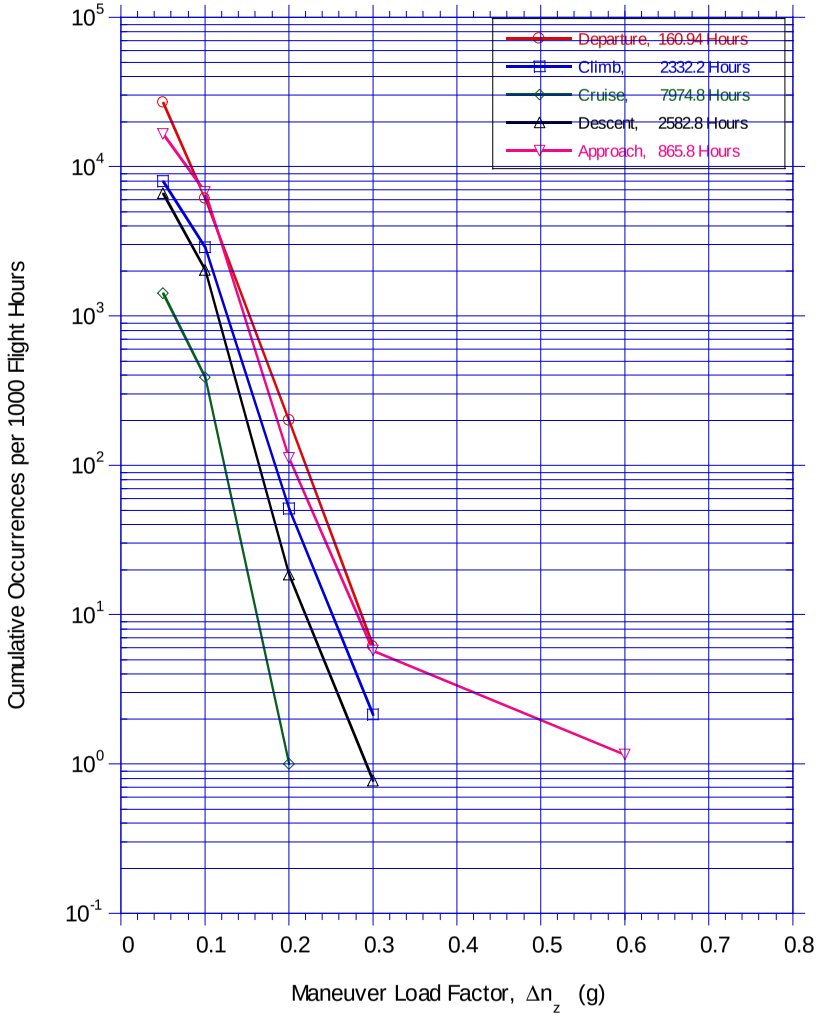

FIGURE A-54. CUMULATIVE OCCURRENCES OF MANEUVER LOAD FACTOR PER 1000 HOURS BY FLIGHT PHASE

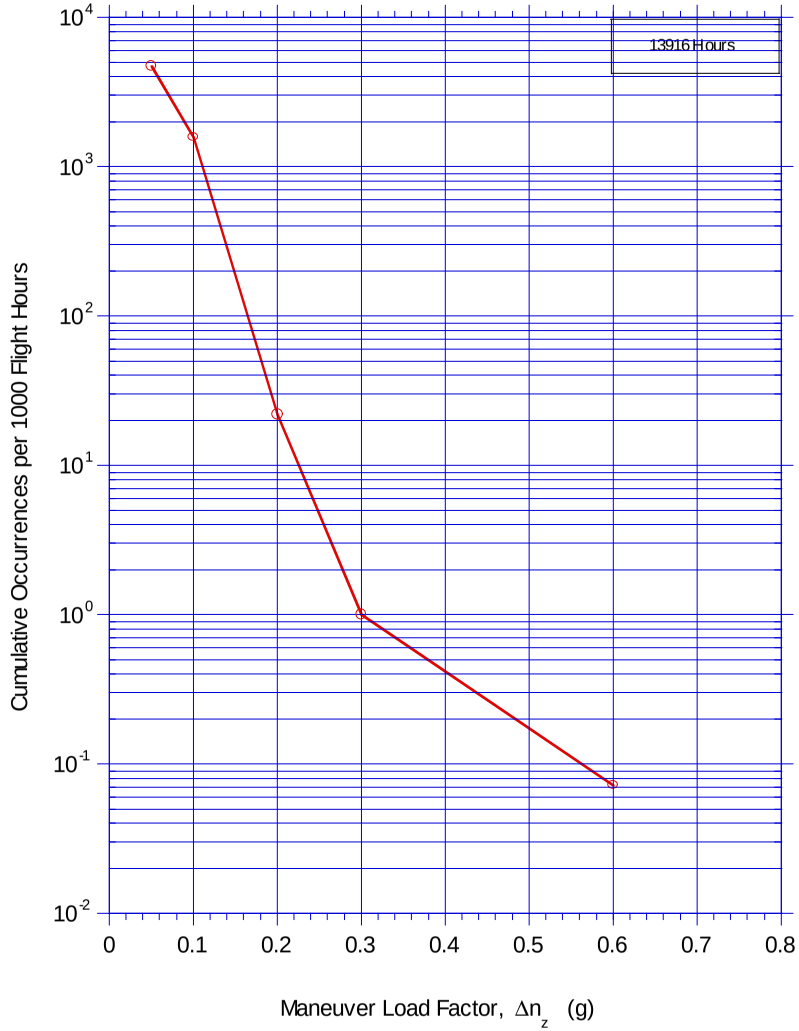

FIGURE A-55. CUMULATIVE OCCURRENCES OF MANEUVER LOAD FACTOR PER 1000 HOURS, COMBINED FLIGHT PHASES

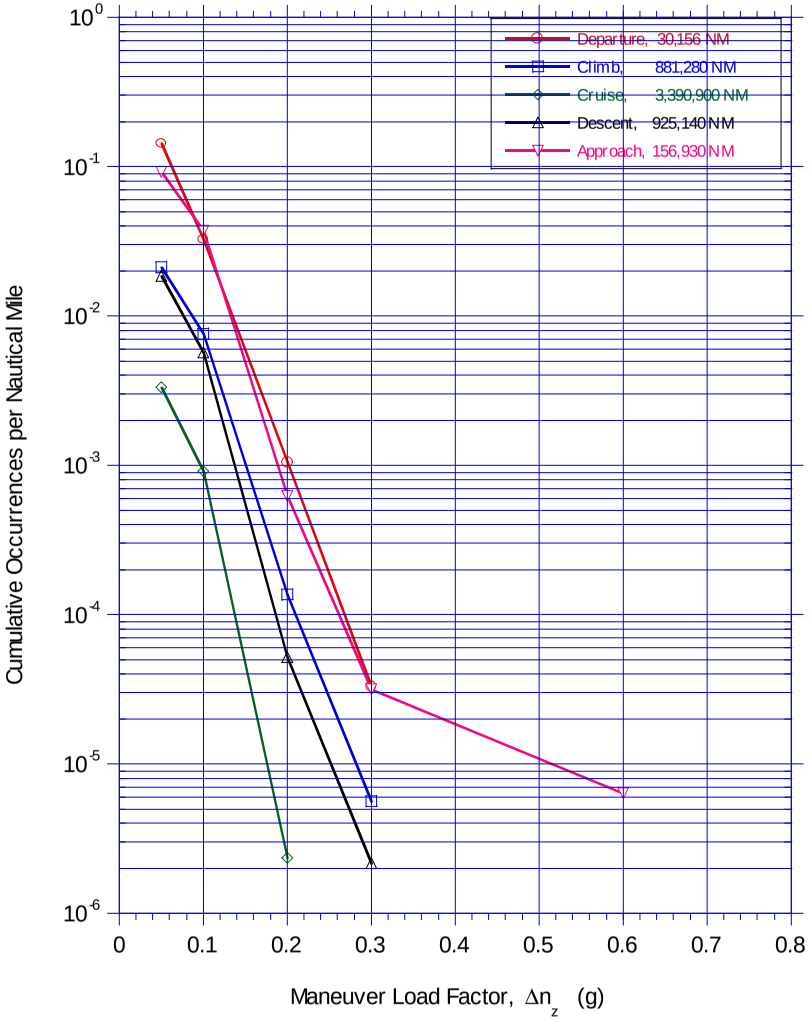

FIGURE A-56. CUMULATIVE OCCURRENCES OF MANEUVER LOAD FACTOR PER NAUTICAL MILE BY FLIGHT PHASE

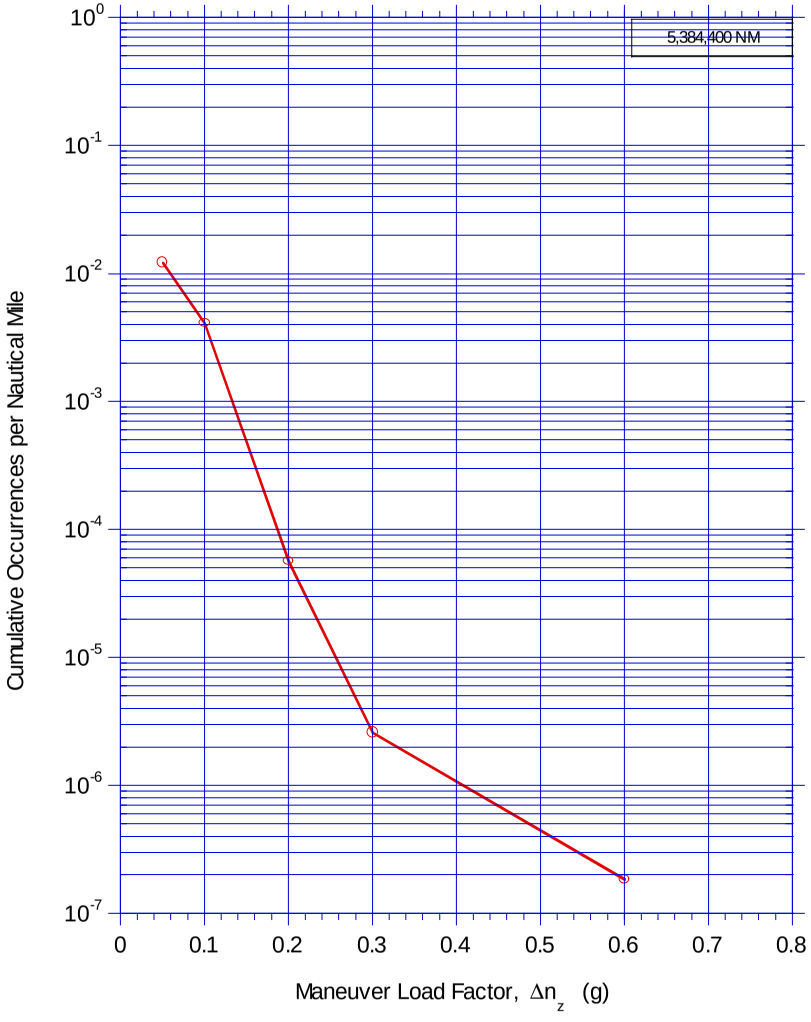

FIGURE A-57. CUMULATIVE OCCURRENCES OF MANEUVER LOAD FACTOR PER NAUTICAL MILE, COMBINED FLIGHT PHASES

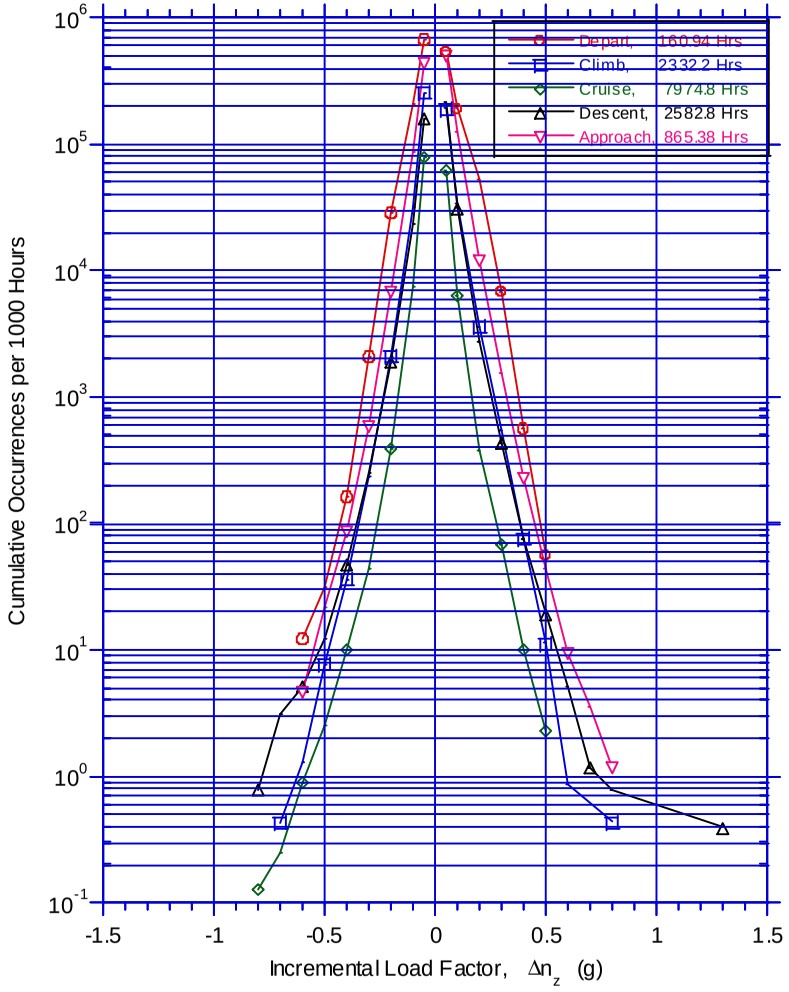

FIGURE A-58. CUMULATIVE OCCURRENCES OF COMBINED MANEUVER AND GUST VERTICAL LOAD FACTOR PER 1000 HOURS BY FLIGHT PHASE

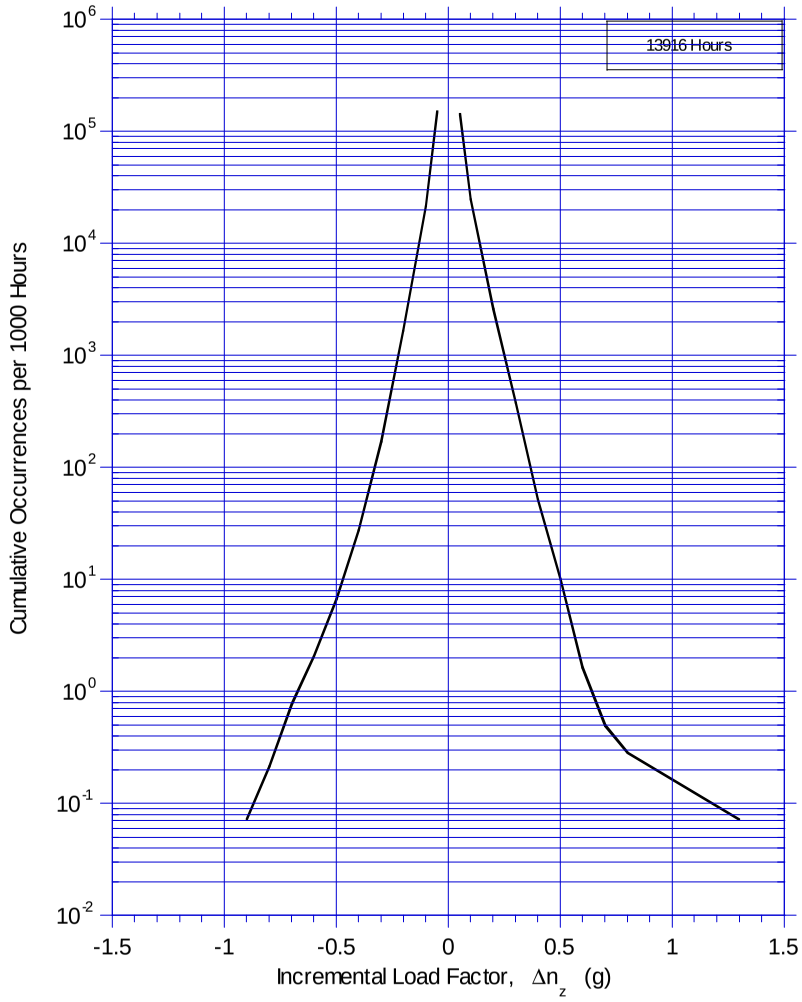

FIGURE A-59. CUMULATIVE OCCURRENCES OF VERTICAL LOAD FACTOR PER 1000 HOURS, COMBINED FLIGHT PHASES

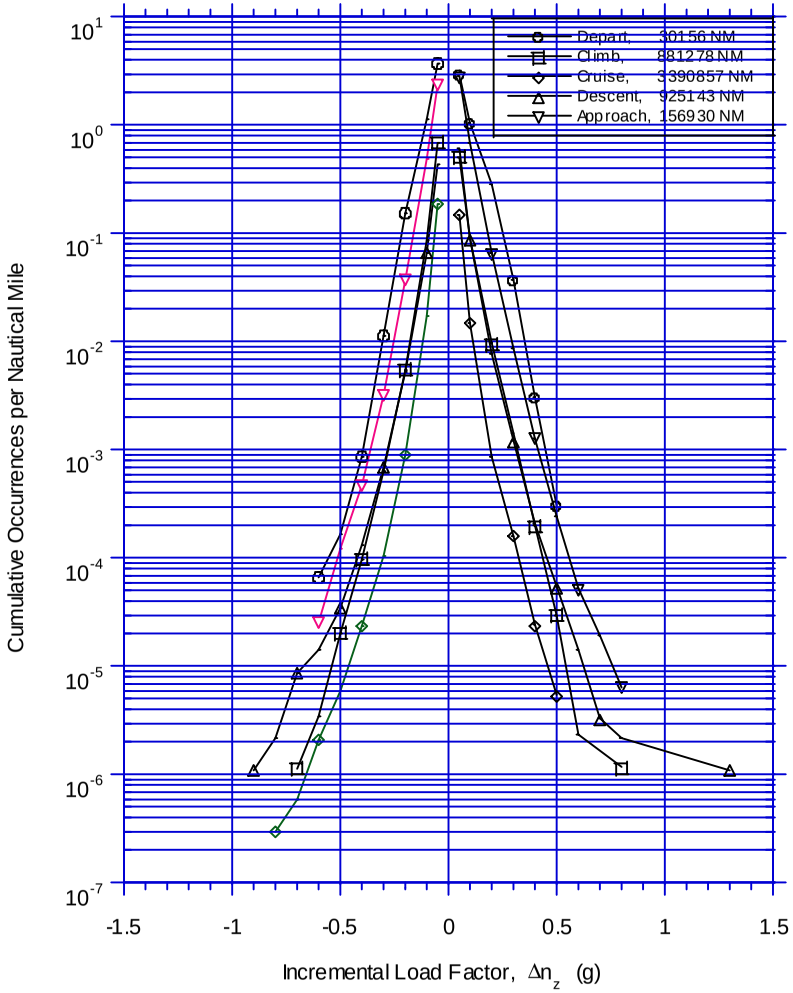

FIGURE A-60. CUMULATIVE OCCURRENCES OF VERTICAL LOAD FACTOR PER NAUTICAL MILE BY FLIGHT PHASE

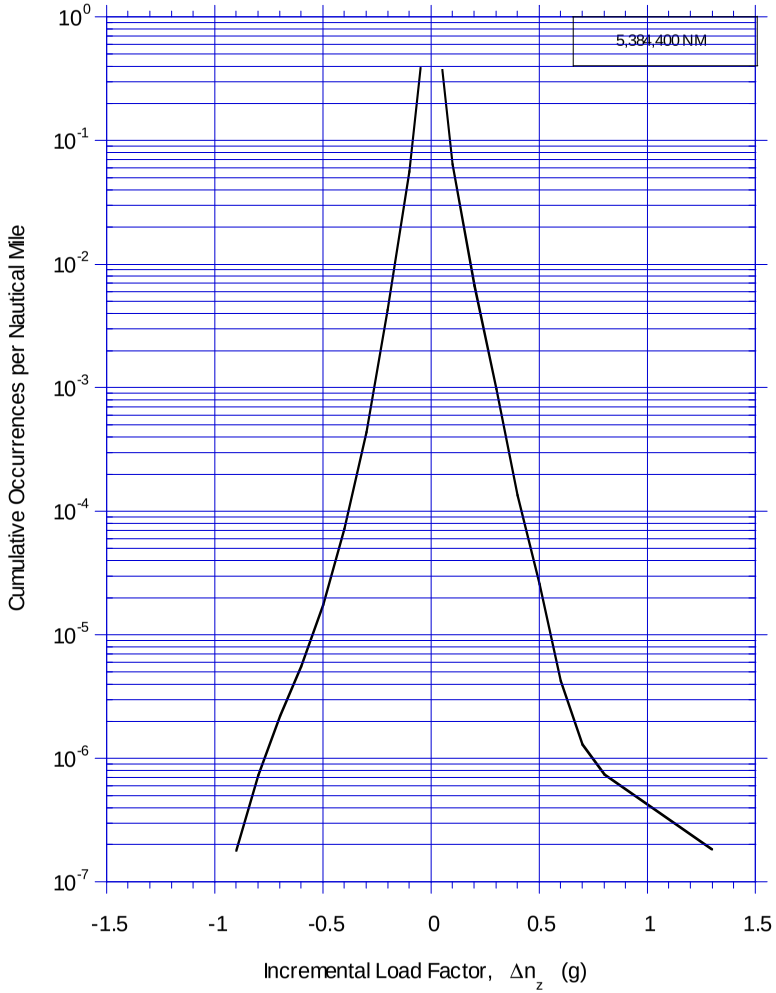

FIGURE A-61. CUMULATIVE OCCURRENCES OF VERTICAL LOAD FACTOR PER NAUTICAL MILE, COMBINED FLIGHT PHASES

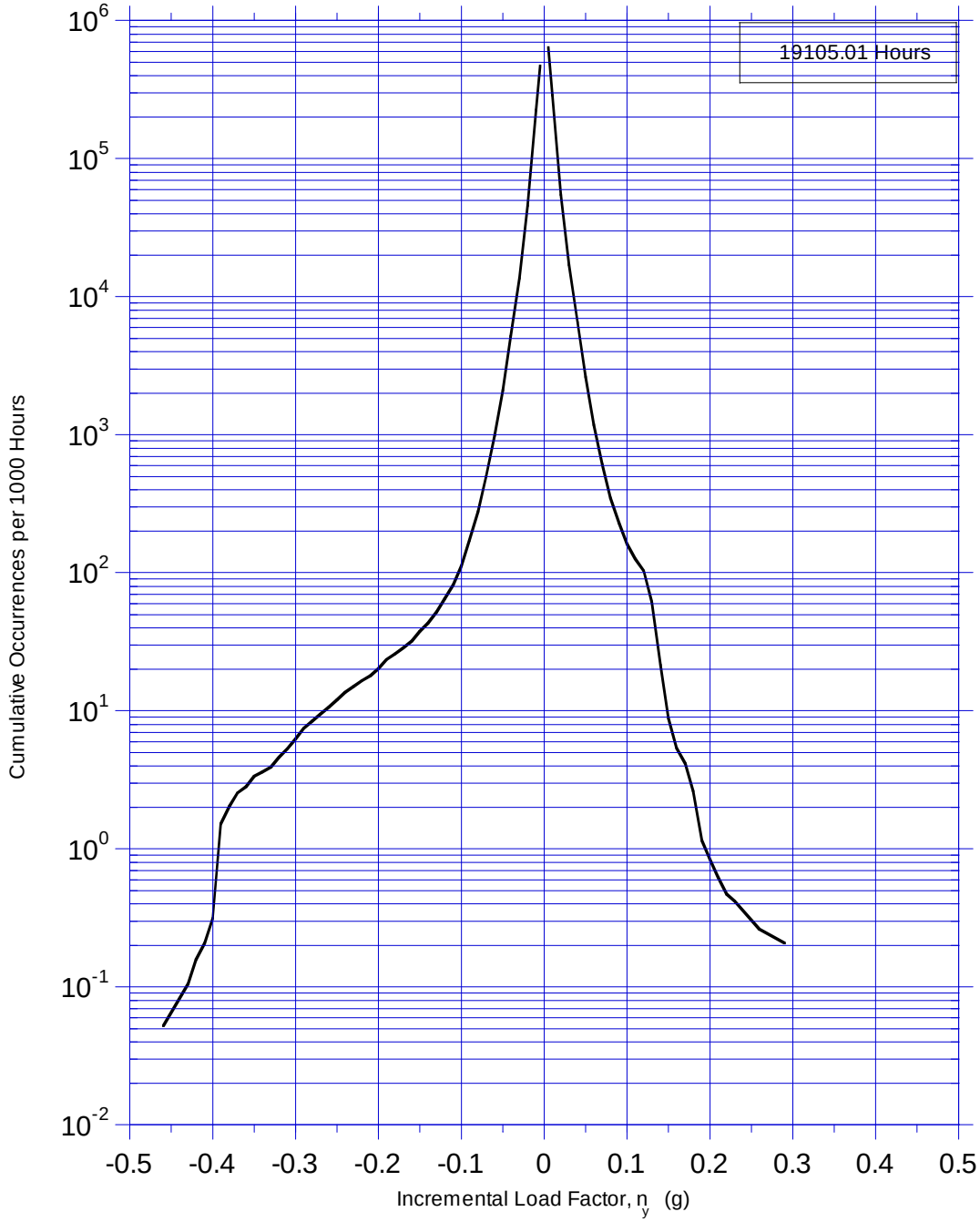

FIGURE A-62. CUMULATIVE OCCURRENCES OF LATERAL LOAD FACTOR PER 1000 HOURS, COMBINED FLIGHT PHASES

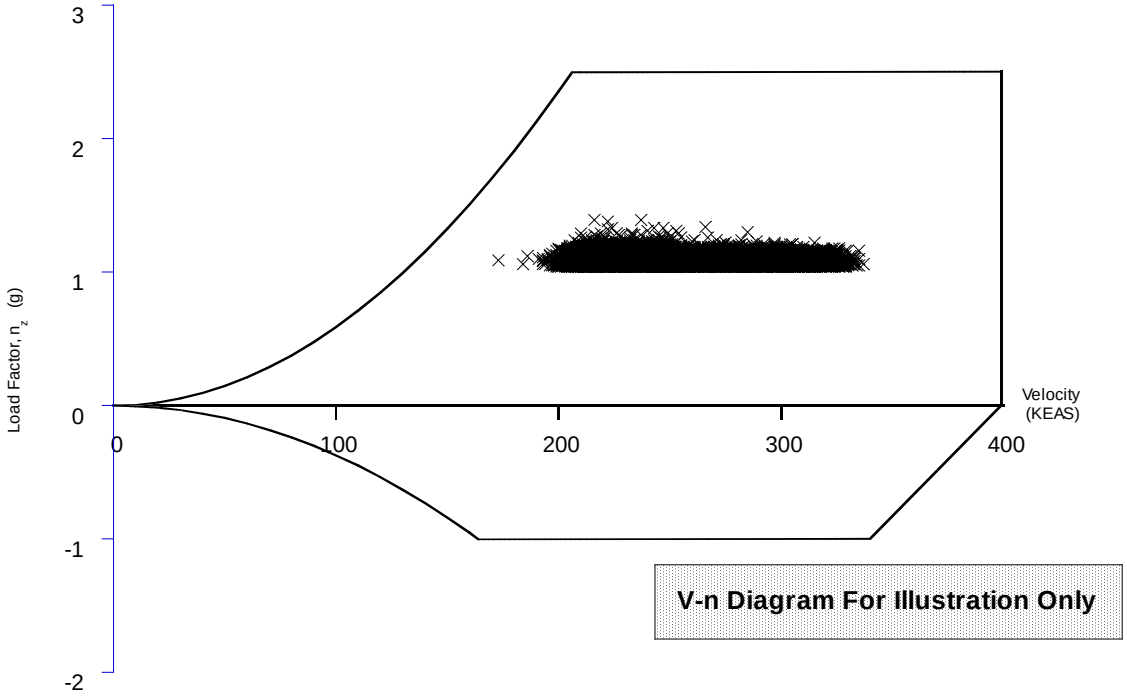

FIGURE A-63. COINCIDENT MANEUVER LOAD FACTOR AND SPEED VERSUS V-n DIAGRAM FOR FLAPS RETRACTED

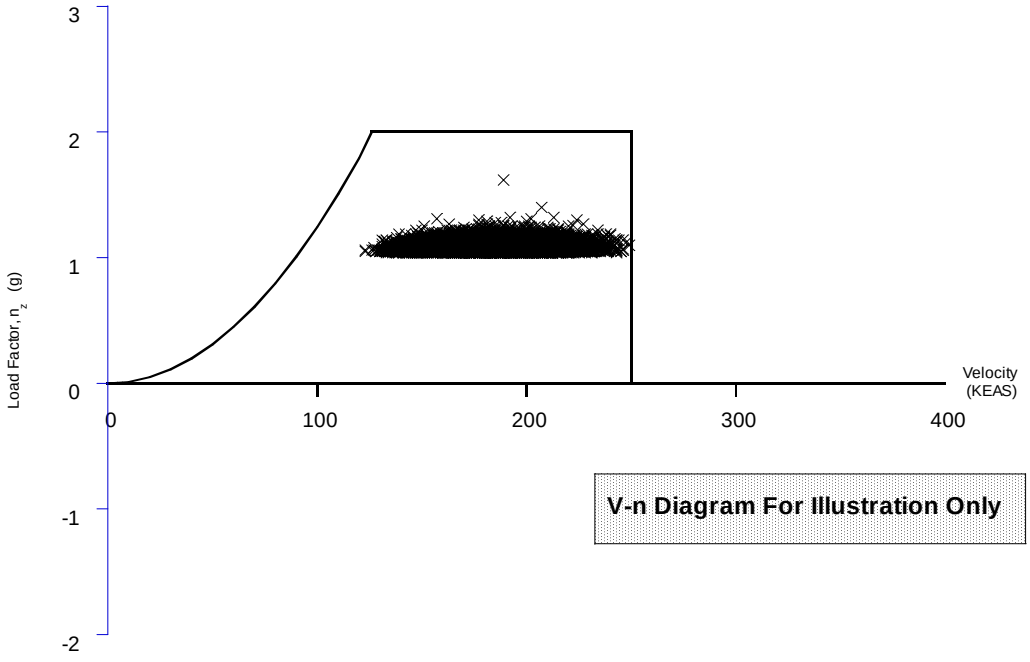

FIGURE A-64. COINCIDENT MANEUVER LOAD FACTOR AND SPEED VERSUS V-n DIAGRAM FOR FLAPS EXTENDED

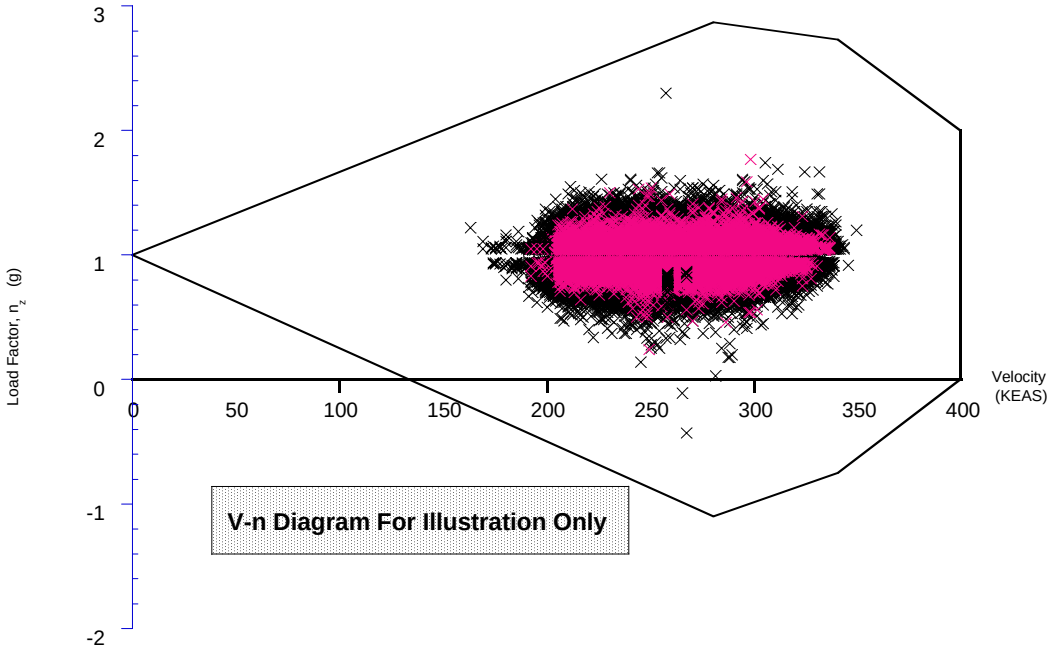

FIGURE A-65. COINCIDENT GUST LOAD FACTOR AND SPEED VERSUS V-n DIAGRAM FOR FLAPS RETRACTED

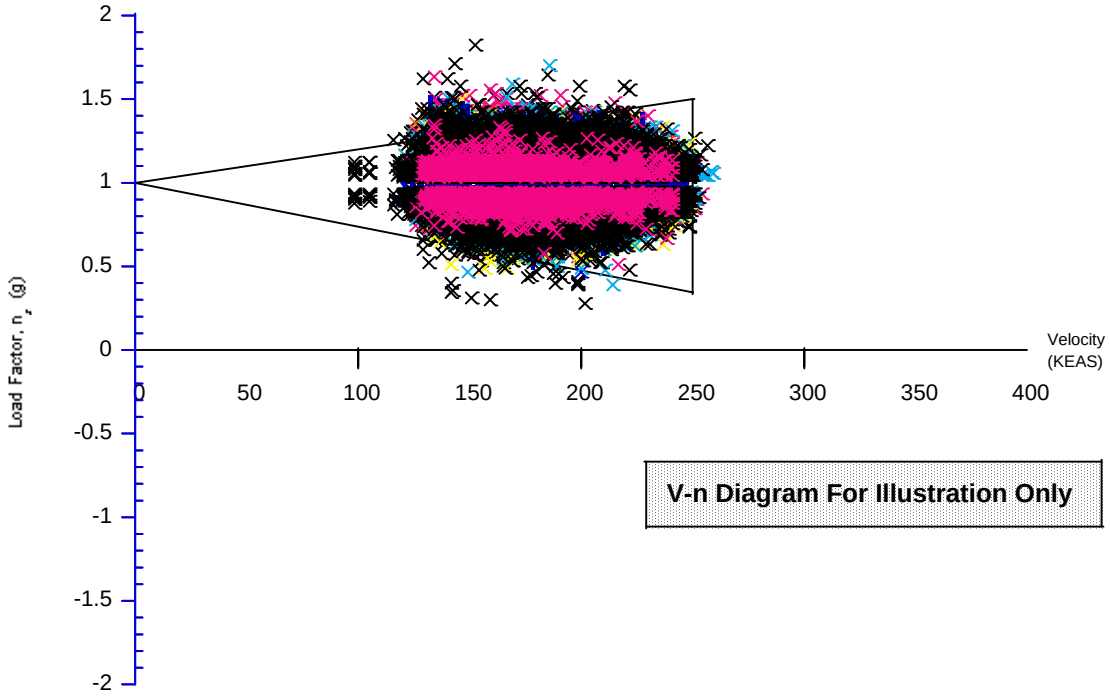

FIGURE A-66. COINCIDENT GUST LOAD FACTOR AND SPEED VERSUS V-n DIAGRAM FOR FLAPS EXTENDED

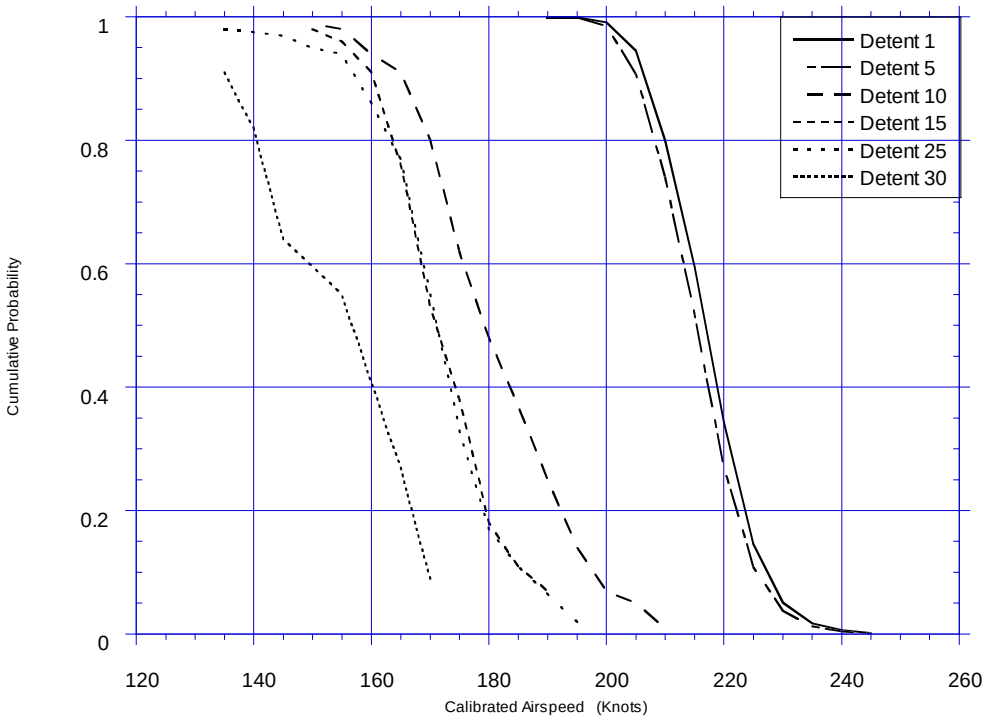

FIGURE A-67. CUMULATIVE PROBABILITY OF MAXIMUM AIRSPEED IN FLAP DETENT DURING DEPARTURE

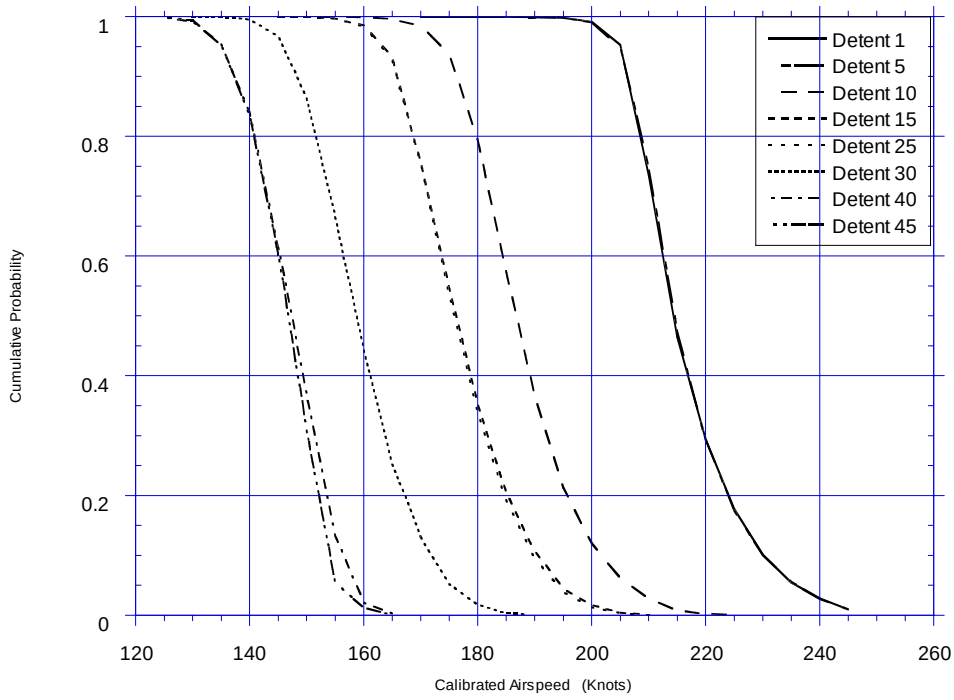

FIGURE A-68. CUMULATIVE PROBABILITY OF MAXIMUM AIRSPEED IN FLAP DETENT DURING APPROACH

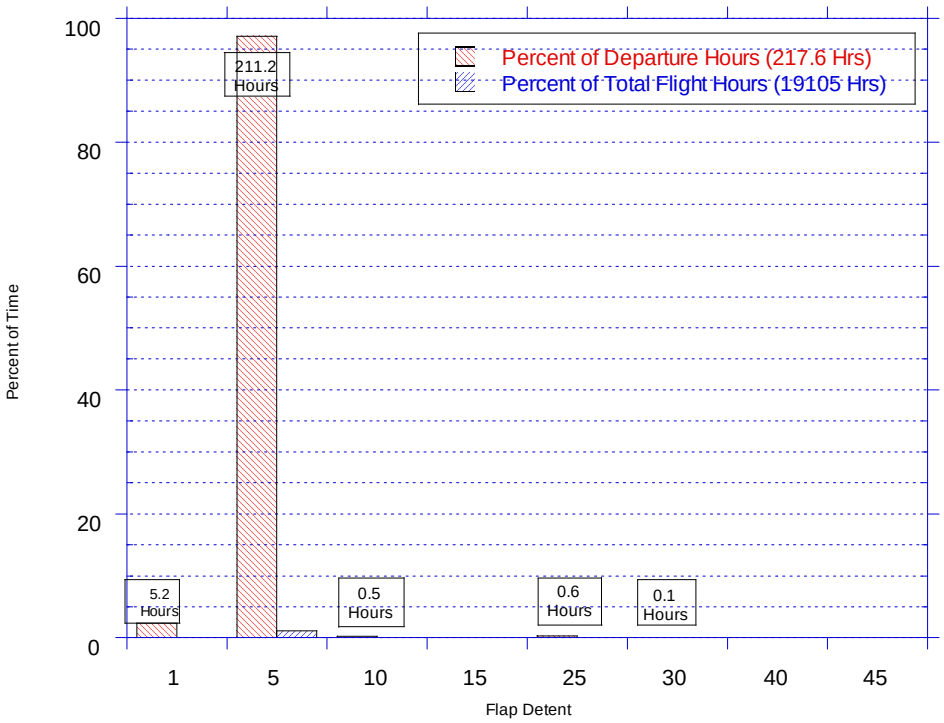

FIGURE A-69. PERCENT OF TIME IN FLAP DETENT DURING DEPARTURE

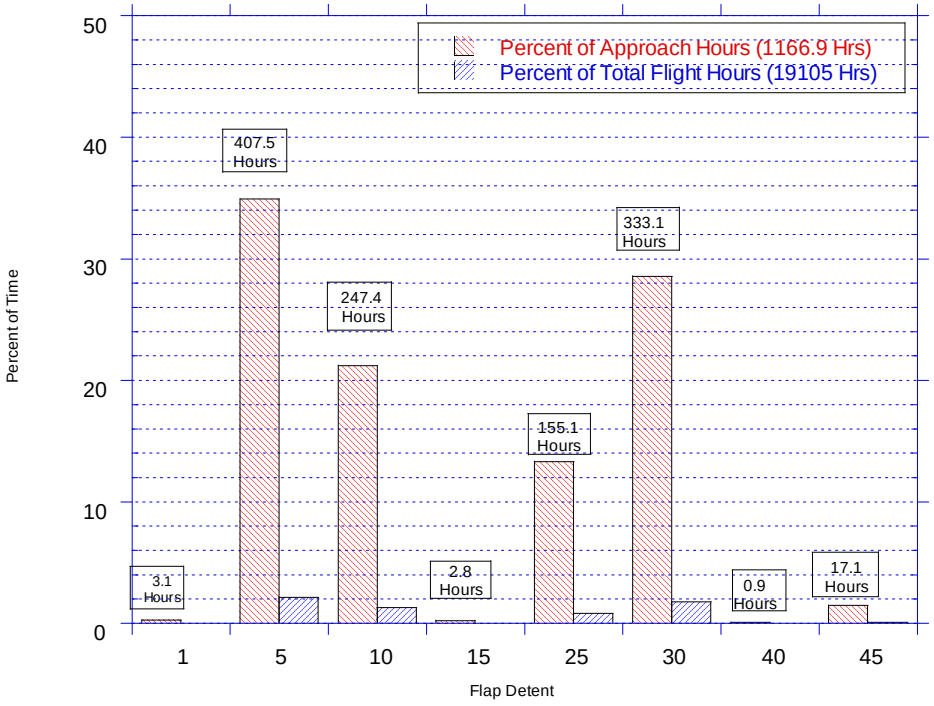

FIGURE A-70. PERCENT OF TIME IN FLAP DETENT DURING APPROACH

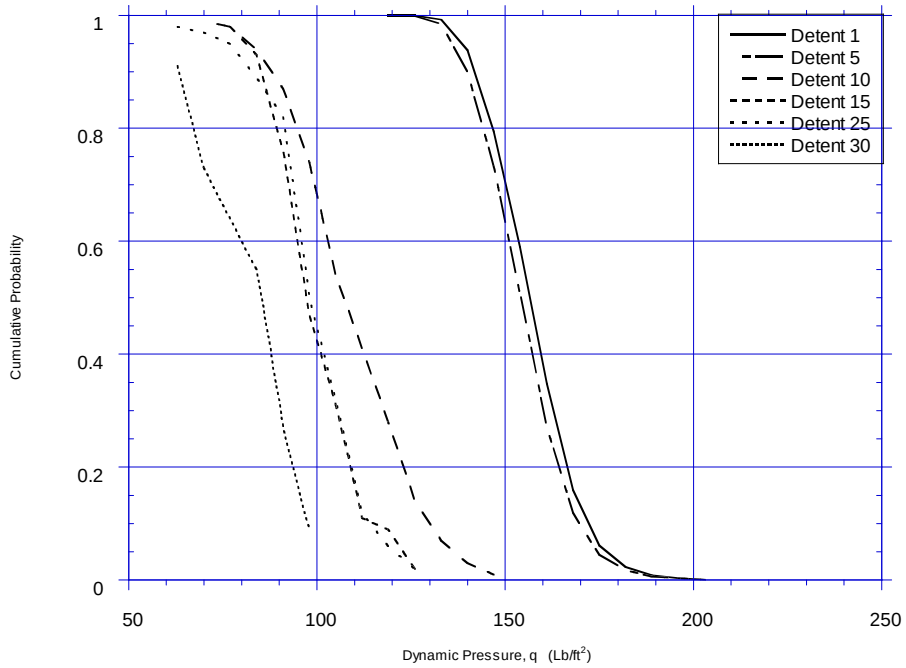

FIGURE A-71. CUMULATIVE PROBABILITY OF MAXIMUM DYNAMIC PRESSURE IN FLAP DETENT DURING DEPARTURE

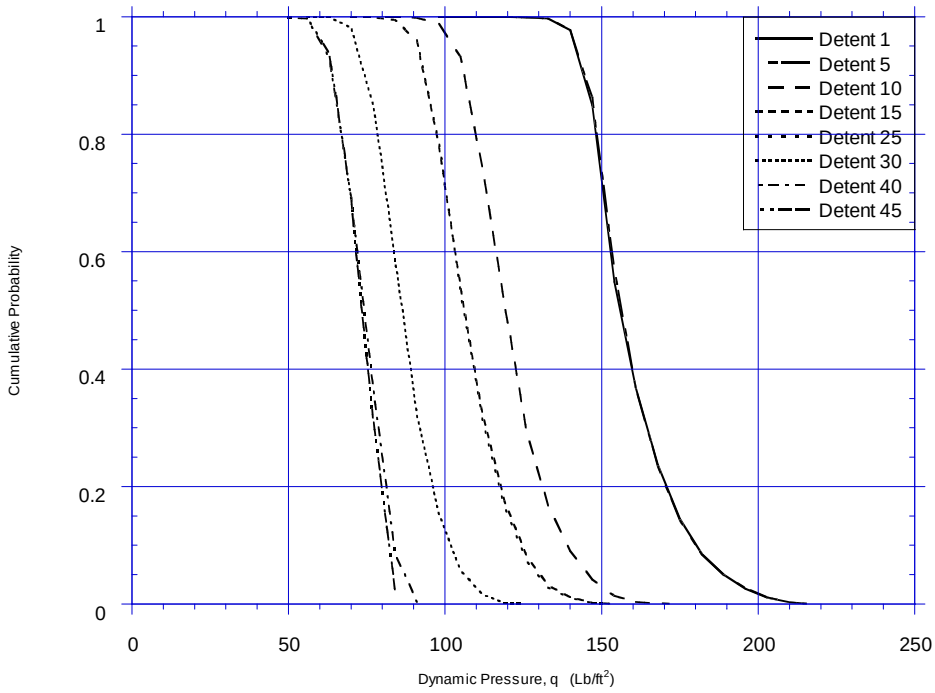

FIGURE A-72. CUMULATIVE PROBABILITY OF MAXIMUM DYNAMIC PRESSURE IN FLAP DETENT DURING APPROACH

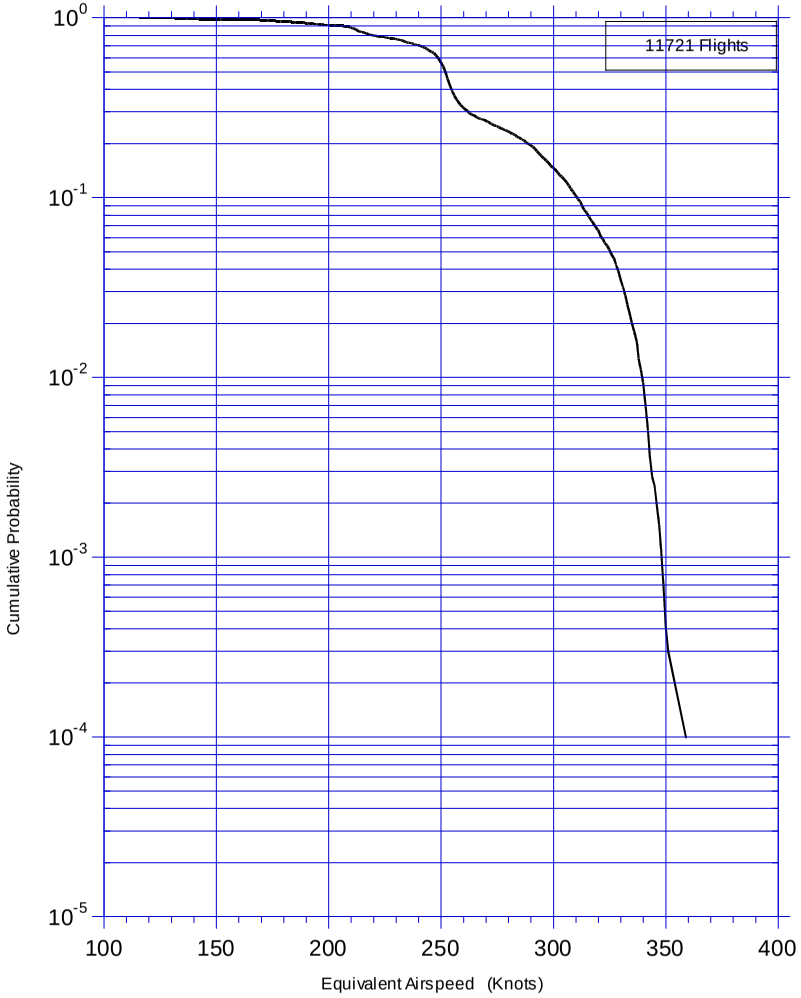

FIGURE A-73. CUMULATIVE PROBABILITY OF MAXIMUM SPEED DURING SPEED BRAKE DEPLOYMENT

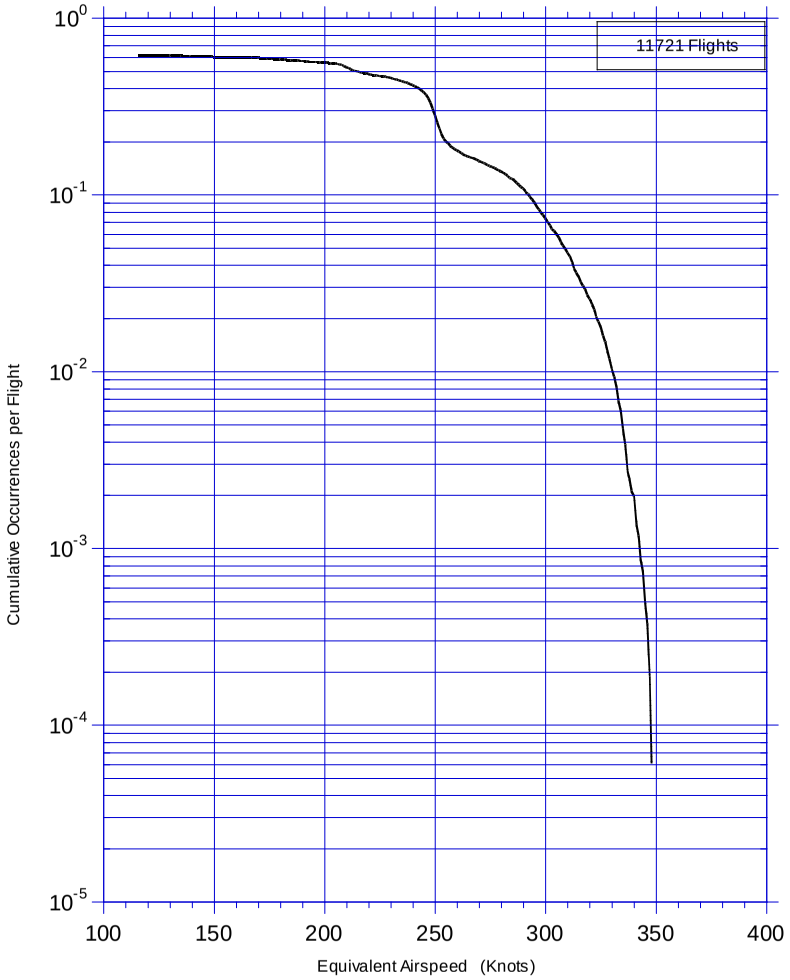

FIGURE A-74. CUMULATIVE FREQUENCY OF SPEED AT SPEED BRAKE DEPLOYMENT

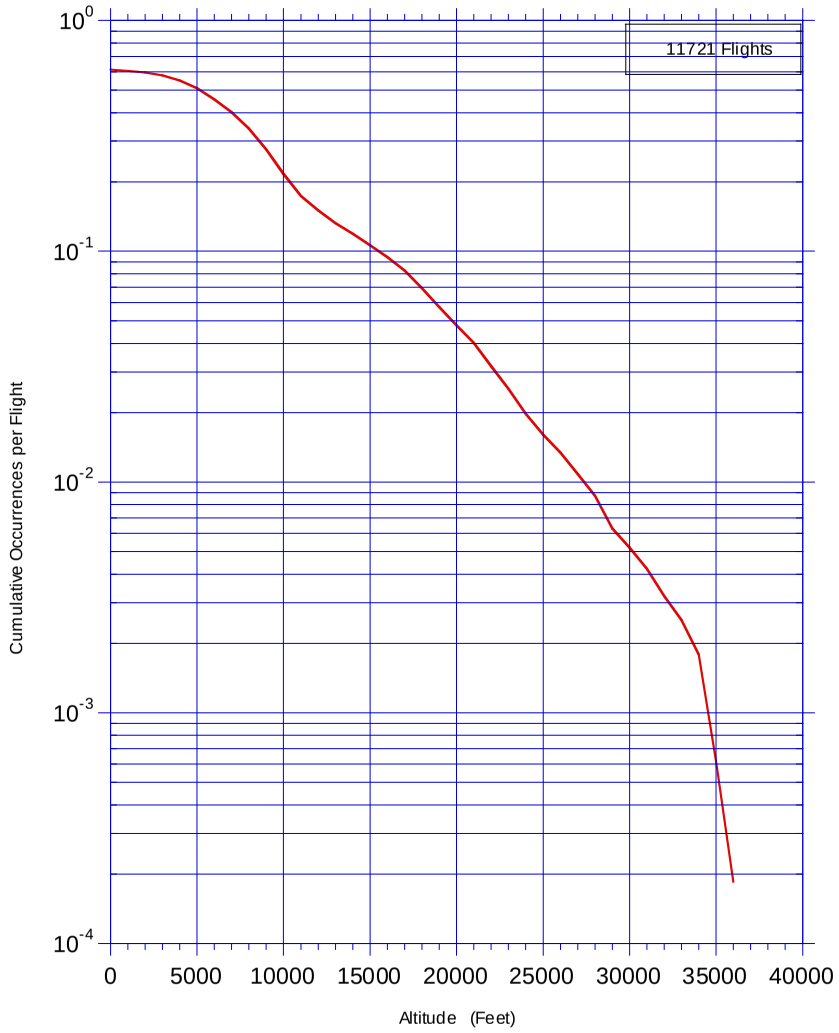

FIGURE A-75. CUMULATIVE FREQUENCY OF ALTITUDE AT SPEED BRAKE DEPLOYMENT

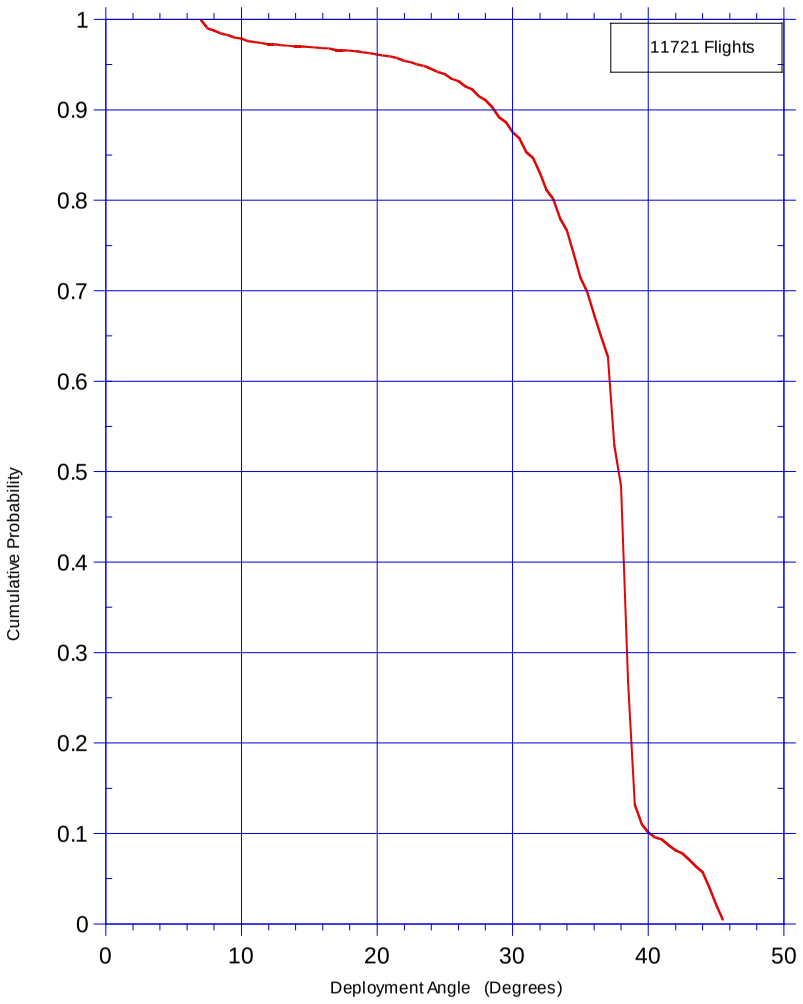

FIGURE A-76. CUMULATIVE PROBABILITY OF MAXIMUM DEPLOYMENT ANGLE DURING SPEED BRAKE DEPLOYMENT, FLAPS RETRACTED

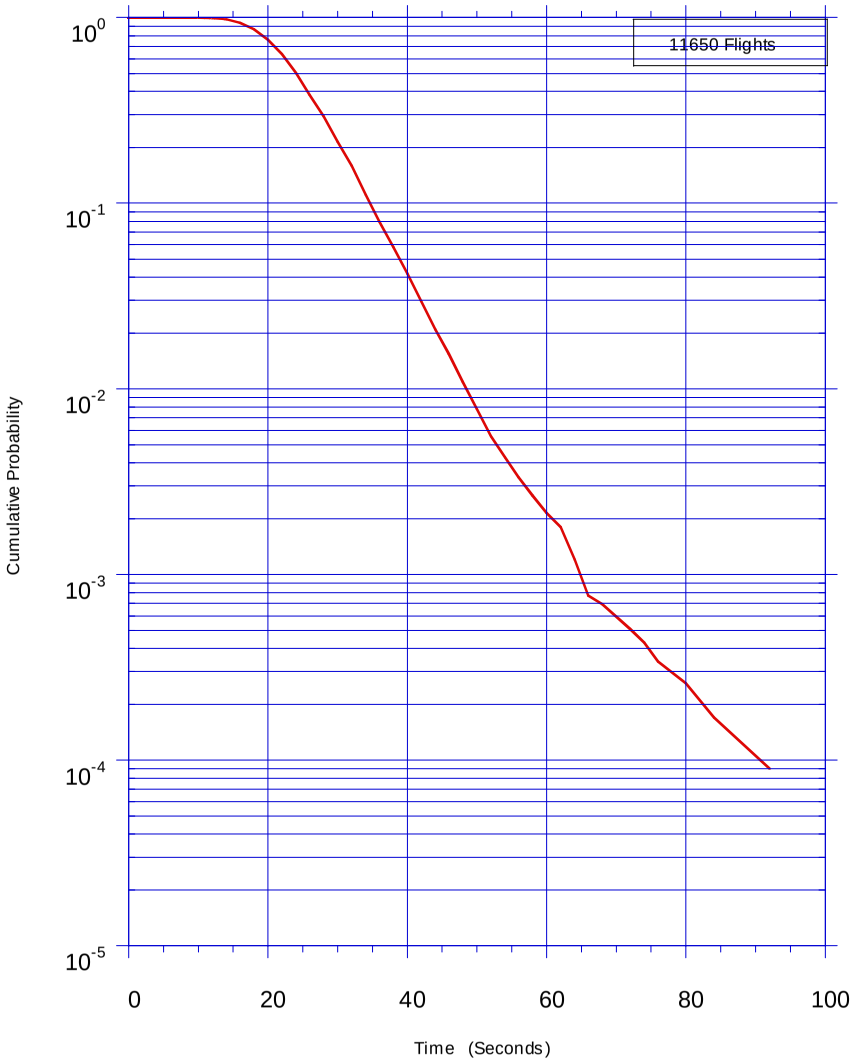

FIGURE A-77. CUMULATIVE PROBABILITY OF TIME WITH THRUST REVERSERS DEPLOYED

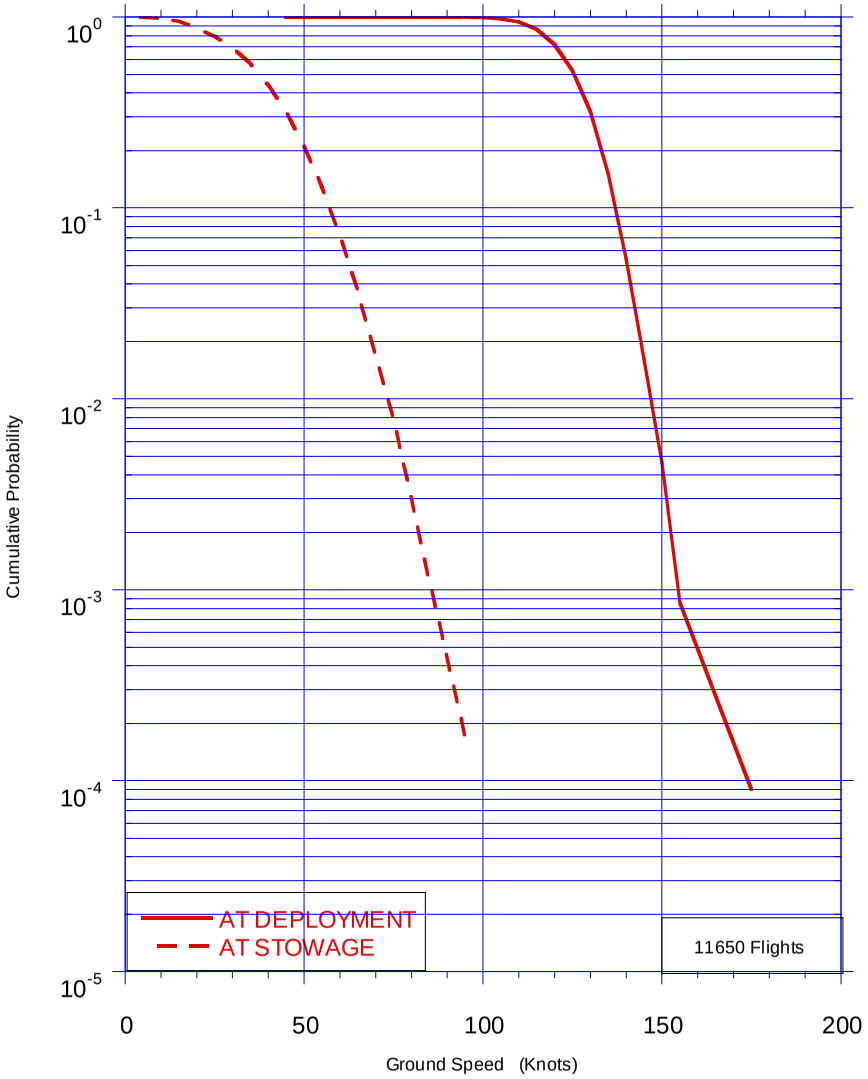

FIGURE A-78. CUMULATIVE PROBABILITY OF SPEED AT THRUST REVERSER DEPLOYMENT AND STOWAGE

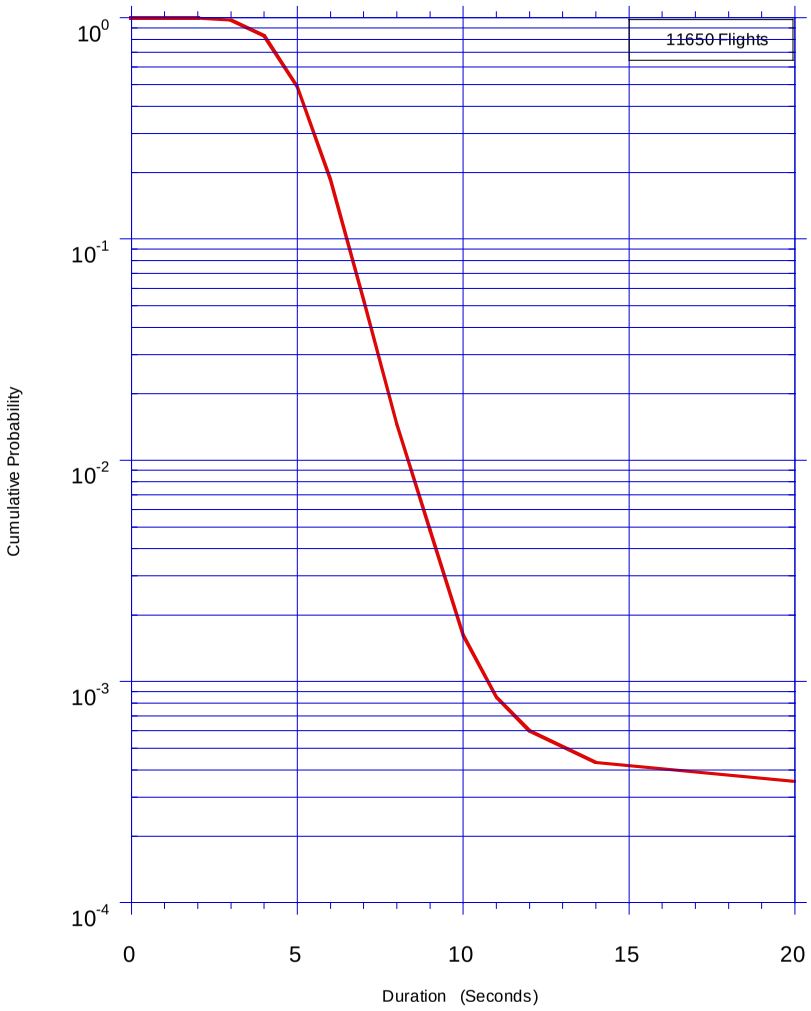

FIGURE A-79. CUMULATIVE PROBABILITY OF TIME WITH LANDING GEAR EXTENDED AFTER LIFTOFF

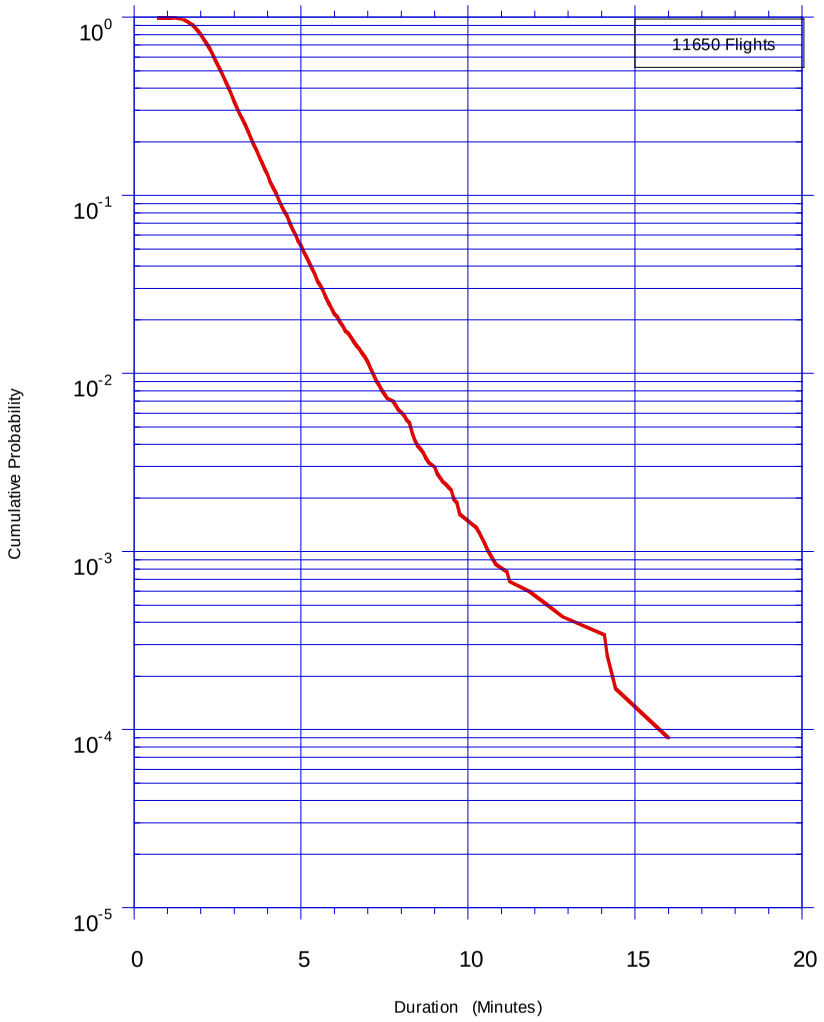

FIGURE A-80. CUMULATIVE PROBABILITY OF TIME WITH LANDING GEAR EXTENDED PRIOR TO TOUCHDOWN

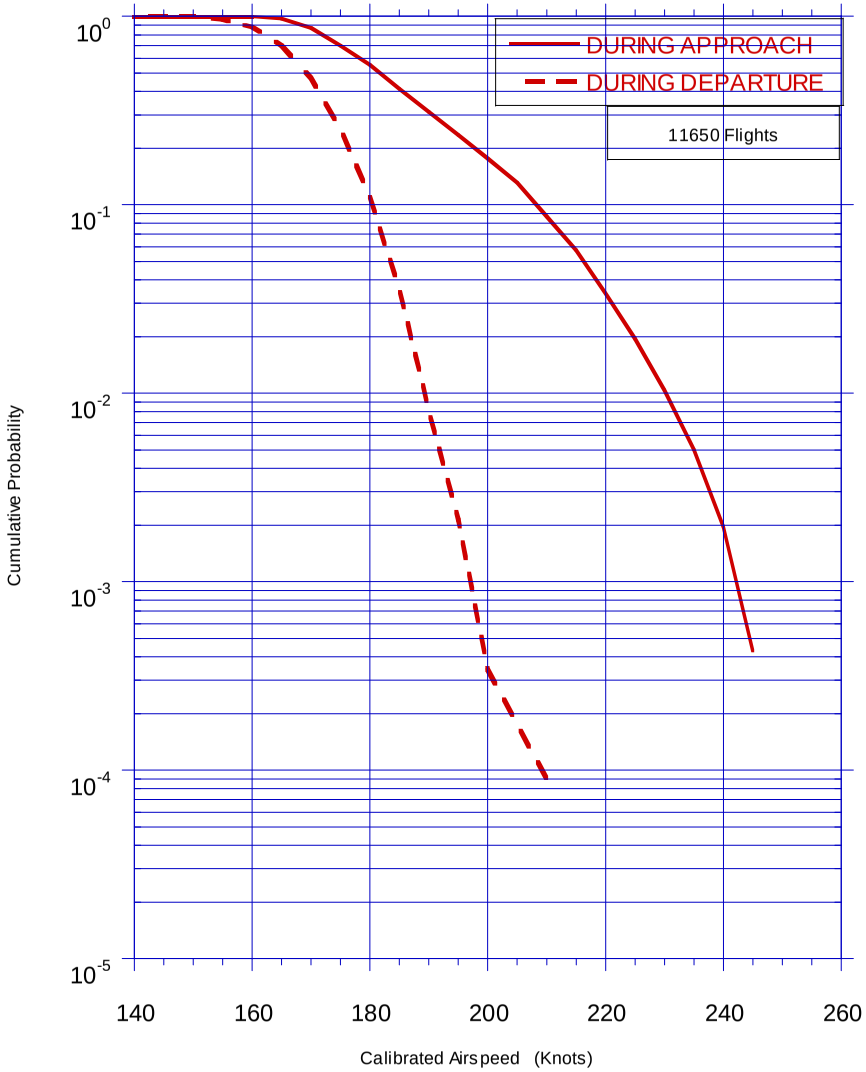

FIGURE A-81. CUMULATIVE PROBABILITY OF MAXIMUM AIRSPEED WITH GEAR EXTENDED

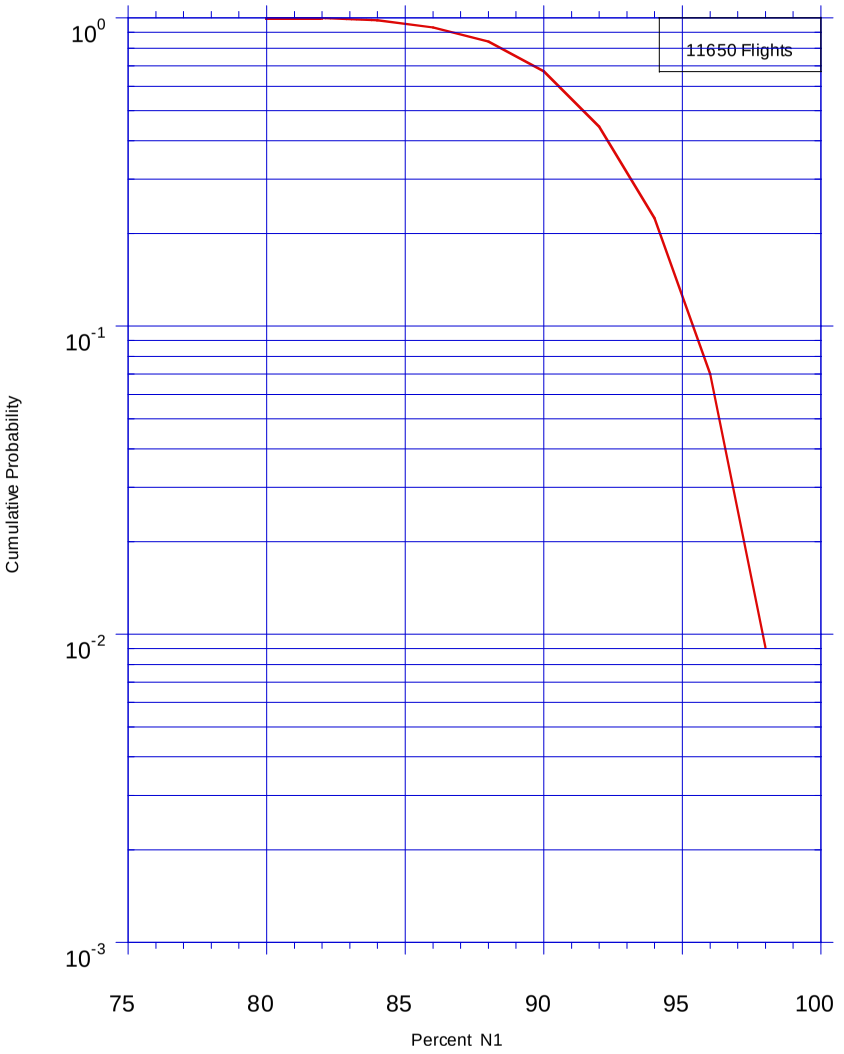

FIGURE A-82. CUMULATIVE PROBABILITY OF PERCENT OF N_1 AT TAKEOFF

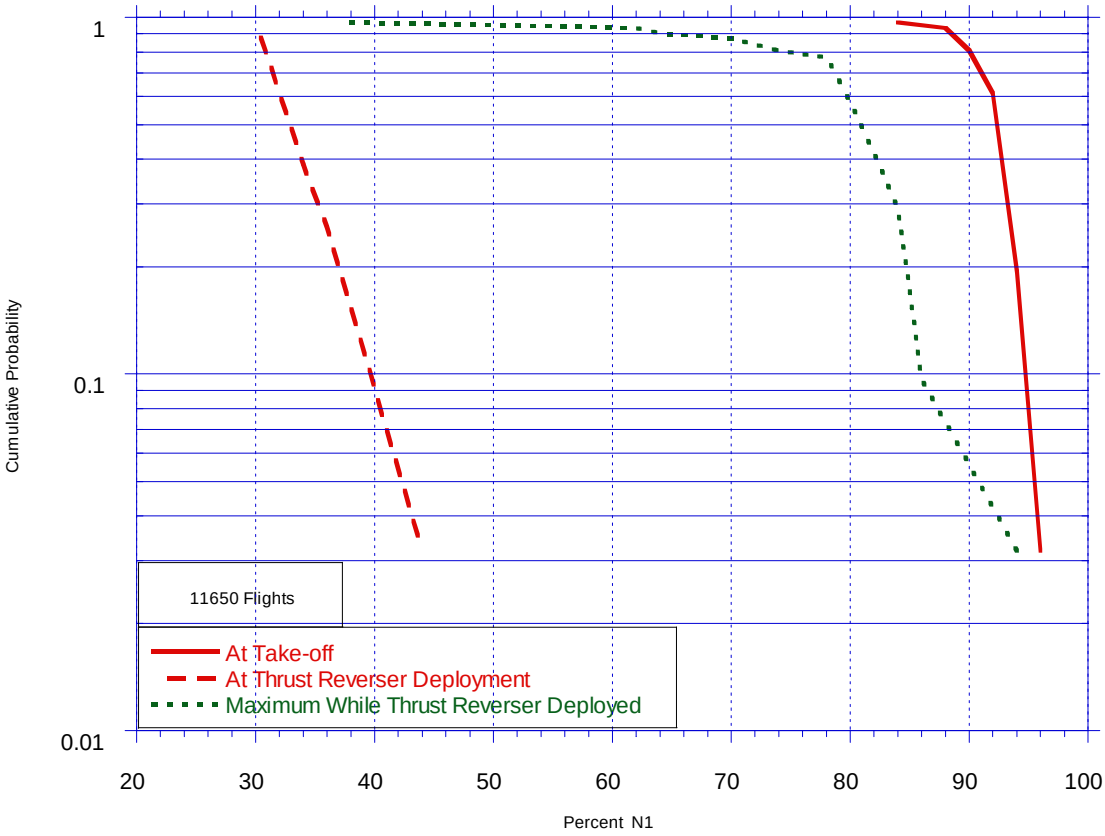

FIGURE A-83. CUMULATIVE PROBABILITY OF PERCENT OF N_1

APPENDIX B—GREAT CIRCLE DISTANCE CALCULATION

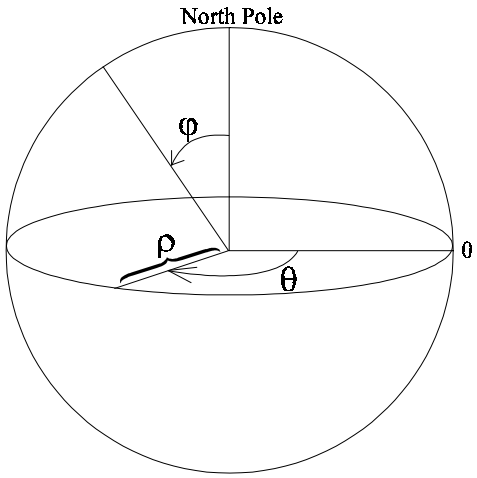

Given:

Latitude and Longitude	ρ = distance from center
of Departure and	φ = angle from North Pole
Destination Airports	θ = angle E/W of prime meridian

Procedure: (see sketch)

The standard mathematical system for spherical coordinates is shown, where three variables specify location: ρ,φ, and θ.

Let *a* = Great Circle Distance in angular measure.

Latitude is measured away from the Equator (0°) to the North Pole (+90°) and the South Pole (-90°); whereas in the standard spherical coordinate system, the North Pole, Equator, and South Pole lie at 0°, 90°, and 180°, respectively. Therefore,

$$\varphi = 90° - \text{latitude}$$

transforms latitude readings into equivalent angles (φ) in the standard spherical coordinate system.

Then

$$b = 90° - \text{Latitude}_{Dep}$$
$$c = 90° - \text{Latitude}_{Des}$$

where *b* and *c* are values of φ for the departure and destination locations, respectively.

Longitude is measured away from the prime meridian (0°). Longitudes to the east are positive and to the west negative. However, the standard spherical coordinate system measures its angles in the opposite direction. Therefore,

θ = - longitude

transforms longitude readings into equivalent angles (θ) in the standard spherical coordinate system.

Then

$$\begin{aligned} A &= (-\text{ Longitude}_{Des}) - (-\text{ Longitude}_{Dep}) \\ &= \text{Longitude}_{Dep} - \text{Longitude}_{Des} \end{aligned}$$

where *A* is the value of θ between the departure and destination locations.

The following equation, based on the spherical coordinate system, allows the computation of the Great Circle Distance, *a*. (Law of cosines for oblique spherical triangles)

$$\cos a = \cos b \cos c + \sin b \sin c \cos A$$

Substituting for *b*, *c*, and *A* from the above equalities,

$$\begin{aligned} \cos a = &\cos (90° - \text{Lat}_{Dep}) \cos (90° - \text{Lat}_{Des}) \\ &+ \sin (90° - \text{Lat}_{Dep}) \sin (90° - \text{Lat}_{Des}) \cos (\text{Lon}_{Dep} - \text{Lon}_{Des}) \end{aligned}$$

Since

$$\begin{aligned} \cos (90° - \text{Lat}_{Dep}) &= \sin \text{Lat}_{Dep} \\ \cos (90° - \text{Lat}_{Des}) &= \sin \text{Lat}_{Des} \\ \sin (90° - \text{Lat}_{Dep}) &= \cos \text{Lat}_{Dep} \\ \sin (90° - \text{Lat}_{Des}) &= \cos \text{Lat}_{Des} \end{aligned}$$

by replacement one obtains

$$\cos a = \sin (\text{Lat}_{Dep}) \sin (\text{Lat}_{Des}) + \cos (\text{Lat}_{Dep}) \cos (\text{Lat}_{Des}) \cos (\text{Lon}_{Des} - \text{Lon}_{Dep})$$

Thus *a*, the angular measure of the great circle arc connecting the departure and destination locations, is obtained as

$$a = \cos^{-1} [\sin (\text{Lat}_{Dep}) \sin (\text{Lat}_{Des}) + \cos (\text{Lat}_{Dep}) \cos (\text{Lat}_{Des}) \cos (\text{Lon}_{Des} - \text{Lon}_{Dep})]$$

So, for *a* expressed in radians

$$GCD = a \text{ radians} \left(\frac{180 \text{ deg.}}{\pi \text{ radians}} \right) \left(\frac{60 \text{ min.}}{1 \text{ deg.}} \right) \left(\frac{1 \text{nm}}{1 \text{ min.}} \right) = \left(\frac{10800a}{\pi} \right) \text{nm}$$

and for *a* expressed in degrees,

$$GCD = a \text{ degrees} \left(\frac{60 \text{ min.}}{1 \text{ deg.}} \right) \left(\frac{1 \text{ nm}}{1 \text{ min.}} \right) = 60a \text{ nm}$$

Appendix – List of FAA Technical Reports Published in FY98

Report Number	Title
R&D Highlights 1998	Highlights of the major accomplishments and applications.
DOT/FAA/AR-TN97/50	Comparison of Radial and Bias-Ply Tire Heating on a B-727 Aircraft
DOT/FAA/AR-97/99	Fire-Resistant Materials: Research Overview
DOT/FAA/AR-95/18	User's Manual for the FAA Research and Development Electromagnetic Database (FRED)
DOT/FAA/AR-97/7	Advanced Pavement Design: Finite Element Modeling for Rigid Pavement Joints, Report II: Model Development
DOT/FAA/AR-97/26	Impact of New Large Aircraft on Airport Design
DOT/FAA/AR-97/64	Operational Evaluation of a Health and Usage Monitoring Systems (HUMS)
DOT/FAA/AR-TN98/15	Fire Testing of Ethanol-Based Hand Cleaner
DOT/FAA/AR-95/111	Stress-Intensity Factors for Elliptical Cracks Emanating from Countersunk Rivet Holes
DOT/FAA/AR-97/9	An Acoustic Emission Test for Aircraft Halon 1301 Fire Extinguisher Bottles
DOT/FAA/AR-97/37	Development of an Improved Magneto-Optic/Eddy-Current Imager
DOT/FAA/AR-97/69	Automated Inspection of Aircraft
DOT/FAA/AR-97/5	Marginal Aggregates in Flexible Pavements: Field Evaluation
DOT/FAA/AR-97/87	A Predictive Methodology for Delamination Growth in Laminated Composites, Part I: Theoretical Development and Preliminary Experimental Results
DOT/FAA/AR-TN97/103	Initial Development of an Exploding Aerosol Can Simulator
DOT/FAA/AR-97/56	Applications of Fracture Mechanics to the Durability of Bonded Composite Joints

Report Number	Title
DOT/FAA/AR-96/97	Stress-Intensity Factors Along Three-Dimensional Elliptical Crack Fronts
DOT/FAA/AR96/119	Vertical Drop Test of a Beechcraft 1900C Airliner
DOT/FAA/AR-98/22	FAA T53-L-13L Turbine Fragment Containment Test
DOT/FAA/AR-97/85	Response and Failure of Composite Plates with a Bolt-Filled Hole
DOT/FAA/AR-98/26	A Review of the Flammability Hazard of Jet A Fuel Vapor in Civil Transport Aircraft Fuel Tanks
DOT/FAA/AR-TN97/108	Effects of Concentrated Hydrochloric Acid Spills on Aircraft Aluminum Skin
DOT/FAA/AR-TN98/32	Cargo Compartment Fire Protection in Large Commercial Transport Aircraft
DOT/FAA/AR-98/28	Statistical Loads Data for Boeing 737-400 Aircraft in Commercial Operations
DOT/FAA/AR-97/47	Development of Advanced Computational Models for Airport Pavement Design
DOT/FAA/AR-98/34	Health Hazards of Combustion Products From Aircraft Composite Materials
DOT/FAA/AR-97/81	Bioremediation of Aircraft Deicing Fluids (Glycol) at Airports
DOT/FAA/AR-TN97/8	Heats of Combustion of High-Temperature Polymers
DOT/FAA/AR-95/29 ***FACT SHEETS***	Fiber Composite Analysis and Design: Composite Materials and Laminates, Volume I Note: This document's PDF is unique from the above documents in that some of the Adobe navigational tools cannot be used such as searching and bookmarking. To navigate in this document, page down to the Table of Contents, List of Figures, and List of Tables where the entries are linked to the body of the document.